Università di Pisa

Dexterous grippers: between simple industrial grippers and complex robotic hands

Doctoral School of Engineering "Leonardo da Vinci"
PhD Program on Automatic, Robotics and Bioengineering
XXVI cycle
SSD: ING-INF/04

Author:
Vinicio Tincani

Tutors:
Prof. Antonio Bicchi
Prof. Gualtiero Fantoni

2011 - 2014

Abstract

This thesis addresses the issue of introducing dexterity, namely the ability to manipulate objects in hand, into simple mechanical grippers. Among the many possibilities to give dexterity to a gripping device we opted to intervene at the finger-pad surface since it is the part of the end effector directly in contact with the object to be manipulated.

The first contribution is the development of an under-actuated gripper with Active Surfaces on the inner side of the fingers which allow to in-hand manipulate the grasped objects. The gripper, named Velvet Fingers, was designed from the theoretical concepts, manufactured, assembled and then turned into an applicative scenario.

A second main contribution of this thesis, carried out in collaboration with AASS Research Center, of the University of Örebro (Sweden), is a grasp execution routine using the Active Surfaces of the Velvet Fingers to achieve a robust power grasp starting from an initial fingertip grasp. This routine is very useful and effective in cluttered environment where an initial fingertip grasp is much more likely to be feasible than a bulky power grasp.

The third main contribution is the development of a small gripper for

small household objects such as cans, small bottles, little boxes, tennis balls etc. This gripper, named Velvet-II, is able to perform in-hand manipulation tasks, to elicit information from the grasped object, namely the contact point location and the components of the grasping forces and to detect incipient slippage between the gripper and the object. Within a collaboration with AASS Research Center the gripper has been employed on a robotic platform for autonomous picking and palletizing.

Acknowledgements

I have a long list of people to thank, since I have the fortune to live and work with very special persons. First and foremost, I would like to thank my supervisors Antonio Bicchi and Gualtiero Fantoni for giving me the opportunity to work close to them and for their precious support over the past years together. Then I would like to extend my thanks to all my colleagues and friends at the University for making this place the friendly and productive environment that it is. Thank you Manuel C., Giorgio and Manolo for being great colleagues always available for fruitful discussions and ready to help the others. Thank you Manuel B. for your pleasant company and for sharing with me our pilgrimages to Bremen. Then I would like to thank two special colleagues and friends I had the fortune to meet in the RobLog project. Thank you Todor and Robert for showing me that discipline, professional competence, kindness, availability and desire to enjoy the life can coexist in the same person. Finally I want to thank my family: Thank you Dad, thank you Mum, thank you Giulia for your unwavering support. Always in my mind!

Contents

1 Introduction **19**
1.1 Outline of the thesis . . . 23
1.2 Contributions . . . 24
1.3 Publications . . . 25

2 Background **29**
2.1 The grasping process . . . 29
2.2 Industrial grippers . . . 31
2.3 Robotic hands . . . 41
2.4 Medium complexity gripping devices . . . 44
2.5 Dexterous grippers . . . 55

3 The Velvet Fingers dexterous gripper **63**
3.1 Theoretical concept . . . 64
3.1.1 Conceptual design . . . 64
3.1.2 Active Surfaces . . . 66
3.1.3 Kinematic Design for Grasping Closure . . . 72
3.1.4 Manipulability Analysis . . . 77
3.2 Design of the Velvet Fingers . . . 81
3.2.1 Palm . . . 83
3.2.2 Proximal Phalanx . . . 84
3.2.3 Distal Phalanx . . . 85
3.3 Physical implementation of the Velvet Fingers . . . 86

3.3.1 Electronics . . . 87
3.3.2 Grasping experiments . . . 89
3.4 Active Surface control . . . 91
3.4.1 Positioning control . . . 93
3.4.2 Variable friction control . . . 96
3.5 Discussion . . . 107

4 Autonomous grasp acquisition with the Velvet Fingers 111
4.1 Grasp planning for an under-actuated gripper with Active Surfaces . . . 113
4.2 Grasping pipeline . . . 116
4.3 Grasping execution for cluttered scenes . . . 119
4.4 Evaluation and results . . . 124
4.5 Velvet Fingers upgrade . . . 127
4.6 Grasp execution on the Parcel Robot . . . 136
4.7 Discussion . . . 139

5 The Velvet II 141
5.1 Concept and specifications . . . 142
5.2 Sensitive Active Surfaces . . . 148
5.2.1 Contact point location . . . 150
5.2.2 Variable friction coefficient control of the SAS . . . 155
5.3 The Velvet II: physical implementation . . . 162
5.3.1 The fingers . . . 164
5.3.2 Palm . . . 168
5.4 Grasping experiments . . . 170
5.5 The Velvet-II on an autonomous picking and palletizing platform . . . 173
5.5.1 Autonomus forklift . . . 175
5.5.2 Grasping & Manipulation System . . . 178
5.5.3 Robust Grasp Execution . . . 182
5.5.4 Evaluation . . . 182
5.5.5 Discussion . . . 183

6 Conclusion and future works 187

A Contact Point Algorithm 191

List of Publications **205**

Bibliography **209**

List of Figures

1.1 Grasping devices 22

2.1 Grasp principles 30
2.2 Vacuum gripper 33
2.3 Passive magnetic grippers 34
2.4 Active elctromagnetic grippers 35
2.5 Magnetoadhesive grippers 35
2.6 Scheme of an electroadhesive gripper 36
2.7 Cryogenic grippers 37
2.8 Needle grippers 38
2.9 The Needle Roller 39
2.10 Mechanical grippers 40
2.11 Bernoulli grippers 40
2.12 The Robonaut 2 Hand. 43
2.13 The Shadow Hand 44
2.14 The Barret Hand 46
2.15 The Pisa/IIT SoftHand 47
2.16 Grasps executed with the Soft Hand 47
2.17 The Soft Gripper and the Shape Gripper 48
2.18 Grasps performed by the Velo 2G Gripper 48
2.19 The Velo 2G Gripper 49
2.20 The Robotiq 3-Finger Adaptive Robot Gripper 50

2.21 Robotiq 3-Finger: fingertip and power grasp 51
2.22 Robotiq 3-Finger: operation mode 51
2.23 The SDM Hand 52
2.24 The SDM Hand: the differential transmission 53
2.25 Grasps executed with the SDM Hand 54
2.26 The Universal Gripper 55
2.27 Omnidirectional driving gears 57
2.28 Datseris and Palm dexterous gripper 58
2.29 The Roll-on Gripper 58
2.30 Roll-on Gripper: grasping 59
2.31 Roll-on Gripper: in-hand manipulation 60
2.32 The Robin Read Gripper 60
2.33 The DxGrip-II 61
2.34 The DxGrip-II: operative modes 62

3.1 Heterogeneous goods in the RobLog project 64
3.2 Basic idea for grasping in RobLog 65
3.3 Friction modulation at micro scale 68
3.4 Tangential push at micro scale 68
3.5 Friction modulation at macro scale 69
3.6 Tangential push at macro scale 69
3.12 Free closure and enveloping grasp of the gripper 74
3.13 Kinematics of the gripper 74
3.14 Grasping of a small object 76
3.15 Manipulability ellipsoids 78
3.16 Cut view of the Velvet Fingers 83
3.17 Velvet Fingers: the palm 84
3.18 Velvet Fingers: the proximal phalanx 85
3.19 Velvet Fingers: the distal phalanx 86
3.20 Refinements of the Velvet Fingers 87
3.21 Physical implementation of the Velvet Fingers 88
3.22 Free closure of the Velvet Fingers 90
3.23 Embracing grasp of the Vlevet Fingers 91
3.24 Grasping with touching fingertips 91
3.25 Grasps executed with the Velvet Fingers 92
3.26 Dynamical model of the conveyor belts 93
3.27 Object expulsion 94

3.28 In-hand object rotation . . . 95
3.29 In-hand roto-tranlsation . . . 96
3.30 Combined effect of Active Surfaces and under-actuation . . . 97
3.31 Lift of a box . . . 98
3.32 Dahal friction model . . . 99
3.33 External pushing force Vs tangential emulated friction force. . . . 100
3.34 Sinusoidal external force . . . 101
3.35 Low friction level . . . 102
3.36 Medium friction level . . . 103
3.37 High friction level . . . 103
3.38 The tilted plane experiment . . . 104
3.39 Emulated friction coefficient: upper and lower bound. . . . 105
3.40 Grasping of a big cylinder . . . 106
3.41 Opening a bottle with high friction to balance the torque . . . 106
3.42 Grasp equilibrium . . . 108

4.1 Parcel Robot . . . 112
4.2 Preset contact locations . . . 115
4.3 A set of fingertip grasps . . . 116
4.4 Grasping pipeline . . . 117
4.5 Grasp retrieval . . . 119
4.6 Autonomous grasping execution . . . 120
4.7 Control architecture of the pull-in strategy . . . 123
4.8 Electronic board for the pull-in strategy . . . 123
4.9 Platform in Pisa . . . 124
4.10 Planning results:isolated objects . . . 126
4.11 Final version of the Velvet Fingers: CAD . . . 130
4.12 The driver cylinder . . . 130
4.13 Driver cylinder and guide roll . . . 132
4.14 Distal phalanx . . . 133
4.15 The finger . . . 134
4.16 Cut view of the finger . . . 135
4.17 The palm . . . 136
4.18 Photograph of the final version . . . 136
4.19 From tip grasp to power grasp . . . 138
4.20 A sequence of an autonomous grasp . . . 139

5.1 Extrinsic and intrinsic sensors . . . 143
5.2 SAS concept . . . 144
5.3 Joint arrangement . . . 145
5.4 Notation used for the kinematic design of the finger . . . 146
5.5 Kinematic scheme of a finger . . . 147
5.6 SAS physical implementation . . . 148
5.7 Experimental set up . . . 150
5.8 Contact point detection: HI . . . 151
5.9 Contact point detection: actuation . . . 152
5.10 Contact point detection:random trajectory . . . 153
5.11 Contact point detection:perimeter . . . 153
5.12 Contact point accuracy on the plane . . . 154
5.13 Contact point accuracy on the driven cylinder . . . 154
5.14 Variable friction experimental setup . . . 158
5.15 Accuracy of the variable friction algorithm . . . 159
5.16 Experiment with low friction . . . 160
5.17 Variable friction experiment with a variable external wrench . . . 161
5.18 Overall view of the Velvet-II . . . 163
5.19 Velvet-II main dimensions . . . 163
5.20 Tip grasp and power grasp . . . 164
5.21 The finger . . . 165
5.22 The tendons . . . 166
5.23 c(a) function . . . 167
5.24 First and second joint . . . 167
5.25 The splicing . . . 168
5.26 The palm . . . 169
5.27 A photograph of the Velvet-II . . . 171
5.28 Grasping . . . 171
5.29 Slippage detection of a battery . . . 172
5.30 Slippage detection of a hammer . . . 173
5.31 The APPLE platform . . . 175
5.32 Human detection . . . 178
5.33 Grasp interval . . . 180
5.34 Truncated grasp interval . . . 181
5.35 Grasp execution . . . 184
5.36 Final evaluation of the APPLE platform . . . 185

LIST OF FIGURES

A.1 Left cylinder reference frame 192
A.2 External wrench applied on the left cylinder 193
A.3 Solution of Eq.A.4 195
A.4 Right cylinder reference frame 198
A.5 Reference frame of the plane 201
A.6 Reference system of the 6-axis F/T sensor 201

List of Tables

4.1 Motor comparative table 122
4.2 Predefined parameters 126
4.3 Planning results: cluttered scenes 127
4.4 Characteristics of REMAX17 131
4.5 Grasp statistics 137

5.1 Specifications of the F/T transducer 149
5.2 Specifications of the motor for opening and closing 170

Chapter 1

Introduction

One of the most important aspect in many robotic applications across all domains is the interaction between the robot and the environment. The apparatus a robot manipulator interacts directly and actively with the environment falls under the name of "end effector" and usually it is the last link of its kinematic chain. End effector can be divided into two distinct groups:

- *non-prehensile end effectors*: This class includes substantially tools, often with no degrees of freedom (DoF), attached to the wrist of a manipulator. They perform their functions while being carried along certain trajectories by the manipulator and they do not execute any grasp. There are many instances of non-prehensile end effector in industry, for example the spot welding heads or the spray guns on the assembly lines of automotive industry. Again from industry, cutting tools and sanders. From surgery, lasers for eye surgery or scalpels.

- *prehensile end effectors*: This class includes devices whose main

task is to firmly grab and hold objects. There exists a huge variety of end effectors for prehensile tasks. Industrial grippers and robotic hands fall into this class.

Grasping and manipulation are very complicated tasks even though for human beings their complexity is usually underestimated being natural and instinctive. This underestimation relies on the goodness of the "hardware" and "software" a human being is provided to accomplish such tasks. Indeed the human hand, with four fingers, an opposable thumb, 19 DoFs in total, with a big amount of sensory nerve endings of different kinds which form an outstanding efficient sensor equipment, is very effective and allows to accomplish both firm power grasps and nimble and fine manipulation. The arrangement of the fingers and the large number of DoFs allows a good adaptability of the hand to the shape of the objects which contributes to the firmness of the grasp. Moreover Neuroscience states that the largest fraction (30-40%) of the motor cortex, (the region of the brain responsible for movement planning and execution) is dedicated to the control of the hand [1]. All this tremendous system (the hand and the portion of the cortex dedicated) is continuously trained since the first moments of life, so that a three years old child (even if it might still take a few years before reaching the full grasping and manipulation maturity [2]) can be an extraordinary "gripping device" more effective and skillful than the most sophisticated robotic hands today.

For a robot, successfully grasping an object entails solving the problems of object perception and grasp synthesis, as well as hand and manipulator motion planning and control. However the grasping process can be simplified reducing the variability of the parameters which affect the stages of grasping: perception, grasp synthesis, grasp execution and motion planning. For instance, limiting the shape of the target objects, their pose and making the surrounding free from possible collisions can

remarkably simplify the hardware and the control of the end effector. In some contexts, these aspects are or can be brought under control. This is the case of the structured or semi-structured environment of factories where, just to mention an instance, a smart feeding system can furnish the robot with properly oriented workpieces fostering and facilitating the following grasping and handling. All of this often results in the use of simple grippers which allows to boost other aspects, which are very valued in industry, like robustness, reliability, speed and cost-effectiveness.

At the increase of the variability and uncontrollableness of such parameters, the complexity of the end effector tends to increase up to human like robotic hands which are conceived to mimic the human hand behavior. An example is the hand/arm system in [3] which is one of the most advanced anthropomorphic platform today (see Fig.1.1 a)). Such humanoid hands can accomplish not only grasping tasks, using the palm and the inner surfaces of the fingers to achieve enveloping grasps, but also manipulative grasps contacting the objects with their fingertips and performing dexterity tasks. In this dissertation the word "dexterity" is used in the sense of the capability of changing the position and orientation of the manipulated object from a given reference configuration to a different one, arbitrarily chosen within the hand workspace [4].

However, anthropomorphism is not mandatory for dexterity. There exist many impressive gripping devices with alternative mechanical solutions like the 3-fingered High-Speed Hand in [5] (Fig.1.1 b)) and the Barret Hand in [6] (Fig.1.1 c)) which possess simple in-hand manipulation capability. These gripping devices belong to a medium complexity region between simple industrial gripper and complex robotic hands.

Since industrial grippers often lack flexibility, (i.e. the aptitude of a device to be responsive to variations of the objects such as in the shape, dimension, roughness, weight etc. with respect to the ones a device is

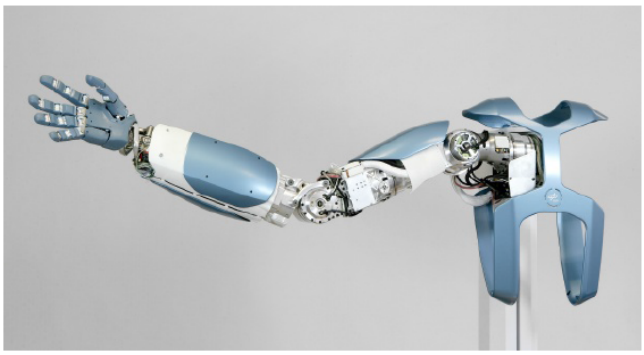

(a)

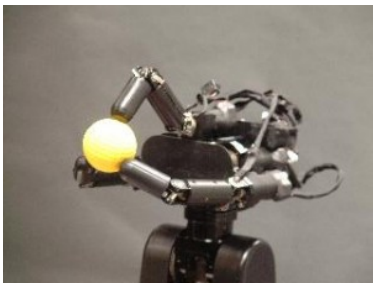

(b)

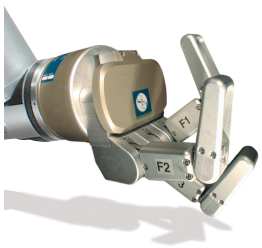

(c)

Figure 1.1: a) the DLR hand/arm system, one of the most advanced human-like robotic platforms, b) the 3-fingered High-Speed Hand, c) the Barret Hand.

designed for, yet achieving a stable grasp) medium complexity devices like the Barret Hand consolidate many specialized gripper tools into a single gripping device avoiding the need for changing end effector on a task-to-task basis and fuse together the dexterity and versatility typical of of robotic hands with the simplicity of control and robustness of simple grippers.

In the medium complexity region, which is the background of this dissertation, is often difficult to distinguish a simplified robotic human-

like hand from a complex industrial gripper. In the last years complexity reduction and reliability enhancement from the complex hand side and flexibility and dexterity augmentation from the simple industrial gripper side have populated this zone with many interesting devices.

The work presented in this dissertation introduces enhanced capabilities, which usually belong to the region of the robotic hands, into industrial grippers while maintaining low the general complexity of the device. Several novel approaches are investigated, focusing on the kinematics and mechanical structure of the device, on the surfaces which directly come into contact with the grasped object, on the sensing system and on the control which can exploit the features of the gripper. Doing so, particular attention was payed on the ease of manufacturing, assembling and use, since the grasping devices object of this dissertation have been designed from the theoretical concepts, manufactured, assembled and then turned into applicative scenarios.

1.1 Outline of the thesis

The rest of this thesis is organized as follows.

- In Chapter 2 we put end effectors for prehensile purposes within a background context where usually antithetical characteristics, such as complexity and dexterity on one hand and simplicity and reliability on the other hand, are active. Within this scenario industrial grippers and anthropomorphic robotic hands assume a neat and opposite position. In between this two classes lies a whole gray scale where many other gripping devices fall, whose position is usually function of the complexity of the tasks they are designed to carry out.

- In Chapter 3 we introduce a novel under-actuated mechanical gripper with Active Surfaces within the an EU-funded project.
- In Chapter 4 we discuss a grasp acquisition strategy and present an improved version of the previous gripper prototype.
- In Chapter 5 a novel gripper with Sensitive Active Surfaces is introduced and used in an applicative case
- Chapter 6 finally concludes this dissertation and summarizes the major contributions and directions of future research based on the presented work.

1.2 Contributions

The major contribution of this thesis can be summarized as follows:

- Development of the Velvet Fingers a novel under-actuated gripper with Active Surfaces for medium size objects. The gripper has been designed from the theoretical concepts, to the employment in an applicative scenario
- A control scheme of the Active Surfaces of the Velvet Fingers for active in-hand manipulation and variable friction emulation
- In collaboration with AASS Research Center, of the University of Örebro (Sweden) a grasp execution routine using the Active Surfaces of the Velvet Fingers to achieve a stable power grasp in cluttered environment.
- A re-design of the Velvet Fingers to facilitate more robust grasp acquisition and for integration and tests on a robotic platform for

automatically unloading shipment containers packed with heterogeneous loose goods.

- Development of the Velvet-II, a gripper with Sensitive Active Surfaces for small size objects.
- A control scheme of the Sensitive Active Surfaces for in-hand manipulation, friction coefficient emulation and contact point location
- In collaboration with AASS Research Center, of the University of Örebro (Sweden), a robotic mobile platform for autonomous picking and palletizing has been developed

1.3 Publications

- Tincani, V., Catalano, M. G., Farnioli, E., Garabini, M., Grioli, G., Fantoni, G., & Bicchi, A. (2012, October). Velvet fingers: A dexterous gripper with active surfaces. In Intelligent robots and systems (IROS), 2012 IEEE/RSJ International conference on (pp. 1257-1263). IEEE.
- Tincani, V., Grioli, G., Catalano, M. G., Garabini, M., Grechi, S., Fantoni, G., & Bicchi, A. (2013, May). Implementation and control of the velvet fingers: a dexterous gripper with active surfaces. In Robotics and Automation (ICRA), 2013 IEEE International Conference on (pp. 2744-2750). IEEE.
- Tincani, V., Grioli, G., Catalano, M. G., Bonilla, M., Garabini, M., Fantoni, G., & Bicchi, A. (2013, November). Controlling the active surfaces of the Velvet Fingers: Sticky to slippy fingers. In Intelligent Robots and Systems (IROS), 2013 IEEE/RSJ International Conference on (pp. 5494-5499). IEEE.

- Krug, R., Stoyanov, T., Bonilla, M., Tincani, V., Vaskevicius, N., Fantoni, G., Birk, A., Lilienthal, A. J., & Bicchi, A. (2014, May). Velvet fingers: Grasp planning and execution for an underactuated gripper with active surfaces. In Robotics and Automation (ICRA), 2014 IEEE International Conference on (pp. 3669-3675). IEEE.

- Krug, R., Stoyanov, T., Bonilla, M., Tincani, V., Vaskevicius, N., Fantoni, G., Birk, A., Lilienthal, A. J., & Bicchi, A. (2014). Improving grasp robustness via in-hand manipulation with active surfaces. In IEEE International Conference on Robotics and Automation-Workshop on Autonomous Grasping and Manipulation: An Open Challenge.

- Vaskevicius, N., Mueller, C., Bonilla, M., Tincani, V., Stoyanov, T., Fantoni, G., Pathak, K., Lilienthal, A. J., Bicchi, A., & Birk, A. (2014, August). Object recognition and localization for robust grasping with a dexterous gripper in the context of container unloading. In Automation Science and Engineering (CASE), 2014 IEEE International Conference on (pp. 1270-1277). IEEE.

- Tincani, V., Catalano, M. G., Grioli, G., Bonilla, M., Garabini, M., Farnioli, E., Fantoni, G., & Bicchi, A. "Design, Implementation and Control of the Velvet Fingers Dexterous Gripper" International Journal of Robotics Research (IJRR), 2015, under review.

- Krug, R., Stoyanov, T., Tincani, V., Andreasson, H., Mosberger, R., Fantoni, G.,Bicchi, A., & Lilienthal, A. J. On Using Optimization-based Control instead of Path-Planning for Robot Grasp Motion Generation.

- Krug, R., Stoyanov, T., Tincani, V., Andreasson, H., Mosberger, R., Fantoni, G.,Bicchi, A., & Lilienthal, A. J. The Autonomous

Picking & Palletizing (APPLE) Robot: A Research Platform for Intralogistics Applications. IEEE/RSJ International conference on (IROS),2015, under review.

- Tincani, V., Catalano, M., Grioli, G., Stoyanov, T., Krug, R., Lilienthal, A., Fantoni, G.,Bicchi, A. Sensitive Active Surfaces on the Velvet II Dexterous Gripper.

Chapter 2

Background

2.1 The grasping process

Over the years, engineers have proposed many different devices with the purpose of grasping and manipulating objects. Such devices are collectively identified by the term end effectors (EEs). A wide overview of the most employed EEs can be found in [7].

The grasping principle on which a gripper relies, can be defined as " the physical principle which causes the force effect necessary to get and maintain the part in a relative position with respect to the gripping device" [8]. EE grasping principles are extremely various; there are mechanical, electrostatic, suction, magnetic, adhesive, Bernoulli EEs, just to mention a few. Fig.2.1 shows a survey of the gripping principles adopted to grasp parts ([9]).

At reducing of the scale, the number of gripping principles employable increases, since other kinds of interaction between the gripper and the micro-parts, which are usually negligible at macro domain, arise. Surface forces, which are generally not significant at macro scale, acquire a

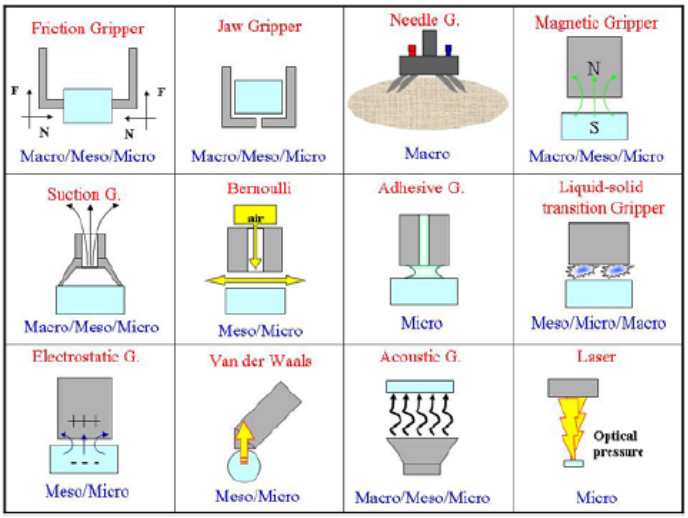

Figure 2.1: Grasp principles

remarkable or even predominant role with respect to body forces at meso and micro scale. Aside from the grasping principle the purpose of a gripper is to generate a force on a target object so as to firmly attach it to the gripping device, keeping hold in spite of all possible disturbances (external forces, slippages, vibrations, etc.), generally with the aim afterwards at changing the pose of the grasped part respect to a fixed frame of reference. In general (with some exceptions) the grasping process can be described as follows:

- **Approaching**: the gripper is positioned nearby the object.
- **Contact**: the gripper touches the object.
- **Force enhancement**: the gripper starts exerting the force on the object.
- **Securing**: the grasping force continues to increase until every de-

grees of freedom of the object is removed.

- **Moving**: the object changes its position respect to a fixed frame. Most of the time the gripper is moved by the robot with the object securely attached, sometimes the gripper itself handles the object.

- **Releasing**: the grasping force decreases until the object and the gripper are separated. At the macro-scale, usually gravity releases the object. Conversely at micro-domain some releasing strategies are often necessary since surface forces might overcome gravity.

At macro scale, two clearly distinct camps of grippers can be identified: simple industrial grippers and robotic hands, which are described in the next Sections.

2.2 Industrial grippers

Industrial grippers usually have only a few (generally one or two) degrees of freedom (DoFs) and show a reduced complexity in terms of hardware components, a simple structure and a basic sensing system. The main task of these simple grippers is to ensure a robust grasp, i.e., to securely attach the objects to the manipulator, keeping hold in spite of all possible disturbances (external forces, slippages, vibrations, etc.). This reduction in complexity simplifies movement planning, actuation and control at the cost of low flexibility and high specialization for limited task types. Devices belonging to the first class generally find applications in industrial environments where cost-effectiveness, speed and reliability are at a premium. In the following a short description of the most common types of gripper utilized in industry, classified on the grasping principles they rely on, is provided.

Suction grippers

Suction grippers can be divided in two classes: active vacuum suckers and passive suction cups. The former operates on the vacuum technique usually generated by vacuum pumps or Venturi vacuum suction generators. Deformable suction cups, made in elastomeric material, are hermetically pushed against the surface of the object to be grasped. Subsequently a low pressure is produced inside the suction heads resulting in a prehension force F given by:

$$F = (\sigma_0 - \sigma_u)A \tag{2.1}$$

where:

σ_0 is the atmospheric pressure $[bar]$

σ_u is the applied vacuum pressure $[bar]$ within the sealed suction volume

A is the total area between all suction cups of the gripper and the object $[m^2]$

For common applications the applied vacuum σ_u ranges from 10% to 60%.

In passive suction caps the vacuum is produced by pressing a disk sucker which has a relatively soft rim against the surface of the object. The releasing of the object is usually enabled through a mechanism which connects the low pressure region inside the cups with the atmosphere. Since vacuum grippers require a hermetic contact between the suction cups and the object, they are restricted to airtight materials. However, providing continuous suction power they can also retain slightly porous and permeable materials. A vacuum gripper for parcel handling is depicted in Fig.2.2.

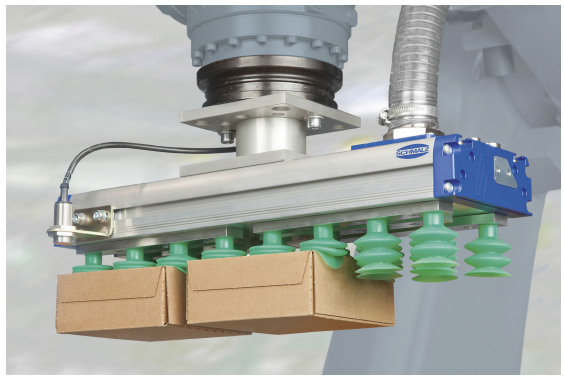

Figure 2.2: Handling of two parcels executed with a vacuum gripper

Magnetoadhesive grippers

Magnetoadhesion may be implemented in passive or active forms. Magnetic grippers, makes use of (passive) permanent magnets to attract magnetically susceptible objects. These grippers incorporate a switch mechanism for the purposes of magnetic flux diversion as depicted in Fig.2.3. In Fig.2.3 a) the flux is forced to pass through the surface of the object generating an attraction force F. In Fig.2.3 b) the magnet is turned of 90° resulting in a magnetic flux which does not pass through the object; in this fashion the object can be easily released.

Electromagnetic grippers relies on a magnetic field electrically generated as shown in Fig.2.4. A current I, either direct or alternating, runs through one or more coils wound on a core of high magnetic permeability generating an attractive force F which can be expressed as:

$$F = \frac{\mu_0 \mu_r N^2 I^2 l}{2p} \tag{2.2}$$

where:

μ_0 is the permeability of free space $[4\pi 10^{-7} H/m]$

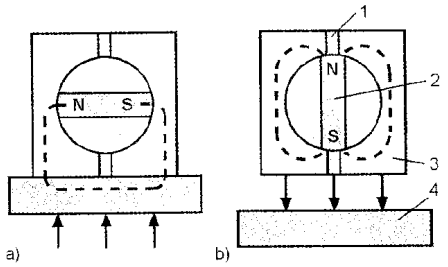

Figure 2.3: Mechanical control of the magnetic flow implemented in magnetic grippers. 1) non-magnetic material, 2) permanent magnet 3) ferromagnetic housing, 4) object

μ_r is the relative permeability of the core

N is the number of the coil windings

I is the intensity of the current $[A]$

l is the length of the conductor $[m]$

p is the magnetic path length $[m]$

Magnetoadhesive grippers (Fig.2.5) are widely used with ferrous materials, thanks to their simple and compact construction (with no moving parts in case of electromagnetic grippers). Permanent magnet or electromagnetic grippers using direct current may induce some residual magnetization in the object after release. This effect can be hindered by using alternating current in electromagnetic grippers.

Electroadhesive grippers

Electroadhesive grippers use an electrostatic field to generate an attractive force on the surface of the target object. The simplest implementation of an electroadhesive prehension for electrical conductive objects is

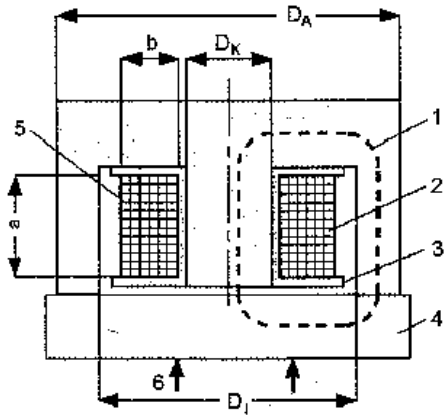

Figure 2.4: Electromagnetic gripper working principle. 1) magnetic flux path, 2) 5) coils, 3) coil former 4) object, 6) prehension force

(a) (b)

Figure 2.5: a) Magnetic gripper. b) Ferromagnetic sheet handled by magnetic grippers.

depicted in Fig.2.6 with the associated electric circuit. The object is electrically connected to one side of the supply through the gripper central electrode and forms the plate of a capacitor subjected to an attractive force F given by:

$$F = \frac{\epsilon_0 \epsilon_r V^2 A}{2d^2} \tag{2.3}$$

where:

ϵ_0 is the permittivity of free space $[8.85410^{-12} C^2/(Nm^2)]$

ϵ_r is the relative permittivity of the dielectric

A is the interface between the gripper and the object $[m^2]$

V is the applied potential $[Volts]$

d is the dielectric thickness $[m]$.

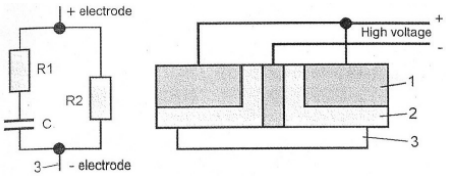

Figure 2.6: Scheme of an electroadhesive gripper with the associate electric circuit. 1) electrodes, 2) dielectric, 3) electrically conductive object

Electrostatic grippers are widely used to clamp and transport silicon wafers and photovoltaic cells efficiently ([10]), since, unlikely vacuum cups, they can work in vacuum environment, as required in chip manufacturing, and can hold also partially machined wafers which contain holes.

Cryogenic grippers

In cryogenic grippers, small droplets of water suspended between the surfaces of the gripping head and the object are frozen by an application of a small quantity of liquid carbon dioxide or nitrogen. The ice which is formed works as an temporary adhesive layer. The releasing of the object

is enabled by heating the gripping surface which causes the melting of the ice. Some cryogenic grippers for micro-components utilize Peltier modules as a heating and cooling system simply switching the polarity of the cells. Fig.2.7 a) shows the grasping and handling of a textile which is another application field of cryogenic grippers ([11]).

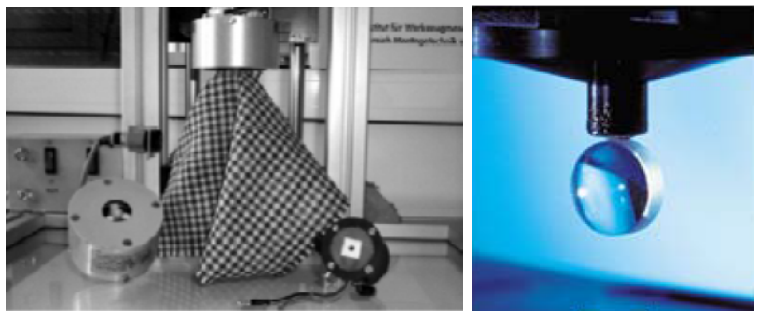

(a) (b)

Figure 2.7: a) Grasping and handling of a textile with a cryogenic gripper. b) a cryogenic gripper for small parts which utilizes Peltier cells as a heating and cooling system

Intrusive grippers

The term "intrusive" is used to refer to those gripping methods which penetrate a material surface to some given depth. The action of ingression, carried out by means of pins or needles, applies to a single surface and allows to hold the object without the need to maintain an applied force. Intrusive techniques are used almost exclusively with soft materials. A typical application field is the textile industry where intrusive grippers are utilized for the acquisition of the single uppermost panel from a stack of the same.

Usually the intrusive mechanism consists of needles mounted on a rigid

platform with a DoF to enable the intrusion and the releasing. Typical intrusive grippers employ between 10 and 40 fine polished needles with diameter from 0.5mm to 2mm and oriented in different directions. The capability to remove one single layer at time requires a fine and adjustable stroke of the needles. Fig.2.8 shows two instances of needle gripper and an applicative case.

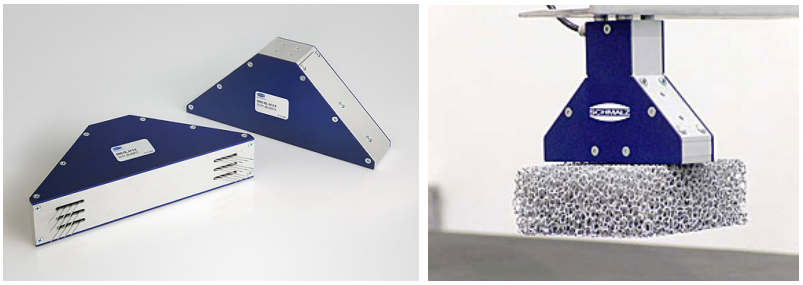

(a) (b)

Figure 2.8: Needle grippers

The Needle Roller (Fig.2.9) is a gripping system for unloading coffee sacks out of shipping containers. It falls in the class of intrusive grippers since the method employed a roller with needles to drag coffee sacks on a conveying system located behind the gripper. The roller with radial needles is longitudinally attached to the front of a movable conveyor. A curved metal sheet partially covers the needles while a series of slots allows the needles to extend out of the panel. When the gripper is pushed against the lateral surface of the uppermost coffee sack, the needles penetrate the jute and carry the sack on the conveyor.

Mechanical grippers

The object retention force of the mechanical grippers is based on the physical effect of classical mechanics. Two or more jaws are pressed against

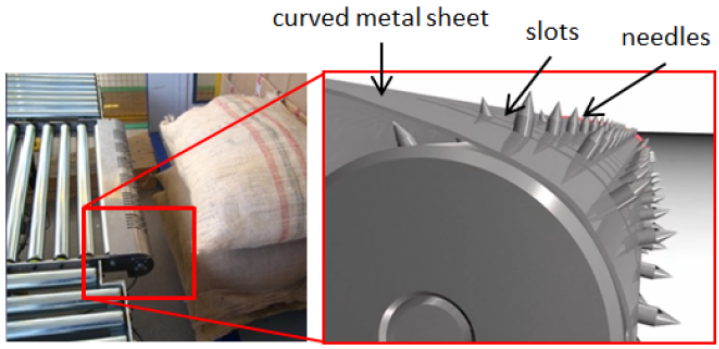

Figure 2.9: The frontal side of the Needle Roller gripper and a detailed view.

the surface of the object. Once grasped, any movement of the object is hindered by the jaws of the gripper and the friction forces. Mechanical grippers are the most frequently used gripping devices thanks to their versatility, robustness, reliability and cost. There exist a large variety of mechanical grippers which differ for the drive system, for the number and trajectory of jaws for the kinematics and many other aspects. Fig.2.10 depicts four different industrial mechanical grippers.

Contact-less grippers

The most frequently used contact-less devices is the Bernoulli gripper. It operates on the Bernoulli principle whereby air flow over the surface of an object generates a low pressure region between the gripper and the objects which results in a lift. The object is therefore lifted in the immediate vicinity of the gripper without contact. The gripper is widely employed in the electronic industry to handle silicon wafer, which demands a breakage-free handling method since they are very thin and brittle and thus prone to fracture. Bernoulli grippers are also employed to handle light and deformable objects like pliable textile, packaging film, and also slices of fruit and vegetables thanks to their simplicity and high operating speed.

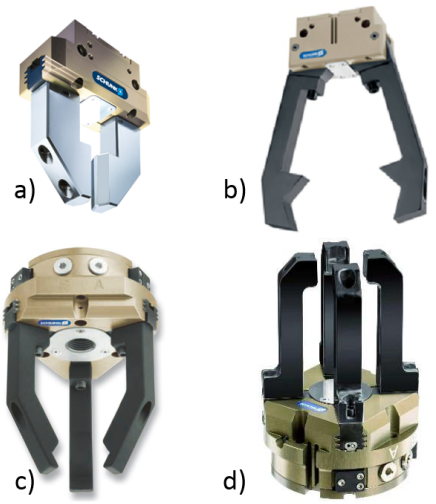

Figure 2.10: Some instances of mechanical industrial gripping devices.

Fig.2.11 shows an example of Bernoulli gripper for wafers and for sliced food [12].

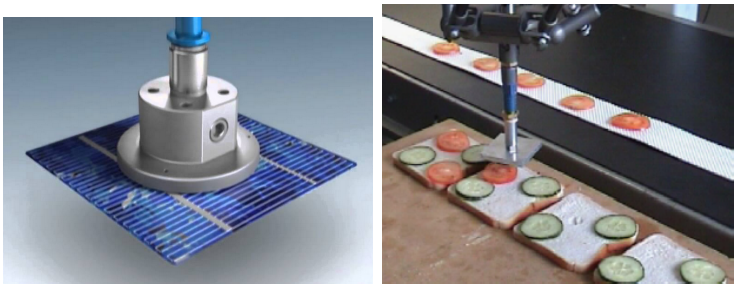

(a) (b)

Figure 2.11: Bernoulli gripper for silicon wafer and photovoltaic cells a) and for sliced of fruit and vegetables b)

Other contact-less gripper less known are the ultrasonic based gripper [13] which generate pressure waves able to lift up parts and laser grippers

[14] which produce a pressure able to trap and move micro-parts in a liquid medium.

2.3 Robotic hands

Opposed to industrial grippers, complex hands incorporate many DoFs into multi-fingered hand designs with the aim of imitating some of the human hand characteristics. The complexity of such devices is very high which entails sophisticated control systems, but the resulting performances are impressive. Several four- and five-fingered hands are able to fulfill not only grasping tasks, using the palm and the fingers to achieve enveloping grasps, but also manipulative grasps contacting the objects with their fingertips and performing in-hand manipulation tasks.

Some hands for tele-manipulation are human-like (even though there exist many examples of not at all anthropomorphic hands like the grippers of the Da Vinci Robot for laparoscopic operations [15], the end effectors on the arms of explosive ordnance disposal robots [16], robots for underwater application [17], and many others). A good match between the master human hand and the slave robotic hand makes it easier for the operator to translate his natural manipulation capabilities into commands for the remote system. Particularly representative of this type of artificial hands is the Robonaut 2 Hand [18]. The Robonaut [19] is a the tele-operated humanoid robot for space applications conceived with the aim at replacing astronauts in tasks where humans might be in danger. It is of human size, has a three Degrees of Freedom (DOF) articulated waist, two 7-DOF arms and two human-like hands giving it an impressive work space for interacting with the environment. A pan/tilt head with multiple stereo camera systems provides data for both tele-operators and computer vision systems.

It can work in the same corridors as the crew, use a significant subset

of the Extra-Vehicular Activity (EVA) tool set, and is designed to safely work alongside a human crew. Additionally, Robonaut can serve as a minuteman, providing mission controllers with a highly dexterous device for dealing with an EVA emergency in far less time than the several hours it takes to prepare an astronaut for a space walk. Its two 5-fingered hands, with four fingers and one thumb and a total of 20 DoFs, allow manipulation of a wide range of tools and to mimic and to have similar dexterity of the human hand. The Robonaut 2 Hand, depicted in Fig.2.12 a) is an improvement of the first version in terms of dexterity, overall joint travel, wire reduction and durability. The hand has 12 DoFs which are driven by 16 actuators by means of tendons. The drivers and avionics are packaged inside the forearm, with two further motors for the 2 Dofs of the wrist. The hand is endowed with three types of sensor; hall-effect sensors which monitor the angular position of each independent joint, six Dofs force torque sensors on each phalanx and tendon tension sensors. Fig. 2.12 b) shows that the hand is able to perform the 90% of Cutkosky's grasp taxonomy [20], which is a good benchmark for evaluating dexterity.

Another example of a complex anthropomorphic hand is the Shadow Hand [21]. The hand, shown in Fig.2.13 is an advanced humanoid robot hand system with 24 DoFs which mimics the kinematics and dexterity of the human hand. The thumb is fully actuated, while the other fingers have three actuated joints each, since the distal and middle joints are coupled. The little finger is moreover endowed with an additional actuated DoF in the palm to perform pinch grasps with the thumb. Finally the wrist comprises of two DoFs. The total 20 actuators, packed into the hand base, are pneumatically or electrically activated. The hand has been designed to provide comparable force output and movement precision to the human hand. It is used for research in grasping, manipulation, neural control, brain computer interface, industrial quality control, and

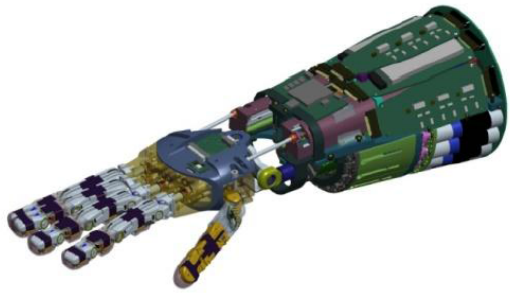

(a)

(b)

Figure 2.12: The Robonaut 2 Hand. In a) depicted is the hand and the forearm with motors and avionics embedded. b) shows that the hand is able to perform 15 of the 16 grasps of Cutkosky's grasp taxonomy.

hazardous material handling. Five pressure sensors embedded in the fingertips enable tactile sensing.

Figure 2.13: The Shadow Hand: all actuation and sensing is built into the hand and the forearm

2.4 Medium complexity gripping devices

The main reason for the big differences between simple grippers and robotic hands lies in the very different context in which they operate. The first category operates usually in structured environments (typical for factories): well-defined workpieces, often fed in well-defined poses, with high throughput requirements. Opposed to this, the ultimate goal of robotic hands is to function in unstructured environments, with different kinds of objects, executing complex tasks and tolerating many potentially unexpected situations.

In between these two classes lies a whole gray scale where tradeoff among flexibility, efficiency, reliability, robustness, cost and many other aspects are active. The design of devices belonging to the middle area

generally obey to the engineering principle of "minimalism": choose the least complex solution that will do the job. For sake of clarity, it is helpful to pinpoint also the definition of the term "flexibility". In this thesis, flexibility is the aptitude of a device to be responsive to variations of the objects (in shape, dimension, roughness, weight etc.) with respect to the ones a device is designed for, while still being able to achieve a stable grasp.. Flexibility and dexterity enhancement from one side and complexity reduction and reliability from the other side makes the middle gray scale to be populated by numerous devices whose position between simple grippers and robotic hands is usually function of the complexity of the tasks they are designed to carry out.

Ulrich in [22], perceived the need of medium-complexity end effectors which combine the ease of control of simple grippers with the flexibility of complex hands. In his work he describes a concept of a middle complexity gripper for grasping and assembly tasks that, afterwards evolved into the Barret Hand [6], a very successful commercial product depicted in Fig.2.14. The Barret Hand consolidates many specialized gripper tools into a single versatile and dexterous gripping device avoiding the need for changing end-effectors on a task-to-task basis. Also Mason in [23] addressed the issue of the tradeoff between simplicity and "generality" in a robot hand, where the term "generality" means "that the hand should address a broad range of tasks and task environments".

The under-actuation concept, authoritatively described in [24], pursues the intent of the hardware and control complexity reduction, since it does not involve an active coordination of all joints, while keeping an intrinsic adaptability to the shape of the grasped object. One of the most representative under-actuated robotic hands which addresses the simplification goal is the Pisa/IIT SoftHand [25]. It has an antropomorphic design with 19 DoFs arranged in four fingers with four DoFs each

Figure 2.14: The Barret Hand dexterous gripper

and an opposable three DoFs thumb. The hand is equipped with only one motor which pulls a tendon routed through all joints using passive anti-derailment pulleys, as in a differential mechanism. The hand offers, simplicity of control and good shape-adaptive capability. Moreover the rolling contact articulations and elastic ligaments in polyurethane rubber increase the resilience of the hand against external forces, overexertion and collisions with the surroundings, resulting in an extremely robust gripping device.

The under-actuation idea has involved also the side of the grippers. Under-actuated grippers combine the flexibility and adaptability to the shape of the object, characteristic of complex hands, with the low number of actuators and the simplicity of traditional industrial grippers. Perhaps two of the first instances of passively adaptive grippers are the Soft Gripper, introduced by Hirose and Umetani [26] (depicted in Fig2.17 a)) and the Shape gripper (Fig.2.17 b)), both based on the idea of a differential transmission carried out through tendons and pulleys to distribute motion of a prime mover to many DOFs [27].

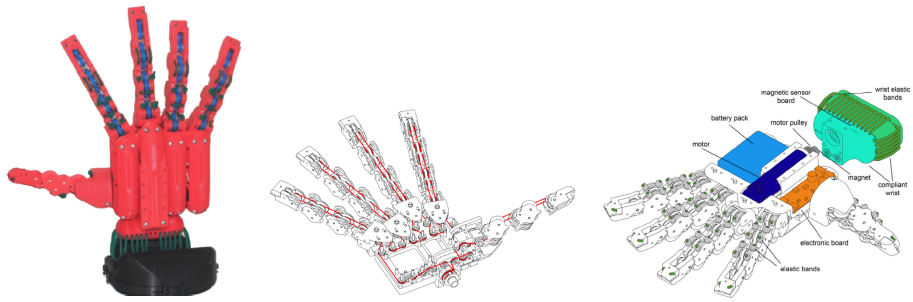

(a) (b) (c)

Figure 2.15: A picture of the Pisa/IIT SoftHand a). b) Partially exploded line sketch of the hand where the red line represents the tendon which distributes the motion to all joints. c) Main components of the hand, joints and wrist architecture.

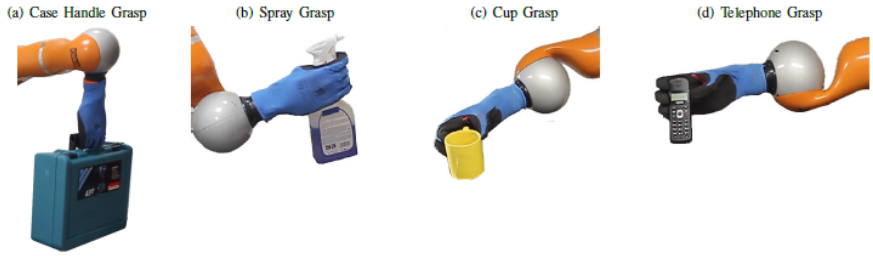

Figure 2.16: Grasps of household objects executed with the Pisa/IIT SoftHand

A more recent example of under-actuated gripper is the Velo 2G Gripper [28]. The " Velo Gripper ", shown in Fig.2.18 during grasping of many different objects, is an under-actuated gripper with parallel closure. This is an economic grasping device, versatile, able to grasp and to adapt to a wide range of objects.

The gripper consists of two fingers with the same size and shape which are symmetrically arranged with respect to the middle plane of the palm and actuated by only one driver contained in the wrist. Each finger

(a) (b)

Figure 2.17: The Soft Gripper a) and the Shape Gripper b) of Hirose and Umetani.

Figure 2.18: Grasps executed with the Velo 2G Gripper. Note that some grasps result in a non-symmetrical configuration of the phalanges.

is composed of two phalanges forming a RR serial manipulator. The motion of the fingers is driven by means of tendons; each finger has three, as depicted in Fig.2.19 a) and b). The red wire actuates the closure, the blue one ensures a passive opening by means of a return spring in the palm and the green tendon constrains a parallel motion of the distal phalanges during opening and closing with no object between the fingers. Furthermore a spring at the first joint facilities the passive opening. The aforementioned elements are illustrated in Fig.2.19.

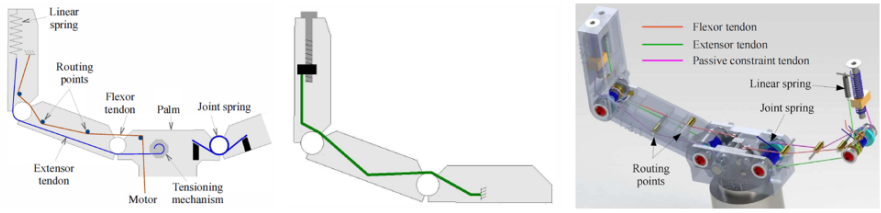

Figure 2.19: On the left the tendon for the closure in red and the passive elements for opening in blue. In the picture in the middle depicted is the constrain wire which ensures a parallel movement of the distal links. On the right a CAD model of the gripper.

The kinematics of the gripper ensures a parallel movement of the distal phalanges during the free closing or when external wrenches are applied only on them. When the proximal phalanges are blocked by an object and the actuator continues to be powered, the distal phalanges turn around the second joint resulting in an enveloping grasp. Moreover the fingers can assume a non-symmetrical configuration adapting to the shape of the objects as can be seen in some pictures in Fig.2.18. These features render the Velo gripper a reliable and adaptable gripping device [29].

Another well known gripper which belongs to the medium complexity region is the Robotiq 3-Finger Adaptive Robot Gripper [30]. It is a robotic peripheral designed for industrial applications. It has three independent articulated fingers with three rotary joints. Fig.2.20 a) shows a picture of the gripper. Referring to picture b) two fingers have an additional DoF which allows them to rotate, approaching or distancing their finger-tips.

The torque is applied at the first joint of the fingers (left picture of Fig.2.21 shows the kinematic design of a finger) and the proximal and medial phalanx rotate rigidly while the finger-pad of the distal phalanx

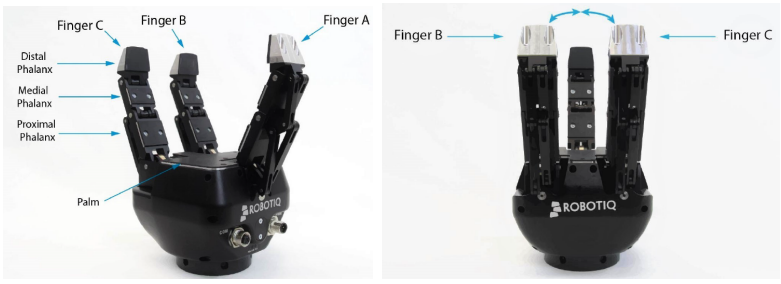

(a) (b)

Figure 2.20: a) The Robotiq 3-Finger Adaptive Robot Gripper. b) the additional DoF at the first joint of fingers B and C changes the operation mode of the gripper.

remains vertical. When the movement of the proximal phalanx is hindered by an object it stops and the other phalanges continue their movement around the second joint. When also the movement of the medial phalanx is hindered, the distal one turns around the third joint. Two types of grips occur when the EE closes on an object: fingertip grip or encompassing grip, depicted in the middle and right pictures of Fig.2.21 respectively. In fingertip grasp configuration the object is held only by the distal phalanges as in conventional industrial parallel grippers. In encompassing grip, the fingers embrace the object keeping it well attached to the palm in a firm power grasp.

The gripper can grasp the object with different modalities thanks to the additional DoFs of fingers B and C:

1. *basic mode*: the trajectories of the fingers are parallels. It is the most versatile operation mode and it is suitable for objects that have one dimension larger than the other two.

2. *wide mode*: fingers B and C are divergent. This configuration is optimal for gripping round or large objects.

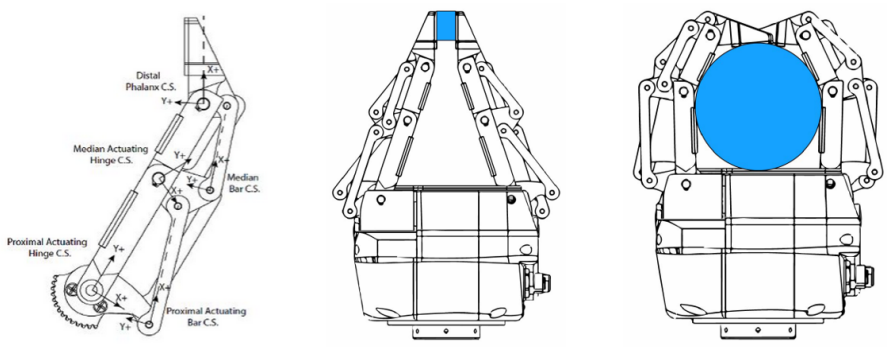

Figure 2.21: a) The design of a finger. b) Fingertip grasp of a small object which is held only by the distal phalanges of the gripper. c) Encompassing grasp of a ball in which the object is surrounded by the fingers.

3. *pinch mode*: fingertips B and C touch. It is used for small objects that have to be picked precisely. This operation mode can only grip objects between the distal phalanges of the fingers.

4. *scissor mode*: in this modality, finger A is not involved in the grasping process. The additional DoF at the base of finger B and C is utilized to approach their fingertips resulting in precise tip grasp for tiny objects.

Fig.2.22 illustrates the four operation modalities described above.

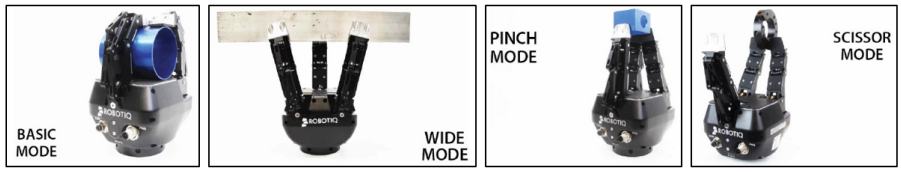

Figure 2.22: Operation mode of the Robotiq 3-Finger Adaptive Robot Gripper

Another interesting under-actuated grasping device is the SDM Hand depicted in Fig.2.23([31], [32]). It comprises four identical fingers each of

which belongs to a different parallel plane. Every finger has two phalanges with elastic joints in polyurethane and is driven by a pre-stretched, nylon-coated stainless steel cable anchored into the distal link, and running through low-friction nylon 11 tubing to the base. Fig.2.23 b) details a finger of the SDM Hand.

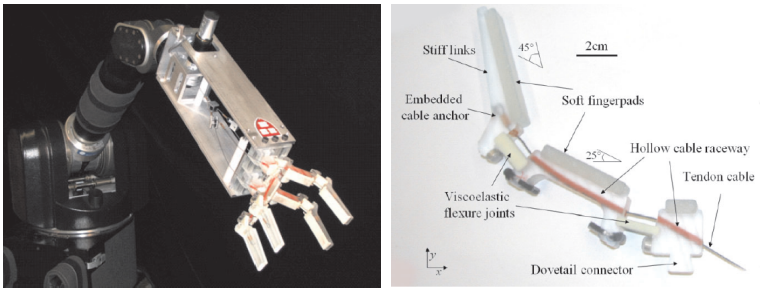

(a) (b)

Figure 2.23: a) The SDM Hand. b) Details of finger parts and its components.

A single actuator drives the four fingers (eight joints) of the hand. Fig.2.24 details the actuation scheme; the motion of the distal links can continue after contact on the coupled proximal links occurs, allowing the finger to passively adapt to the object shape. In addition, the pulley design in this scheme allows the remaining fingers to continue to enclose the object after the other fingers have been immobilized by contact, ensuring that an equal amount of tension is exerted on each tendon cable, regardless of finger position or contact state.

The differential mechanism among the fingers of the hand, which is the same concept employed in the Soft Gripper [26], allows to distribute motion to the fingers even if one or more of them is completely blocked. This constructive solution allows, for instance, to grab an object fixed at the environment, a vertical pipe for example, in presence of positioning error of the wrist of the robot, so that the axis of the pipe does not be-

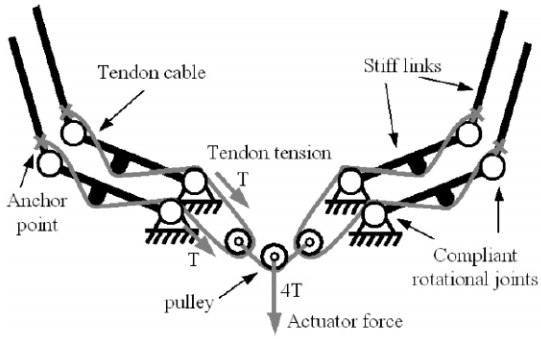

Figure 2.24: Schematic of the differential transmission of the gripper.

long to the middle plane of the hand. Even in this case when some fingers envelop the pipe and are completely immobilized, fingers still mobile can continue their closing trajectories resulting in an embracing grasp of the pipe out of the middle plane of the hand. On the other hand the above described transmission does not allow a fixed reference between the grasped object and the palm, as can be seen on the right column of Fig.2.25; even once grasped, the object maintains one DoF and its position with respect of the palm can change under external forces (gravity, accelerations of the manipulator etc.). Yet, the adaptability and the robustness of the gripper is very impressive. Moreover the overall cost, due to the simplicity of the constructive solution, is very contained. In [33] the design of an underactuated hand, based on the SDM Hand concept, which can be created through fast and commonly accessible rapid-prototyping techniques and simple, off-the-shelf components is proposed.

Finally, a simple gripper which stands out for its simplicity and extremely high adaptability is the Universal Gripper that makes use of a mass of granular material encased in an elastic membrane that passively adapts to the shape of the objects ([34], [35]). Making a positive or negative pressure inside the membrane, the gripper can quickly grip and

Figure 2.25: Grasps executed with the SDM Hand of a ball and a cube

release a wide range of objects. Fig.2.26 depicts the work principles of the gripper and two demonstrations.

The devices presented in this Section are highly effective in adapting to the shape of the object and they don't perform in-hand manipulation, since the achievement of particular postures of the grasped object is fully delegated to the robotic arm. In simple grippers, given their low number of DoFs, dexterity is often achieved by giving some DoFs to the surfaces directly in contact with the object. The following Section addresses this topic.

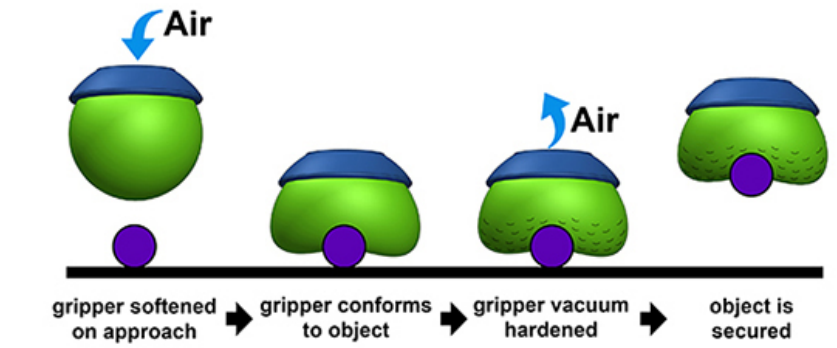

(a)

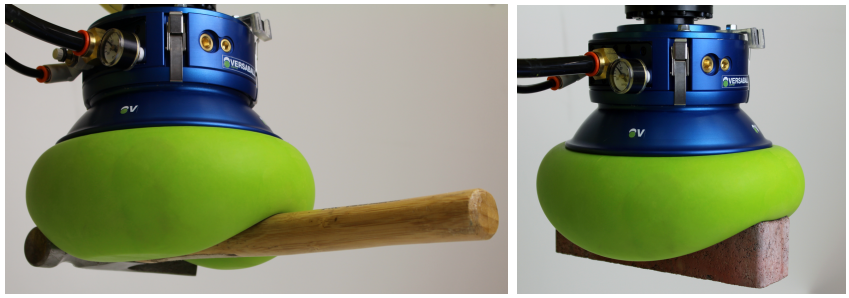

(b) (c)

Figure 2.26: a) Working principles of the Universal Gripper. Two grasps executed with the Universal Gripper b) and c).

2.5 Dexterous grippers

The "medium complexity end effector world" between simple grippers and complex hands is also populated by devices, named here "dexterous gripper". These are generally close to the first class, whose design has been conceived to introduce manipulative dexterity. We define as "dexterous grippers" the end effectors of medium complexity which are able to arbitrarily apply at least one degree of freedom to the object. After

being grasped, a workpiece must often be reoriented to a known orientation and position before further processing can take place. To accomplish this task, conventional grippers require to release and re-grasp the object during the course of their transfer from one work station to the next. This procedure is complicated and time-consuming, and it hampers the effective use of robots in many manufacturing processes. Often the final pose of the workpiece is not known a priori, but it depends on parameters which can change on the specific case; for instance in packaging processes, the final pose of a box in a stack depends on the arrangement of the already placed boxes. In this context a reprogrammable positioning of the workpiece by the gripper can be much more effective than a flexible feeding system.

Furthermore, in complex operations such as assembly of parts, fine motions of workpieces are often required for effective part assembly. These fine motions can be accomplished more precisely by the end effector alone without moving the robot arm. In this fashion, the robot arm provides the gross motion while the gripper provides the necessary fine motion.

Along these lines many attempts to confer dexterity to simple industrial grippers have been done. First studies on relocation of objects lying on flat surfaces are due to Mason [36] and Goldberg [37]. The Freddy II robot [38] is one of the first implementations of in-hand relocation by means of flat surfaces. The robot, conceived for assembling tasks, is a parallel-jaw gripper which lies in a vertical plane above a work table and it can rotate a grasped object around a horizontal axis.

The idea of introducing dexterity into a simple parallel gripper by means of sliding flat surfaces has been recently addressed by Tadakuma et al. in [39]. Fig.2.27 shows a parallel gripper with two additional Dofs for each finger-pads, implemented by omnidirectional driving gears utilized to translate the surfaces of the jaws in any direction in a plane,

performing in-hand manipulation. The grasped object can be translated in any direction in a plane parallel to the sliding surfaces and rotated along any axis belonging to the plane.

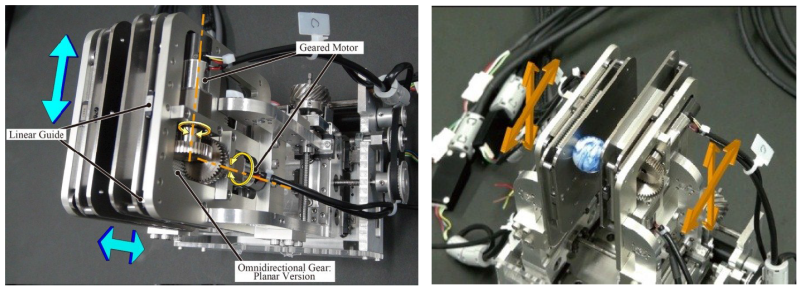

(a) (b)

Figure 2.27: Depicted is a parallel gripper with enhanced manipulability due to two DoFs implemented as sliding surfaces for each finger a). In-hand manipulation of a ball b).

An old end effector belonging to the category of dexterous grippers is the gripper of Datseris and Palm [40] [41]. They substituted sliding flat surfaces with conveyor belts. The gripper is a simple parallel planar gripper with two fingers which takes advantage of an actuated and orientable conveyor belt on the inner side of each jaw to translate and rotate the workpiece (Fig.2.28). With respect to the previous designs, this solution has the advantage that the sliding surfaces, being implemented by conveyor belts, have no end-stroke; in this fashion, for instance, an object can be indefinitely rotated.

A more recent dexterous end effector relying on the same principle of the Datseris and Palm gripper is the Roll-on Gripper [42]. It is a gripper for grasping, manipulation and handling of packed goods which finds application especially in packaging processes. The gripper is an hybrid between a forklift and a gripper, composed of two rigid wedge-shaped

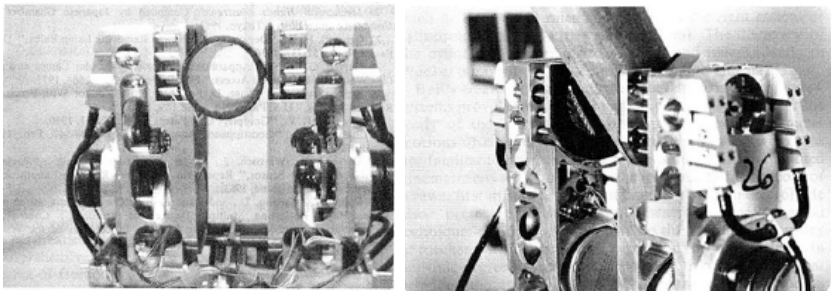

(a) (b)

Figure 2.28: Taking advantages of an actuated and orientable conveyor belt on the jaws a cylinder is in-hand manipulated.

forks with an actuated conveyor belt each. It is composed of a horizontal guide along which the two forks can translate (keeping a symmetrical arrangement) and also rotate of 90 around an axis perpendicular to the guide; this last ability allows to grasp boxes by acting on two opposite sides like a traditional parallel gripper. Fig.2.29 shows the DoFs of the gripper.

Figure 2.29: The Roll-on Gripper. The red arrows indicate the DoFs of the device.

Fig.2.30 b) depicts the working principle of the Roll-on Gripper to lift a parcel in a stack, where often the only free sides for grasp are the frontal and the upper side. From Fig.2.30 is clear that the piles of goods need to have another pile behind or a vertical panel, to compensate the horizontal push of the forks.

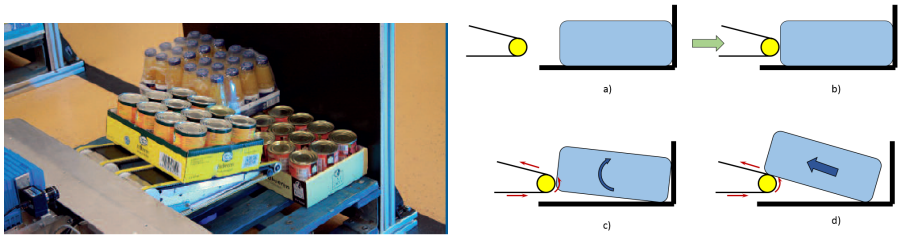

(a) (b)

Figure 2.30: The gripper is composed of two wedge-shaped forks with one actuated and independent belt each, which are pushed on the face side of a box (for this reason the boxes need to lie in front of a vertical panel). Then the belts are actuated and the boxes are first lifted from a border and then transported on the forks by means of the belts.

Once lifted on the forks, a parcel can be manipulated: it can be translated by moving the belts concordant or rotated around a vertical axis by actuating the belts in opposite directions, as shown in Fig.2.31. In this fashion, the gripper can release the parcel onto a target stack with the proper orientation which depends on the arrangements of the previously stacked goods.

A slightly more complex structure, patented by Robin Read [43] is the gripper depicted in Fig.2.32 which was developed as an end effector to be mounted on the arm of a wheelchair for disabled with the aim to support them in simple picking and manipulation tasks of household objects.

It is composed of two pairs of interlinked jaws lying in two parallel planes and mounted on a chassis. A single motor enables the closure of

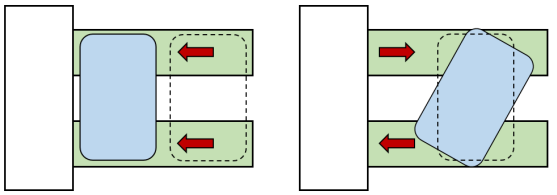

Figure 2.31: Translation and rotation of a parcel on the forks of the gripper by actuating the belts in the same or in opposite directions respectively

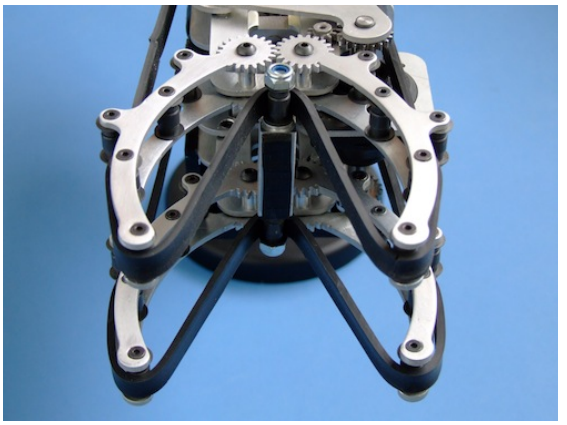

Figure 2.32: A picture of the Robin Read Gripper.

the links through a differential mechanism which allows to independently distribute the motion between the pairs of jaws. Two independent belts, maintained constantly in tension, run on the inner side of the links so that the belts form the jaws of the gripper resulting in a high adaptability to the shape of the object thanks to the deformability of the belts. Moreover the gripper can in-hand rotate a grasped object or, by counter-rotating the belts, it is able to unscrew the caps of bottles. An additional Dof of the belts allows to drag a grasped object towards the palm.

If so far the enhanced dexterity is conferred by sliding surfaces (in form of sliding flat planes or conveyor belts) there exist also some attempts

to pursue this purpose with rotating finger-pads or finger-tips. A first interesting instance, is provided by the DxGrip-II [44]. The gripper has two parallel jaws translating independently which carry two turning disks. Each jaw is driven by a DC motor (mounted within the gripper flange) through gears and a twin four-linkage mechanism, consisting of two four-bar linkages in quadrature. Each jaw has a rotating finger-pad covered by high friction material and actuated by miniature direct-drive brushless motors. Hence, the gripper has four motors in all: two for the motion of the jaws and two more for the rotation of the finger-pads. The hand has a 6-axes force/torque sensor on each finger-pad to elicit information on the location of the centroid of contact, the intensity and direction of contact force, the local torque, the risk of slippage, etc. Fig.2.33 illustrates the gripper and its main components.

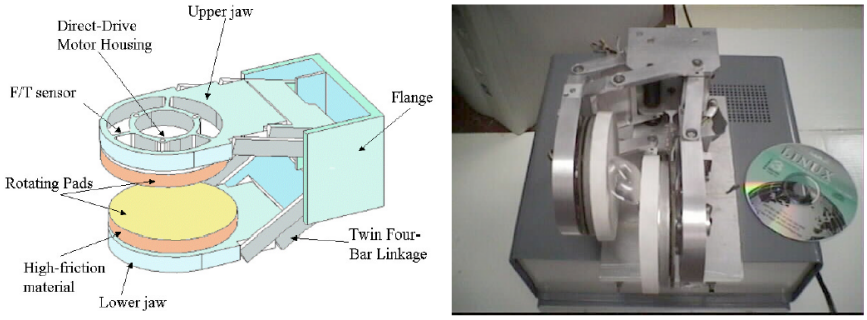

Figure 2.33: a) Main components of the DxGrip-II. b) A photograph of the gripper showing its sizes compared with a CD-ROM.

The gripper can be used as a dexterous manipulator, capable of translating and rolling an object between the fingers or even as a non-grasping manipulating device, by pressing the external surface of the finger-pads on flat parts to translate or rotate them (Fig.2.34).

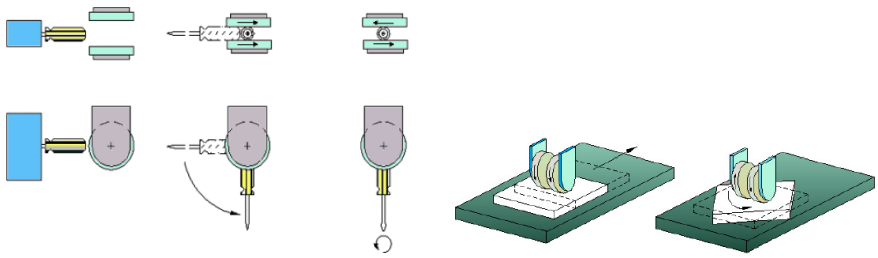

(a) (b)

Figure 2.34: Operation as a device for grasping and in-hand manipulation a) and as a nongrasping manipulation device b).

This end effector scenario, where tradeoff among complexity, flexibility, efficiency, reliability, robustness, cost and skills is active, is the context of this dissertation which can be regarded as an attempt to introduce enhanced capabilities into industrial grippers, maintaining low the general complexity.

Chapter 3

The Velvet Fingers dexterous gripper

The majority of the contents of this dissertation were carried out in the context of FP7 IP European Project RobLog that was aimed at autonomous unloading of shipping containers in a logistics scenario. The RobLog project was structured around two main technology demonstrators, situated in two different application scenarios in the domain of automated container unloading. This dichotomy in the project aimed at producing significant advances in both scientific and technological competences by focusing developments in two qualitatively different areas. The first application domain is directly motivated by a real industrial use-case: namely, unloading of containers packed with 70kg sacks of coffee. The solutions employed in this domain aim to produce a system which is close to an industrial prototype and to further develop competence in directly responding to a real-world industrial need. The second application is embedded in a scientifically more challenging domain: namely, unloading of containers packed with heterogeneous loose goods. In Fig.3.1

depicted are two instances of cluttered scenes in a mock-up of a shipping container (specifically built for the purpose of the project) populated by many different objects. The research carried out in this thesis falls into the context of the latter scenario of the RobLog project and is related to the development and control of the gripping device. The next Section is aimed to introduce the main basic specifications of the end effector we stick with throughout the next sections of this chapter and we kept in mind during the design of the gripper.

(a) (b)

Figure 3.1: Unloading process of heterogeneous goods was tested over many sample scenes, two instances of which are depicted here.

3.1 Theoretical concept

3.1.1 Conceptual design

In general, end effectors are designed on the base of the target objects and the characteristics of the environment in which they operate. The goods involved in the Roblog scientific scenario are 5-liters barrels (161x190mm), boxes (max dimensions 390x290x270mm), different types of bottles and also deformable and soft objects (e.g. a teddy bear or deformable sacks)

in cluttered arrangements. Since the target objects have different shapes, dimensions, and solidity (rigid or deformable) the basic idea is to ensure an embracing grasp with four contact areas for the cylindrical shapes and deformable goods and a grasp which involves the opposing surfaces of the parallelepiped goods such as boxes. Fig.3.2 shows a box and a cylinder grasped through two contact areas on opposing sides and four equidistant contact areas respectively and lifted with an acceleration a (on the left). On the right the free body equilibrium is depicted.

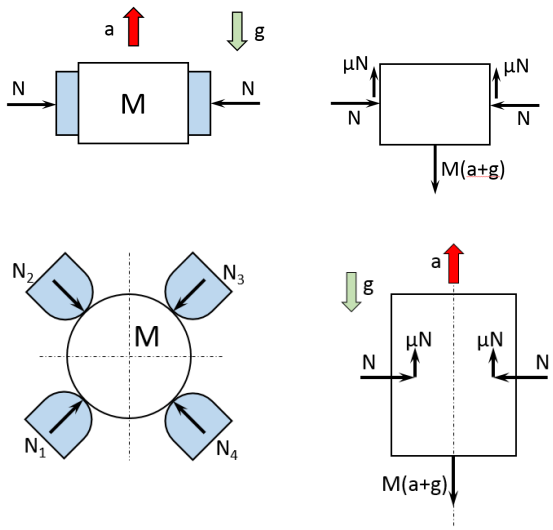

Figure 3.2: In the first row a box is grasped and lifted acting on opposing surfaces and, on the right, the free body equilibrium scheme is illustrated. In the row on the bottom depicted is a power grasp of a cylinder with four contact points. On the right the equilibrium scheme of the grasped cylinder during the lifting is depicted.

Once grasped, the object can be then lifted with an acceleration a which depends on the number of fingers of the gripping device n, on the static friction coefficient between the object and the fingers μ, on the normal force N_i for each contact point and on the mass of the object M,

according to the following equation:

$$a = \frac{\sum_{i=1}^{n} N_i \cdot \mu}{M} - g \tag{3.1}$$

In order to satisfy these grasping requirements we decided to endow the gripper with two fingers, each of which forms a planar rotary-rotary manipulator. In this fashion, all the links are involved in the enveloping grasp of cylindrical and deformable goods, while, for the grasping of boxes, the first links are involved to a lesser extent.

The design of a gripper is also affected by the environment in which it operates. As the containers in RobLog scenario can contain a lot of clutter and closely packed objects, is desirable to contact the goods in the easiest way, that means with a pose of the end effector which minimizes its bulky presence in the scene, and then to achieve the final firm grasping configuration after a grasp acquisition stage, where the object is in-hand manipulated. The possibilities to give in-hand manipulation capability to a simple mechanical gripper will be discussed over the next section. In addition, the operative environment affects another design choice. After the grasp execution, is desirable that the object remains firmly attached to the gripper and the joint configuration does not change under external forces like gravity or accelerations during the complex trajectories of the robot in the escape phase. The design implication of this requirement will be discussed in Sec.3.1.3.

3.1.2 Active Surfaces

Among the numerous possibilities to introduce in-hand manipulation capability, we opted to intervene on the interface between the finger and the object. A possible direction for further improvement of end-effector design for grasping and manipulation is the introduction of adhesive engineered surfaces at the finger-pads of a gripper. The potential for grippers

using extremely high adhesion is clearly very high, although it has been explored so far only to a limited extent, mostly in the micro/nano domain (see e.g. [45]). Bio-inspired designs, such as Cutkosky's Stickybot ([46], [47]), first produced a robot with the ability to climb on flat vertical surfaces, and later led to the development of the gecko-tape [48], an innovative product with many potential and practical applications in nano-technology, military, health care and sport sectors. However, in many applications where the end-effector is required to quickly grasp and release the object, and also performs at least some simple in-hand manipulation tasks, high adhesion surfaces may not be enough.

The ideal would be a surface with variable and controllable adhesion here named "*Active Surfaces*". An Active Surface is, therefore, a surface which can locally enables or disables its adhesion force. Among the many possibilities offered by Active Surfaces, here we will take into account:

- the ability to change friction
- the ability to tangentially push an object in contact with them.

Different means can be imagined to implement the described possibilities of Active Surfaces. In Fig.3.3 and Fig.3.4 a possible implementation is shown, which rely on synchronized control of multiple active adhesion micro-elements. In Fig.s 3.3(a), 3.3(b) and 3.3(c) progressive de-activation of the active adhesive elements is adopted to decrease the friction to the minimum level. In Fig3.4 traveling waves of adhesion, which exploit local dynamics on the wave fronts, are applied to obtain a net push on the object lying on the surface.

Another possible implementation of the effects of the active surfaces is described in Fig.3.5 and Fig.3.6. It is inspired by [49] and is based on actuation of a plane belt.

Given its simplicity, and given that variable and controllable adhesion surfaces are not yet available, the belt solution is adopted in this work,

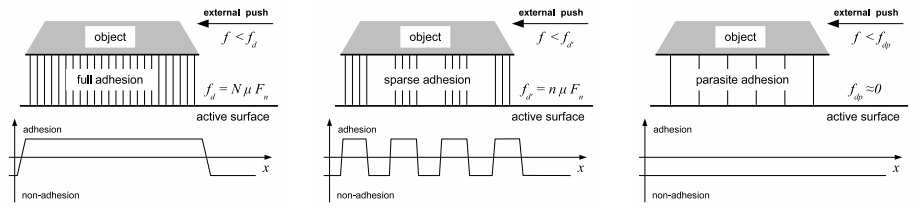

(a) (b) (c)

Figure 3.3: Friction modulation with the proposed active surface implementations: micro/nano adhesion elements. The three pictures show three different levels of friction from high (left), through medium (middle), to low (right). A high static friction force f_d can be achieved by activation of a large number N of adhesion elements. A medium level $f_{d'}$ of friction is obtained through selective activation of a smaller quantity n of adhesion elements. The minimum friction f_{dp} that can be obtained is determined by the parasite friction of the non-active adhesion elements.

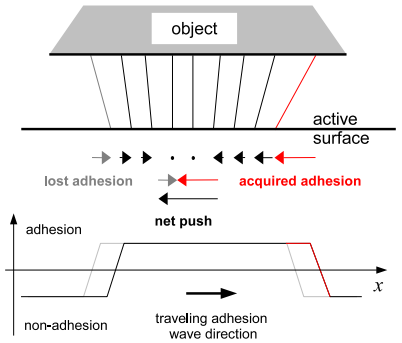

Figure 3.4: Tangential push of the proposed implementation of the active surfaces: coherent waves of adhesion elements.

nevertheless we believe that incoming developments in micro/nano scale adhesion control can, in the near future, tilt the scales of decision. The possibilities offered by the use of Active Surfaces at the finger-pads of a gripper can increase its dexterity and remarkably improve its in-hand

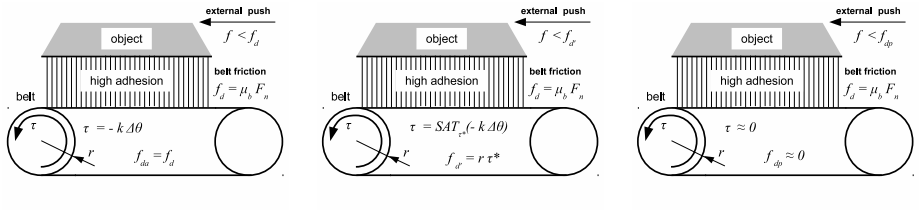

Figure 3.5: Friction modulation with the proposed active surface implementations: controlled conveyor belt. The three pictures show three different levels of friction from high (left), through medium (middle), to low (right). A high static friction force f_d can be achieved by a high gain k negative feedback control on the motor of the conveyor. A medium level $f_{d'}$ of friction is obtained by saturation of the conveyor motor torque to a value τ^* (operation $SAT_{\tau^*}(\cdot)$) related to the desired friction by the conveyor pulley radius r. The minimum friction f_{dp} that can be obtained by the residual torque due to the conveyor motor gear friction and non-perfectly canceled dynamics.

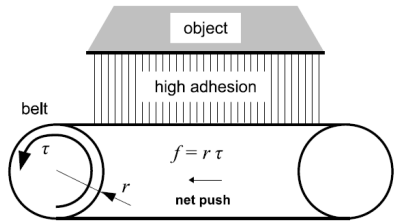

Figure 3.6: Tangential push of the proposed implementation of the active surfaces: belt activation.

manipulation capability as better explained below.

For instance, Fig.3.7 shows how controllable friction can be used to decide the evolution of a tip grasp configuration: keeping it stable with high friction (Fig.3.7(a), 3.7(b)), or letting the object slide toward a different grasp through controlled slipping (Fig.3.7(c) and 3.7(d)). Fig.3.8

shows another example of in-hand grasp reconfiguration where the combined use of Active Surfaces and external forces (in this example gravity) allows to go back from the grasp configuration of Fig.3.8(a) to the original configuration of Fig.3.8(c). Fig.3.9 shows an example of Active Surface operation during grasping: low friction allows the object translation from a configuration with two contact points to a configuration with four contact points.

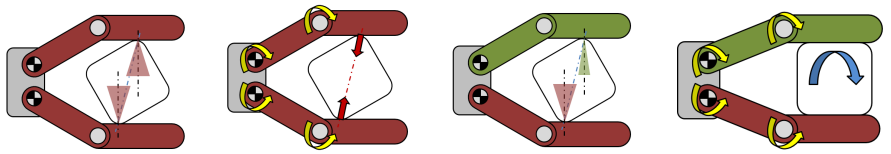

Figure 3.7: Advantages of friction modulation: sticky behavior (red fingers) for increased tip grasping stability (a-b) and slippy behavior (green fingers) for in-hand grasp reconfiguration (c-d).

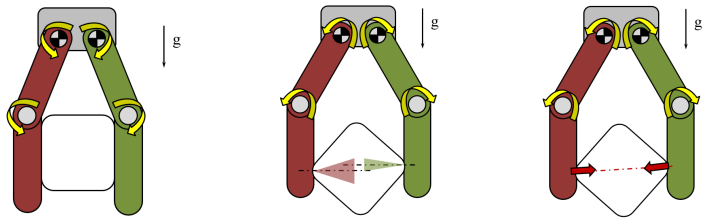

Figure 3.8: In-hand grasp reconfiguration with modulated friction and external forces (in this example gravity). Here, on the green finger-pads low friction is set while on the red finger-pads the friction is high

On the other hand, the possibility to tangentially push the object by means of the Active Surfaces allows other kinds of in-hand manipulations,

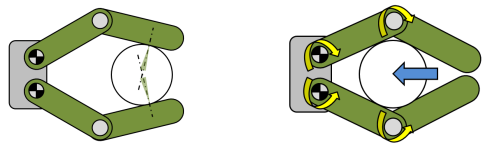

(a) (b)

Figure 3.9: Controlled slipping between Active Surfaces and grasped object for smooth tip-grasp to power-grasp transition.

as rotations and translations, as shown in Fig.3.10 and 3.11. In particular, Fig.3.10 shows as pushing on the object from the Active Surface, in same or opposite verses, it is possible to rotate (a,b,c,d), to translate (f,g), or to combine the two motions (e,h) on a grasped object. Fig. 3.11 shows a controlled inwards dragging of an object performed by the Active Surfaces of the fingers. The pinch-grasped object (a) is moved through a coordinate action of the Active Surfaces (b) and is pulled towards the frame of the gripper (c) till reaching a more robust power grasp (d).

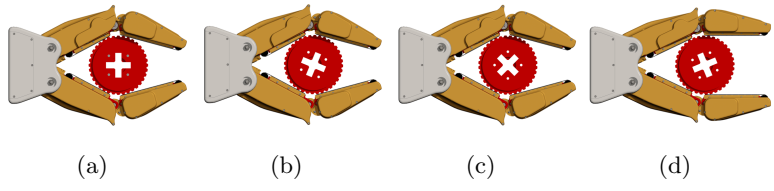

(a) (b) (c) (d)

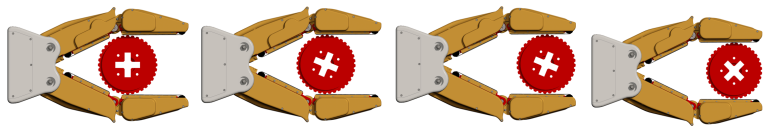

(e) (f) (g) (h)

Figure 3.10: Manipulation enhancement by using pushing Active Surfaces. Pictures show how the grasped object can be rotated (a, b, c, d), translated (f,g), or simultaneously rotated and translated (e,h), combining the two movements.

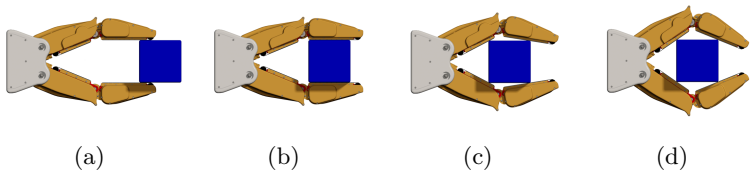

Figure 3.11: Controlled pulling in of an object using tangential pushes of the Active Surfaces. The grasped object is initially contacted in tip grasp (a), then it is moved (b-c) towards the fixed frame of the gripper until it achieves a stable power grasp (d).

3.1.3 Kinematic Design for Grasping Closure

As mentioned earlier, the potentials of the Active Surfaces at the finger-pads of a gripping device can be exploited to achieve a firm grasp starting from the most convenient pose and configuration of the gripper for an untidy environment, which is a tip grasp approach to minimize the bulky presence of the gripper in the scene. Fig.3.11 shows that a power grasp can be reached later through tangential pushes of the finger-pads.

As said before, the Active Surfaces are here implemented by controlled conveyor belts which require one additional motor for each surface with a consequent increase of the complexity, cost, weight, encumbrance and number of components. In order to keep low the total number of actuators, the proposed gripper relies on an under-actuated mechanism for the closure that offers an intrinsic adaptability to the objects.

For the use case of the gripper, two important aspects related to the kinematics have to be taken into consideration, which are necessary to prevent unexpected and uncontrollable collisions between the gripper (in the approach stage) or the gripper with the grasped object (after grasp execution in the escape stage) and other goods or obstacles:

- during the movement to the grasping pose the configuration of the links must be fixed with respect to the frame

- after grasping, during the escape stage, the grasped object must be fixed with respect to the frame

These requirements entail two specifications the under-actuation mechanism has to satisfy which are discussed below.

- During the free opening and closing each link has to stay in a predefined pose the one with respect to the others. The distal and the proximal links can be maintained in a predefined configuration with preloaded elastic elements between the links and an end-stroke at the joint as better explained in Sec.3.2.

- The transmission between the motor and the first joint of each finger is rigid, while the compliance is only at the level of the fingers, between the first and the second joint of the RR kinematic finger representation.

Fig.3.12(a) shows the configuration of the completely open and closed hand. The implemented transmission design ensures a V-shaped closure of the fingers, with both the distal joint variables equal to zero, if no contact interaction occurs. Conversely, if a contact force blocks the first link of a finger, its distal phalanx tends to rotate with respect to the proximal one, determining an enveloping grasp, as shown in Fig.3.12(b). This behavior is obtained with one motor controlling the closure movement of the two fingers, and transmitting its motion to the phalanges by a differential mechanism. With reference to Fig.3.13, the differential mechanism adopted for the under-actuation of the fingers, is described by the system

$$\begin{cases} s = r_1 q_1 + r_2 q_2 & \text{(right finger)} \\ s = r_1 q_3 + r_2 q_4 & \text{(left finger)}, \end{cases} \tag{3.2}$$

where r_1, r_2 are the radius pulleys on the proximal and the distal joints

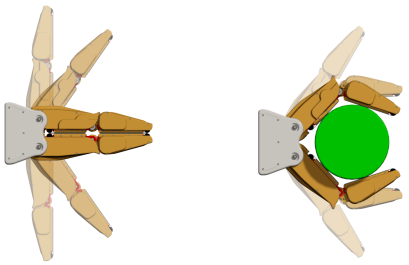

Figure 3.12: Free hand closure movement, panel (a), and constrained enveloping closure around a cylindrical object, panel (b).

respectively, and s is the displacement of the motor belt, winding on the motor pulley of radius r_1. For the sake of simplicity, referring to the right

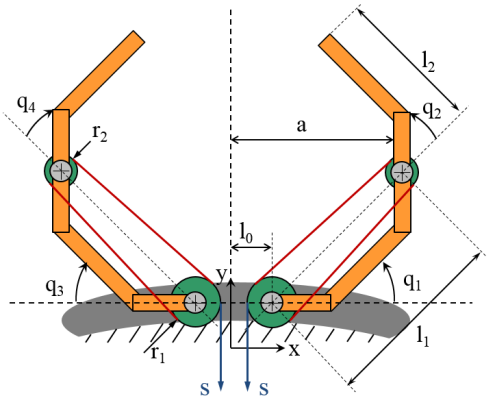

Figure 3.13: Reference frames, kinematic parameters and notation for the kinematic design and manipulability analysis of the proposed hand.

finger, the position of the finger-tip is described by

$$\begin{cases} x = l_0 + l_1 \cos(q_1) + l_2 \cos(q_1 + q_2) \\ y = l_1 \sin(q_1) + l_2 \sin(q_1 + q_2) \\ s = r_1 q_1 + r_2 q_2. \end{cases} \tag{3.3}$$

The length l_0 was chosen such that the gap between the fingers is about $1mm$ in a parallel configuration, in order to allow the gripper to pick up also very small objects, whereas the other parameters were chosen to grasp an object with the main dimension up to $200mm$. Lengths l_1 and l_2 were determined by consequence, following the general guidelines described in [24].

Particular attention was devoted to studying how the kinematic parameters can influence the closure of the hand. From the practical point of view, an interesting case appears to be the one in which the fingertips collide, because of the dimensions and position of the object to grasp. Although other possible critical grasp configurations are possible, an exhaustive analysis was not performed. Empirically, we have found that they occur rarely and are less practically relevant then the case considered. With reference to Fig. 3.14(d), when fingertips collide, keeping actuated the closure movement of the motor ($\delta s > 0$), two cases can happen:

- fingers tend to straighten ($\delta q_1 > 0$), keeping the grasp
- fingers tend to bend ($\delta q_1 < 0$), losing the grasp.

We can say that case (ii) is avoided if the *closure condition* $\delta q_1 / \delta s > 0$ holds for every q_1, q_2 belonging to the end effector workspace. By differ-

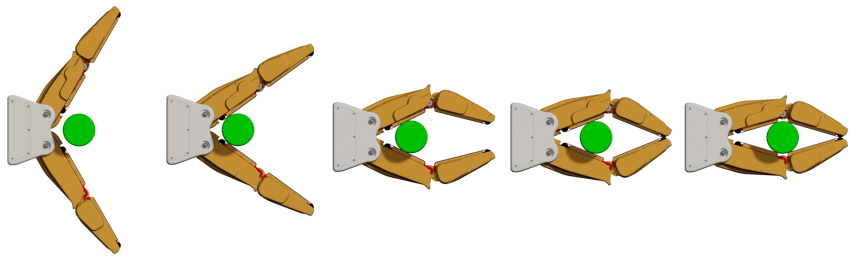

(a) (b) (c) (d) (e)

Figure 3.14: Hand closing with an object in it (sequence). When the hand starts closing, panel (a), the fingers keep moving straight until the first contact with the object occur, panel (b). At this point, the distal phalanges start bending faster than the proximal, panel (c), until the two fingertips touch each other, panel (d). Proper transmission design ensures that, despite the tips interference, the hand keeps squeezing the object, reaching a stable grasp.

entiating (3.3) we obtain

$$\begin{cases} \delta x = -l_1 \sin(q_1)\delta q_1 - l_2 \sin(q_1 + q_2)(\delta q_1 + \delta q_2) \\ \delta y = l_1 \cos(q_1)\delta q_1 + l_2 \cos(q_1 + q_2)(\delta q_1 + \delta q_2) \\ \delta s = r_1 \delta q_1 + r_2 \delta q_2. \end{cases} \tag{3.4}$$

Solving the third equation for δq_2, substituting it into the first, and imposing $\delta x = 0$ for symmetry conditions, we obtain

$$\delta q_1 = \frac{l_2 \sin(q_1 + q_2)/r_2}{l_2 \sin(q_1 + q_2)\left(\dfrac{r_1}{r_2} - 1\right) - l_1 \sin(q_1)} \delta s \,. \tag{3.5}$$

Since, from design constraints, $0 < q_1 + q_2 < \pi$ and $\sin(q_1 + q_2) > 0$, the closure condition is satisfied when

$$\frac{r_1}{r_2} > \frac{l_1 \sin(q_1)}{l_2 \sin(q_1 + q_2)} + 1 \,. \tag{3.6}$$

To evaluate the second member in (3.6) we introduce the object dimension a, cfr. Fig. 3.13, obtaining

$$c := \frac{l_1 \sin(q_1)}{l_2 \sin(q_1 + q_2)} = \sqrt{\frac{l_1^2 - (a - l_0)^2}{l_2^2 - a^2}} \approx \sqrt{\frac{l_1^2 - a^2}{l_2^2 - a^2}}, \tag{3.7}$$

where l_0 was neglected since in our design it is $l_0 \ll l_1$ and $l_0 \ll l_2$. From relation (3.7) it appears that it is desirable to have $l_2 \geq l_1$ because in this case $c \leq 1$, hence, by (3.6), with a ratio $r_1/r_2 > 2$ the closure condition is satisfied. The adopted design choices rise a question about the actual advantage, in terms of manipulative capabilities, of an under-actuated gripping system with active surfaces with respect to a more conventional fully actuated gripper. The next Section tries to tackle this issue.

3.1.4 Manipulability Analysis

To better assess the dexterity increment derived by the adoption of active surfaces, a rigorous manipulability analysis is required, to perform which, the two finger Active Surfaces can be approximated by prismatic joints. The reader can find more information about grasp analysis tools studying for under-actuated hands in [50], and about manipulability indices in [51] and in [52]. Despite the fact that analytical instruments for manipulability analysis give results referring to local properties around an equilibrium configuration, studying more cases helps to better understand the global behavior of the system.

It is possible to demonstrate that a minimum set of equations describing the displacement of the system about an equilibrium configuration can be written in the form $A\delta y = 0$, that is as a *linear* and *homogeneous* set

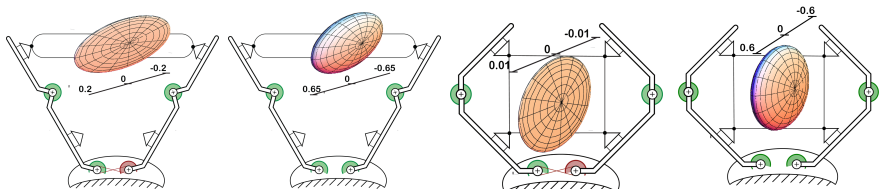

(a) $e_x = none$, $e_y = 0.03$, $e_z = 0.2$, $A = 0.188$

(b) $e_x = 0.001$, $e_y = 0.01$, $e_z = 0.65$, $V = 2.7(10)^{-5}$

(c) $e_x = none$, $e_y = 0.001$, $e_z = 0.01$, $A = 3.5(10)^{-5}$

(d) $e_x = 0.01$, $e_y = 0.1$, $e_z = 0.6$, $V = 0.0025$

(e) $e_x = none$, $e_y = 0.45$, $e_z = 10.7$, $A = 15.1$

(f) $e_x = 0.01$, $e_y = 0.5$, $e_z = 11.8$, $V = 0.24$

(g) $e_x = none$, $e_y = 0.25$, $e_z = 85$, $A = 66.7$

(h) $e_x = 0.1$, $e_y = 0.25$, $e_z = 85$, $V = 8.9$

Figure 3.15: Manipulability ellipsoids in different cases. Actuated joints are green, driven joints are red. Manipulation dexterity of four different hands with same structure and same number of DoA are compared. Manipulability ellipsoids (ellipsis) of hands with Active Surfaces (bottom row) are greatly increased with respect to hands where the same number of DoAs are used elsewhere in the joints (top row).

of equations[1]. The coefficient matrix $A \in \mathbb{R}^{r_a \times c_a}$, also called *Fundamental Grasp Matrix* [50], depends on the *Jacobian matrix*, the *grasp matrix* and the *synergy matrix*, describing the under-actuation of the system.

The vector $\delta y \in \mathbb{R}^{c_a}$ describes the variation of the *augmented configuration* and it composed by (i) the generalized system force variations, including the external wrench variation δw, the contact force variation

[1]For more details about the quasi-static grasp model equations and the manipulability analysis, the reader can refer to [53].

δf_c, the joint torque variation $\delta\tau$, the generalized actuation torque $\delta\eta$, and (ii) the generalized configuration variations, including the object displacement δu, the joint configuration variation δq, and of the actuation variable $\delta\sigma$.

Since A is fat and full row rank, we can introduce a matrix $\Gamma \in \mathbb{R}^{r_\gamma \times c_\gamma}$, with $r_\gamma = c_a$ and $c_\gamma = c_a - r_a$, as a basis for the solution space of A, thus such that $\mathcal{R}(\Gamma) = \mathcal{N}(A)$. Although the matrix Γ does not have a unique formulation, it can always be partitioned in two block columns, one relative to the *internal* perturbed configurations, when there is not any external wrench variation, and the other for the *external* perturbed configurations, when an external wrench variation occurs on the object, without any displacement at the actuation level.

In other words, we can say that all the configuration variations of the system can be written as

$$\begin{bmatrix} \delta w \\ \delta f_c \\ \delta\tau \\ \delta\eta \\ \delta u \\ \delta q \\ \delta\sigma \end{bmatrix} = \begin{bmatrix} 0 & \Gamma_{we} \\ \Gamma_{f_c i} & \Gamma_{f_c e} \\ \Gamma_{\tau i} & \Gamma_{\tau e} \\ \Gamma_{\eta i} & \Gamma_{\eta e} \\ \Gamma_{ui} & \Gamma_{ue} \\ \Gamma_{qi} & \Gamma_{qe} \\ \Gamma_{\sigma i} & 0 \end{bmatrix} \begin{bmatrix} x_i \\ x_e \end{bmatrix}, \tag{3.8}$$

where the left column, composed by matrices of the type $\Gamma_{\bullet i}$, is a basis for the *internal* solutions, and the right column, composed by matrices of the type Γ_{xe}, is a basis for the *external* solutions.

This formulation is very useful in order to study the dexterity of a hand. In fact, as explained in [52], the *internal kinematic manipulability* can be evaluated considering the ratio

$$R_{k_m i} = \frac{\delta u_i^{\mathrm{T}} W_u \delta u_i}{\delta \sigma_i^{\mathrm{T}} W_\sigma \delta \sigma_i}, \tag{3.9}$$

where the matrices W_u and W_σ are positive defined matrices able to accord physical dimension. In later numerical results, these were chosen as identity matrices. Considering (3.8), eq. (3.9) can be also written as

$$R_{k_m i} = \frac{x_i^{\mathrm{T}} \Gamma_{ui}^{\mathrm{T}} W_u \Gamma_{ui} x_i}{x_i^{\mathrm{T}} \Gamma_{\sigma i}^{\mathrm{T}} W_\sigma \Gamma_{\sigma i} x_i}. \tag{3.10}$$

The ratio in (3.10) has the form of a *Rayleigh quotient* which has a maximum corresponding to the maximum eigenvalue λ_{max} of the pencil $\Gamma_{ui}^{\mathrm{T}}\Gamma_{ui} - \lambda\Gamma_{\sigma i}^{\mathrm{T}}\Gamma_{\sigma i}$. The corresponding optimal direction in the object displacement space is given by $\delta u_{max} = \Gamma_{ui} x_{i,max}$. Similar considerations are possible for the others eigenvalues and the corresponding eigenvectors. It is possible to provide a geometrical interpretation of the results of the analysis. In fact, each eigenvector can be seen as the direction of an axis of the *manipulability ellipsoid*, which length is indicated by the corresponding eigenvalue. In the cases in which the number of the eigenvectors is less than three, the ellipsoid degenerates in an ellipse or in a line. In this interpretation, also the volume of the ellispoid, or the area of the ellipse, can be used as a global index of the manipulability capabilities.

The above instruments have been used to compare the effectiveness of the distribution of the degrees of actuation (DoAs) in the hand, in terms of manipulability.

Since in these cases the ellipsoid axis directions are very similar to the reference system ones (sketched in Fig. 3.13), we simply indicate with e_x the length of the ellipsoid axis along the x direction, and similarly for the others. The lengths e_x and e_y are a measure of the ability of the hand

to move the object in the x and y directions respectively, while e_z is a measure of the ability to rotate the object about z.

In our numerical tests, a tip grasp and a power grasp configuration were considered, both studied for the 3 DoAs and 4 DoAs cases. Despite the fact that the gripper has 3 DoAs, arranged as in Fig. 3.15(e) and 3.15(g), the effectiveness of the conveyor belts was evaluated also in the case of complete actuation of the proximal joints of the fingers (Fig.s 3.15(f) and 3.15(h)). For all cases, in Fig. 3.15 are represented the resulting ellipsoids (ellipsis), together with the characteristic lengths of the ellipsoid axes.

As expected, numerical results show how, in the cases of 3 DoAs, ellipsoids collapse into ellipsis. In all cases we can observe that, given the grasp configuration (power grasp or tip grasp) and the number of DoAs we always obtain an axial length increase, using the arrangement with the conveyor belts. The advantage of the solution with Active Surfaces is also highlighted by a two orders of magnitude growth of the ellipsoid volumes (or ellipses areas in the 3 DoA cases), implying a higher dexterity of the hand in manipulating the object.

3.2 Design of the Velvet Fingers

The proposed gripper is named Velvet Fingers. In the overall view of Fig. 3.16 three main mechanical subsystems can be discerned: a palm and, for each finger, one proximal and one distal phalanxes[2]. Each one of the two fingers can be seen as a planar RR manipulator. The hand is under-actuated; one motor actuates the opening and closing and other two motors actuate the Active Surfaces of each finger. The cut view of finger (1) shows the mechanical transmission for the hand closure,

[2]In this section the notation (*number*) refer to the identification number of components.

whereas within finger (2) the transmission system of the conveyor belt, which implements the Active Surface, is shown. The gripper closure is actuated by motor (4) that, by means of gears (6) and (7), transmits the motion to the two fingers. The movement of pulley (21), idlewith respect to proximal 1, is conferred by timing belt (B1). Motion from pulley (21) to pulley (32), fixed on the distal 1, is transmitted by timing belt (B3). The rotation of proximal 1 is transmitted by return springs (27) that link it to distal 1. The springs are preloaded to prevent the rotation of the distal phalanx under the gravity force and they allow a 90° rotation of angle q_2 without overcoming their maximum elongation. The actuator (4) is a $6\,W$ Maxon RE-MAX brushed DC motor with nominal torque $6.82\,mNm$ (peak torque $27.8\,mNm$) with a 316:1 gear-head able to exert a maximum continuous force of $12.6\,N$ on the tip of distal 1 (about $50\,N$ in peak torque condition). Hence the hand is able to grasp a mass of about $1\,kg$ and lift it with an acceleration of $1\,g$. Moreover, the palm is supplied with an additional housing for another motor to independently control the two fingers. In this configuration, gear (7) has to be flipped on shaft (8) not to engage with gear (6). An end-stroke between proximal 1 and distal 1 ensures a minimal value of q_2 equal to zero. On the other hand, if contact forces block the first link, the distal tends to rotate w.r.t. proximal leading to an enveloping grasp (see Fig. 3.12 (b)). Both Active Surfaces on the two links are $40\,mm$ wide conveyor belts actuated in the same verse by the same motor (38). The transmission to implement this is composed of timing belts (B4) and (B5) and pulleys (23), (44) and (45). The pretension of belts (B4) and (B5) is given by tightener (46) and the mobile support of motor (38) respectively.

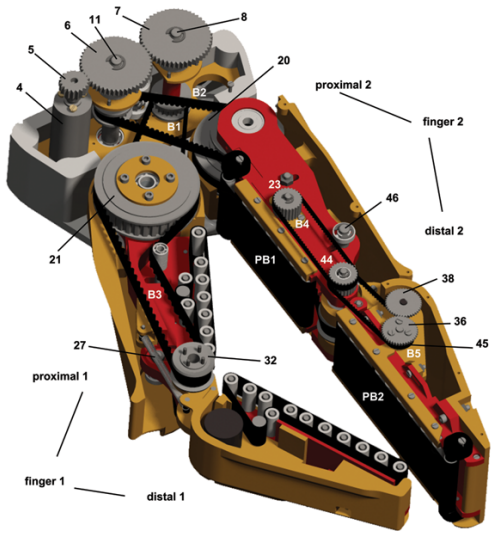

Figure 3.16: Cut view of the hand. Section of the palm shows the transmission between rotational joint actuation unit (11) and (8) and free pulleys (20) and (21) mounted on the proximal phalanges. The transmission is obtained by a combination of linear spur gears (5), (6), (7) and timing belts (B1 and B2). Section of finger 1 shows the transmission between free pulley (21) and pulley (32) fixed on the distal phalanx.

3.2.1 Palm

Fig. 3.17 shows a detailed 3D view of the palm. Pinion (5), actuated by motor (4), transmits the motion to spur gear (6) (transmission ratio -1:2.5), which engages also with gear (7) (transmission ratio -1:1). Gears (6) and (7) rotate, via shafts (11) and (8), timing pulleys (10) and (9) respectively. Each pulley, by means of timing belts (B2) and (B1) (tensioned by tighteners (12) and (13)), transmits the movement to a finger, realizing a 5:1 total transmission ratio between motor (4) and finger pulley (20). The angular position of shaft (11) is measured by a magnetic encoder composed of a magnet (14) and a sensor (15) fixed on the extremity of the shaft. Two electronic boards, fixed to the palm, drive the

motors and read the sensors.

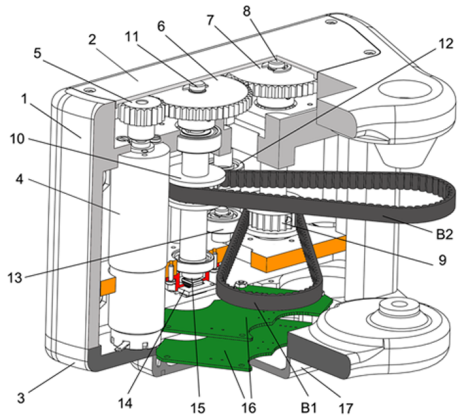

Figure 3.17: 3D section of the palm. Transmission belts (B1) and (B2), gears (5), (6), (7), sensors (14) and (15) and electronic boards (16) are highlighted. One DoA can be added to the hand, decoupling the two finger motions, by mounting one more motor inside the palm frame (1), symmetrically to motor (4). In this configuration gear (8) must be inverted, avoiding the engaging with gear (6).

3.2.2 Proximal Phalanx

Fig. 3.18 shows a 3D section of the proximal phalanx. Pulleys (20) and (21), fixed each other, are idle on axis (19) which is fixed on palm ((1) on Fig. 3.17). Pulley (20) receives motion from pulley (10) with transmission ratio 1:2, whereas pulley (21) transmits motion to the pulley fixed on the second link through belt (B3), tensioned by tightener (22). The distance between the joint axes is 128mm. At the bottom of the first link, plane belt (PB1) wraps around 8mm diameter rollers (25), mounted by ball bearings on steel pins. Pulley (23) moves the motor roller (24) that actuate the plain belt. A mobile roller (48) provides the right pretension to (PB1).

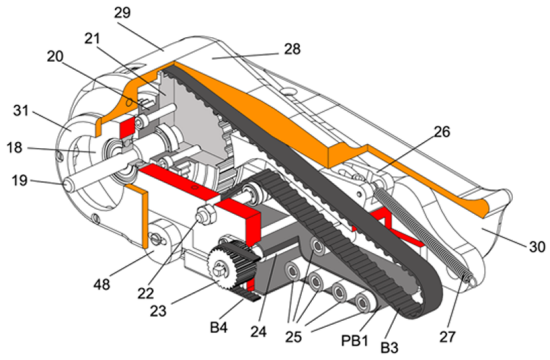

Figure 3.18: 3D section of the proximal phalanx. Belts (B3) and (B4) and the conveyor system are highlighted. Pulleys (21) and (20) are free to rotate around shaft (19), fixed on palm frame (1). The proximal phalanx is mounted on shaft (19) by two ball bearings.

3.2.3 Distal Phalanx

Frame (34) of the distal phalanx (about 132 mm long) in Fig. 3.19 is mounted through ball bearings on pin (49) (fixed on frame (18) of the proximal phalanx), and it is rigidly connected to pulley (32). Springs (27) are hooked on frame (34) by pin (33). Conveyor belt (PB2) wraps around rollers (39) and is put under tension by a mobile roller (similar to (48) in Fig. 3.18), on the tip of the phalanx. The movement of the plane belt is transmitted by motor (38) to motor shaft (35) through a transmission gear. At the end of shaft (35) magnetic encoder (40) is fixed for belt position sensing. Actuator (38) is the same of (4), with a 4.4:1 reduction, so it can exert a force on the belts of about 30N.

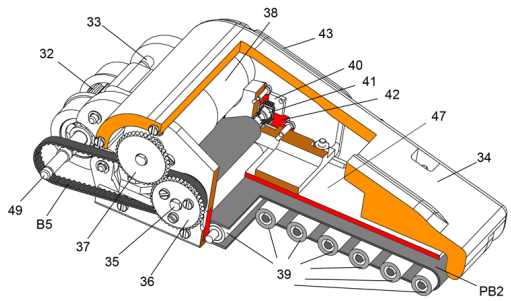

Figure 3.19: 3D section of the distal phalanx. Details about conveyor system and its actuation are shown. Belt (B5) transfers motion from the conveyor on the distal phalanx to the conveyor on the proximal phalanx. Motor (38) is mounted on a mobile frame that can be shifted, along some grooves on frame (47), to tighten plane belt (PB2).

3.3 Physical implementation of the Velvet Fingers

During the realization phase, some small refinements were introduced in the design of the gripper and highlighted in Fig.3.20 a) by red color.

The introduced refinement are described below:

- Two idle rollers were added at the fingertips. This refinement reduces the friction between the fingertip of a finger and the phalanges of the other when they get in contact, and the fingertips can easily slide on the phalanges.

- The belts used in the prototype are composed of a synthetic tissue fixed on a polyurethane layer, with a thickness of 0.8mm, featuring high tensile strength 30MPa and extensional stiffness, yet suitable to wind around 8mm diameter rollers. In order to increase the friction of the belts, they are coated with a Liquid masking film produced

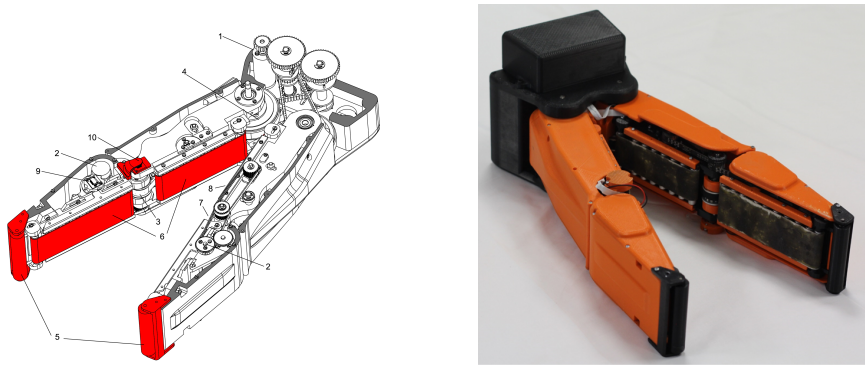

(a) (b)

Figure 3.20: (a) Section view of the Velvet Fingers smart gripper. Parts colored in red are the refinements introduced. (b) A picture of the prototype of the Velvet Fingers

by Talens. It is a liquefied mixture of natural rubber (latex) which, once dried, bonds on the belts. The final result is a high resistance and very flexible thin belt with high friction coefficient.

- an encoder on the second joint of each finger was added to completely reconstruct the gripper configuration and to discern a tip grasp, when the phalanges are aligned, from a power grasp.

The implemented prototype overall weight is 3.46Kg. When completely open the gripper width is 674mm (150mm when fully closed), and its length is 379.5mm, while the maximum gripper depth is 116mm. Fig.3.20 b) shows a picture of the Velvet Fingers.

3.3.1 Electronics

A general schematics of the power and control hardware of the Velvet Fingers hand is shown in Fig. 3.21. Five magnetic encoders AS5045 (Austriamicrosystem) read the rotation angles of the three motors which actuate

the gripper closure and the two Active Surfaces.

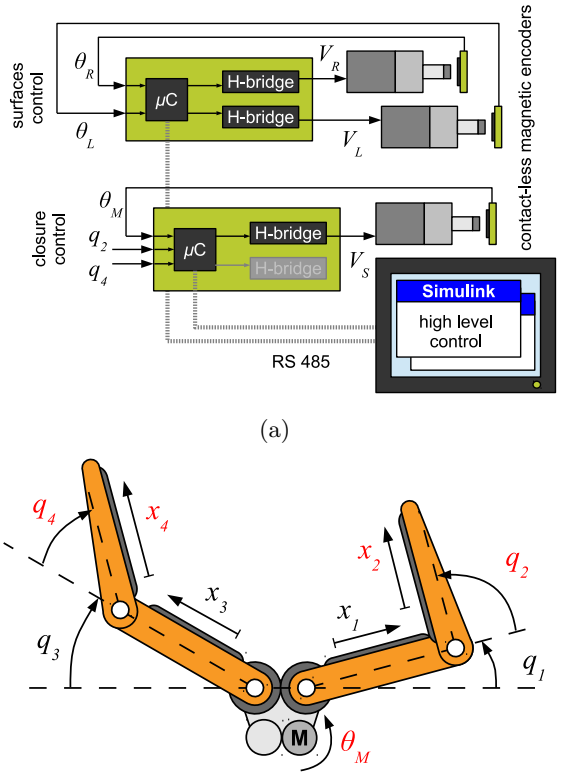

Figure 3.21: (a) Velvet Fingers general control architecture. Two custom boards, designed to drive two motors each, drive the system implementing sensor reading, lower-level loop closure and higher level communication. (b) Kinematic scheme of the Velvet Fingers hand. Variables highlighted in red are measured.

Two custom electronic boards implement motor power driving, encoder reading, low-level closed-loop control and communication with the higher level control. Each board core is a PSOC3 embedded microcontroller and can read up to four rotary magnetic encoders through

SPI bus interface. It communicates with the higher level control (a PC with Matlab/Simulink) through serial RS485 interface, implemented by a MAX1437 IC. Each board uses two ST L6206D H-bridge power drivers to command the voltage to the motors. The first board takes care to control the two Active Surfaces, reading two encoders mounted on the motor rolls of radius r which angular displacement θ_R and θ_L is related to the linear displacement of the conveyors x_i (refer to Fig. 3.21 b)) by

$$\begin{aligned} x_1 = x_2 = r\theta_R \\ x_3 = x_4 = r\theta_L \end{aligned}, \tag{3.11}$$

and driving the two DC motors with voltages V_R and V_L. The microcontroller implements the lower layers of the control loop, implementing the two Active Surface control modalities defined in the following. The second board takes care to control the motor closing the gripper. In doing so it reads the rotation angle of the motor and the two angles q_2 and q_4, thanks to which it is possible to reconstruct the overall kinematic configuration of the hand, through (3.2). The second board also presents a spare power channel to operate the hand in the case that a decoupled fingers assembly is implemented (the hand design accounts for such possibility as described in Sec.3.2.

3.3.2 Grasping experiments

Several experiments were conducted in order to demonstrate and validate the grasping capability of the system and its adaptability to the shapes of the objects.

All trials were performed in the following experimental setup: the gripper is placed horizontally and is fixed on a frame, while some objects are placed on a table lying under the gripper. The relative position between the plane of the gripper and the table is adjusted according to the object shape and the specific task.

All the experiments show preliminary results, carried out with a simplified version of the control. The driving motor for the opening and closing of the fingers is controlled with a PID, without resorting to any kind of impedance control.

Fig. 3.22 shows the closure of the gripper in absence of any kind of external forces; in this situation the fingers are straight and angles q_2 and q_4 are equal to zero.

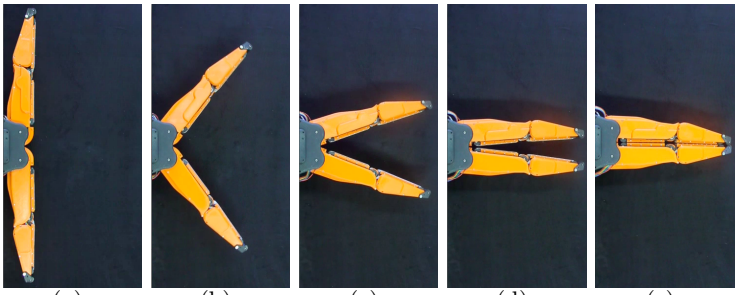

Figure 3.22: Free closure movement. When closing without external forces applied, the device moves in a V-shaped feature, both the second joint variables, q_2 and q_4, are equal to zero.

The gripper presents a very different behavior when external forces, due to contact, act on the first phalanges. Fig. 3.23 shows a sequence where the gripper performs a grasp on a sphere of about $150mm$ of diameter, guaranteeing a good winding on the shape of the object. In some grasps, as in Fig. 3.24, the small dimensions of the grasped objects, can cause fingertips to come into contact, (see frame (d)). Nevertheless (as shown in frames (e) and (f)) a proper closure is always guaranteed thanks to the design of the transmission ratios in the system (Eq.3.6).

Fig. 3.25 shows the grasping configuration of several different kinds of objects, demonstrating the effective adaptation capabilities of the designed under-actuated mechanism.

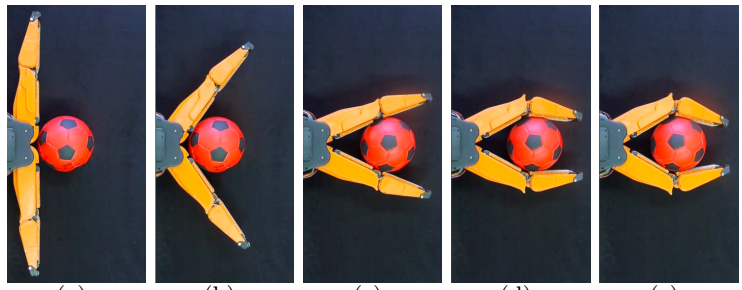

(a) (b) (c) (d) (e)

Figure 3.23: Enveloping closure around a spherical object. In presence of an object, reaction forces arise due to the contact, acting on first phalanges they modify the gripper closure which in turn shows its adaptation capabilities, thanks to which it is able to reach a power grasp.

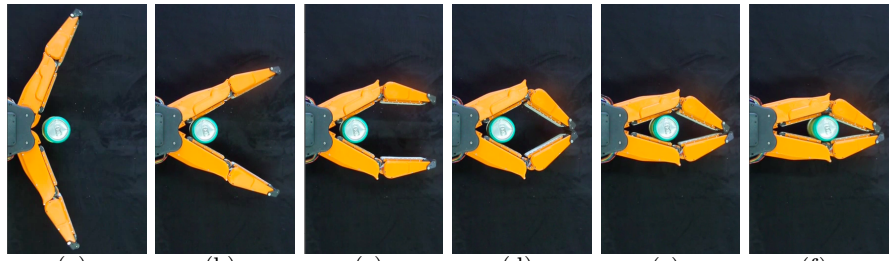

(a) (b) (c) (d) (e) (f)

Figure 3.24: Grasping with touching fingertips. This sequence shows the capability of the system to grasp an object also when fingertips come into contact. After the first contact with the object (b) the distal phalanges start bending faster than the proximal (c) until the two fingertips touch each other (d). Proper transmission design ensures that, despite the tips interference, the hand keeps squeezing the object, reaching a grasp closure.

3.4 Active Surface control

In first approximation the dynamic model of the conveyor belt system can be modeled as in Fig. 3.26, consisting in a three Degrees of Freedoms (DoFs) system, where a mass M (the gripper payload) is in perfect

adhesion with the belt which winds around a driver and a driven roller. The longitudinal elasticity of the belt can be modeled with three lumped linear springs, and finally each components is linked to a linear damper in order to account for energy losses.

The dynamic equations of the system follow:

$$\begin{cases} \ddot{\theta}_l = & \frac{1}{J_l}\Big(-\mu\dot{\theta}_l - kr\left(\theta_l r - x_M\right) - kr^2\left(\theta_l - \theta_c\right) + \\ & + \frac{k_\tau n_m}{R}\left(V - k_c n_m \dot{\theta}_l\right)\Big) \\ \ddot{\theta}_c = & -\frac{1}{J_c}\left(\mu\theta_l + kr\left(\theta_c r - x_M\right) + kr^2(\theta_c - \theta_l)\right) \\ \ddot{x}_M = & \frac{1}{M}\left(-F_{ext} - \mu_M \dot{x}_M - k\left(x_M - \theta_l r\right) - k\left(x_M - \theta_c r\right)\right) \end{cases} \tag{3.12}$$

where the new parameters introduced are the voltage applied to the motor V and its electrical resistance R the torque and speed constant k_τ and k_c, and the transmission ratio from the motor to the driver roller n_m respectively.

In order to fully empower an under-actuated gripper with the ben-

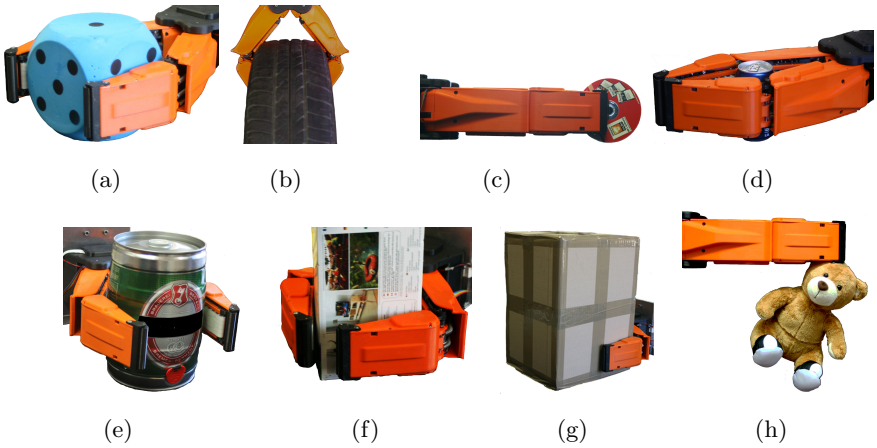

Figure 3.25: The objects grasped are: a cube with an edge of 200*mm (a), a tire (b), a CD-ROM (c), a can (d), a beer keg (e), a small box* 376*x*149*x*122*mm (f), a big box* 390*x*290*x*270*mm (g) and a Teddy Bear (h).*

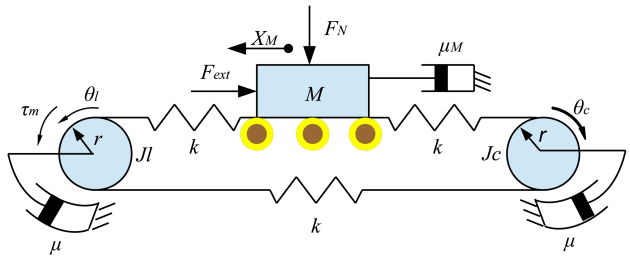

Figure 3.26: Dynamical model of the conveyor belts. It is a three DoFs system whose Lagrangian coordinates (θ_l, θ_c, x_m) are linked through springs with elasticity constant k. The mass M is subjected to normal (F_N) and tangential (F_{ext}) external forces. The driver roller (radius r and moment of inertia J_l with turning elements of the DC motor included) is actuated by motor torque τ_m. The driven roller has radius r and moment of inertia J_c. Damper elements are included to account of the energy dissipation.

efits offered by Active Surfaces, we propose the implementation of two fundamental functions:

- the *position mode control*, in which the conveyor belt moves the contact points with the object squeezed between the fingers.
- the *variable friction mode*, in which the apparent friction "felt" by the contacted object is set to a defined level.

This section analyzes and tests the two control techniques which allow the implementation of the two described fundamental functions.

3.4.1 Positioning control

The force equilibrium on the lumped mass considered on the belts yields that any torque generated by the conveyor motor is then transmitted to the contacted object. Thus, actuating the conveyor belt, when the object is grasped inside the fingers of the gripper, it is possible to perform tasks

of in hand manipulation. Given the slow dynamics of the manipulation, the electric dynamics of the motor current and the counter electro-motive force (CEMF) have been neglected. This simplification leads to a proportional relation between the voltage at the motor V and the tension in the belt F_t. Hence, tangential push control mode is obtained through direct control of the voltage V applied to the motor, accounting for proper transmission ratio. To apply a desired tangential force F_t on the contacted object, a voltage

$$V = F_t \frac{rR}{k_\tau n_m}, \tag{3.13}$$

must be provided to the motor. Fig. 3.27 shows that while controlling the Active Surfaces in order to push the object in the same direction, it is possible to obtain a translation of the grasped object inside the hand.

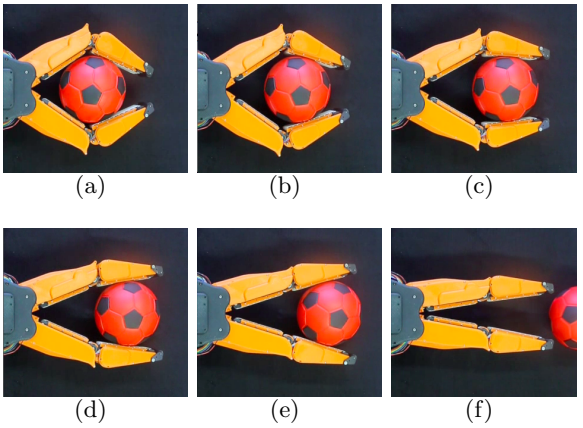

Figure 3.27: Object expulsion. A grasped object (a) is completely expelled out of the hand (f) by pushing it with the Active Surfaces. Adaptability of the under-actuated gripper guarantees grasp stability during the whole movement (b, c, d, e).

On the other hand, controlling the surfaces in order to push in opposite direction it is possible to confer a rotary motion to the object (Fig. 3.28). During the execution of these two kinds of task, the intrinsic adaptability

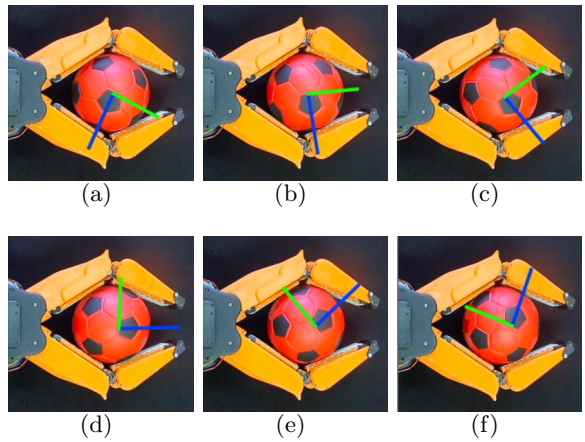

Figure 3.28: In-hand object rotation. Pushing the object in opposite directions causes a pure rotation of the grasped object.

of the under-actuated system guarantees an enveloping grasp throughout the movement.

A more complex control of the Active Surfaces can be adopted to realize more complex tasks, as shown in Fig. 3.29 and Fig. 3.30. In Fig. 3.29 a roto-translational movement is conferred to the grasped object. The sequence shows how the sphere, which is in the starting position (a), moves to a translated and rotated configuration (c) and, afterwards, returns back to the original configuration (f).
Fig. 3.30 shows a sequence where tangential pulling action of the Active Surfaces is used to grasp a cube, thanks also to the adaptivity of the under-actuated mechanism.

Finally, an interesting method of grasp that we want to show occurs through adjacent surfaces. This type of grasp allows for grasp of objects in cluttered environment where the gripper position is limited. The following experiment is explicative from this point of view. Grasping a box can be tricky if its lateral sides are occluded by other goods. Acting on the

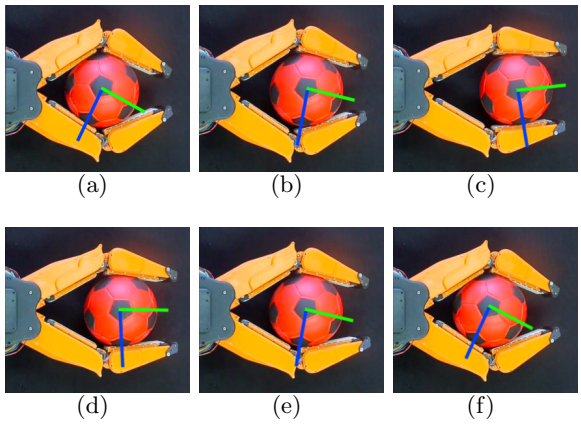

Figure 3.29: In-hand object roto-tranlsation. Suitable combination of tangential pushes by the Active Surfaces, confer the object a movement of roto-translation inside of the hand.

upper and the frontal side of the box and exploiting the tangential pulling actions of the conveyor belts, it can be "sucked" inward the gripper and lifted as shown in the sequence of Fig.3.31.

3.4.2 Variable friction control

Variable friction mode is obtained by applying the algorithm proposed in [54] which is built on the Dahal linear friction model. In emulating friction two important assumptions are made:

1. friction is simulated in terms of its total resulting action, and
2. kinetic friction is assumed equal to the maximum static friction.

While the first assumption is demanded by the physical implementation of the Active Surfaces, i.e. conveyors, the second assumption allows to simplify the control of both the conveyors and the manipulation, by allowing more stable and predictable controlled sliding.

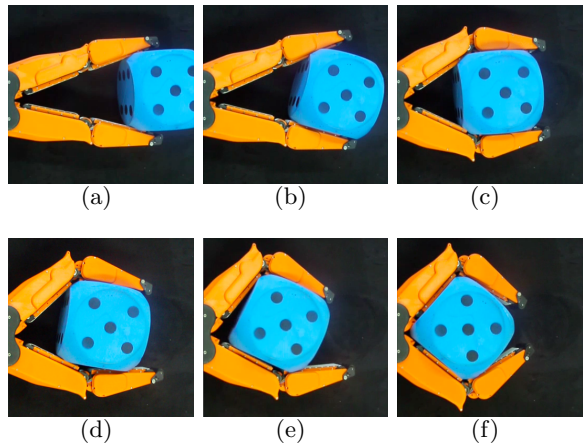

Figure 3.30: Adaptive Active Surface grasping of a cube. The sequence shows the possibilities offered by a combination of Active Surfaces and under-actuation, which give the system the capabilities to reach different configurations of grasp and extend its manipulation capabilities. Pictures (a) and (c) shown, respectively, a tip-grasp and a power-grasp configuration; in the frames from (c) up to (f) a short sequence where the object is put on rotation is shown.

Given a desired static friction coefficient f, it yields a desired maximum friction force $F_{fmax} = fF_N$ where F_N is the total normal force exerted on the contact. The algorithm proposed in [54] models the friction force as a virtual spring between the object and the plane, with stiffness K_s, length at rest null and maximum elongation z_{max}. One side of the spring is attached on the contacted object at point x, the other side is fixed to the surface at point w, its elongation is $z = w - x$ and the emulated friction force is given by $F_f = K_s(w - x)$ (Fig. 3.32(a)). As long as z is smaller than z_{max}, w is stuck on the surface, while, when z reaches the z_{max} value, the spring becomes rigid, no further elongation is permitted and w is dragged toward the (displaced) object.

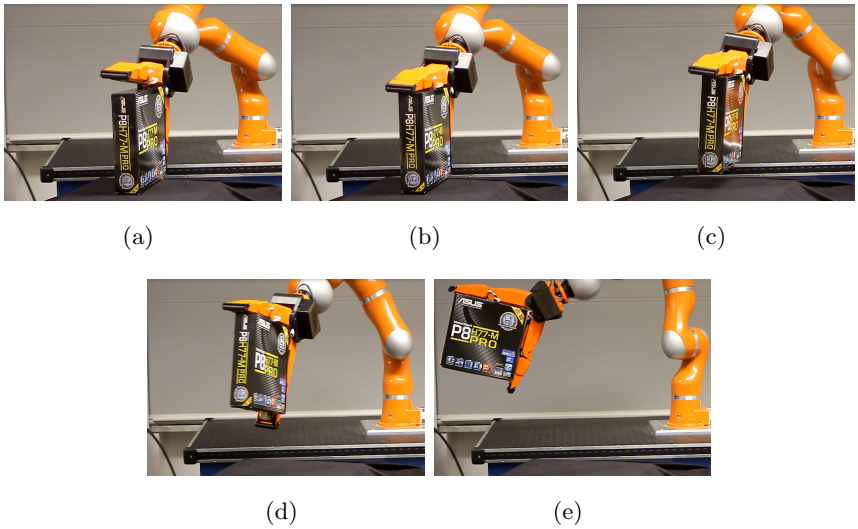

(a) (b) (c)

(d) (e)

Figure 3.31: Tangential thrusts of the conveyor belts used to lift a box in a cluttered environment acting only on its frontal and upper side.

The variable friction control is obtained through a force control where, for a given stiffness K_s the maximum emulated friction force F_{fmax} can be tuned by choosing the threshold $z_{max} = F_{fmax}/K_s$ as shown in Fig. 3.32(b). Since the prototype is not equipped with force sensors and therefore the normal force F_N on the belt is not available, the system can emulate only the tangential friction force, not the friction coefficient F_{fmax}/F_N.

This control is implemented by the following discrete-time system laws:

$$\begin{cases} w(i+1) = \begin{cases} x(i) - z_{max} & \text{if} \quad x(i) - w(i) > z_{max} \\ w(i) & \text{if} \quad |x(i) - w(i)| < z_{max} \\ x(i) + z_{max} & \text{if} \quad x(i) - w(i) < -z_{max} \end{cases} , \\ \\ F_f(i) = K_s SAT_{-z_{max}}^{z_{max}} (x(i) - w(i)) \end{cases} \tag{3.14}$$

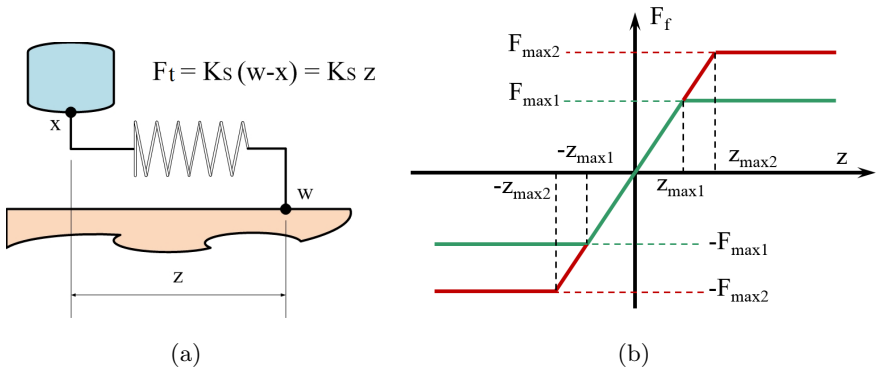

Figure 3.32: Dahal friction model with virtual spring (a). Different values of F_{fmax} obtained by setting different thresholds of z_{max} (b).

where i indicates the sampling time, and $SAT_a^b(y)$ is the saturation of y to the interval $[a, b]$. In (3.14) the first block is the updating of the virtual reference $w(i)$ and the real linear displacement x while the last equation is the function emulating the behavior of the friction force from zero up to the Coulomb force F_{fmax}.

In our system the displacement of the belt x(i) is related through Eq.3.11 to the angular displacement of the driver roll read by encoder, and F_f corresponds to the traction force in the belt F_t. Through Eq.3.13, the control system allows to emulate a desired friction force by applying a saturation to the voltage of the motor by:

$$\begin{cases} w(i+1) = \begin{cases} x(i) - z_{max} & \text{if} \quad x(i) - w(i) > z_{max} \\ w(i) & \text{if} \quad |x(i) - w(i)| < z_{max} \\ x(i) + z_{max} & \text{if} \quad x(i) - w(i) < -z_{max} \end{cases} \\ \\ V(i) = \dfrac{k_\tau n_m}{rR} K_s SAT_{-z_{max}}^{z_{max}} \left(x(i) - w(i)\right) \end{cases}, \tag{3.15}$$

Theoretically, by changing the saturation threshold of the torque resisting to the sliding of a mass located on the conveyor belt and subjected to an external force directed along the direction of the movement of the belt, it is possible to emulate the situation in which the mass is lying on different surfaces with different friction coefficient. When a tangential force exerted on the belt through the grasped object overcomes the maximum emulated friction force, the contact point between the mass and finger moves, driving the belt in a retrograde motion against the tuned resistance exerted by the motor.

Fig. 3.33 and Fig. 3.34 show the results of two simulations that implement the previous claim in a Matlab/Simulink environment. The first plot shows the friction force as function of the external force for different emulated Coulomb force. The second shows the trade of the velocity of the mass under a sinusoidal external force and it allows to test the correctness of the model in presence of stops and motion inversions. The behavior observed in simulation is coherent with the theoretical friction model, in accordance to [54].

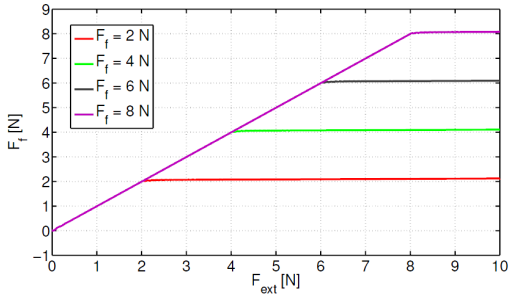

Figure 3.33: External pushing force Vs tangential emulated friction force. Simulation of different levels of emulated friction.

In practice, the bounds of the emulated friction coefficient depends on the real physical system implementing the variable friction.

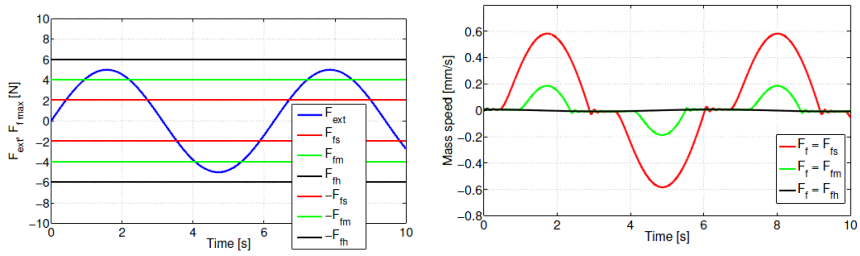

(a) (b)

Figure 3.34: Tangential response of the active surface to external force for different levels of friction. Simulation shows the different behaviors of the contacted object when it is externally pushed/pulled with a force $F(t) = 5\sin(t)$, over a ten second time interval, with different levels of emulated friction. The left panel shows the external force and the three thresholds of static friction $F_{fs} = 2N$, $F_{fm} = 4N$ and $F_{fh} = 6N$. The right panel shows the velocity of the contacted object in the three different cases.

The upper bound is due to the incipient sliding between the belt and the object, that is the real friction coefficient between the belt and the objects. In order to raise it, the conveyor belts are painted with high friction natural rubber. On the other side the lower bound is due to the parasitic internal friction of the conveyor belts. To lower it, all the rotating components are supported by ball bearings and the employed ratio-motors have high-efficiency with a low reduction ratio, in order to allow a retrograde motion with the lowest possible resistance.

To further reduce the friction, in this experiment we removed the transmission of motion between the belts of the proximal and distal inner phalanges in each finger. The inner belt is thus free, effectively resulting in low friction for the object. It was observed experimentally that such modification of the conveyor belt system did not alter much the overall functionality of the gripper. Therefore in the following experiments, the actuated belts were only on the distal phalanges of the Velvet Fingers.

In this experiment we test the capability of the gripper to emulate three different levels of friction: low, medium and high. The gripper is completely open in a vertical plane with a mass lying on the distal phalanx. The mass on the finger is linked to two masses by means of a wire wrapping around a pulley. The hung masses are located at different distances from a table below. With this set up, neglecting any dissipative forces on the pulley, the tangential external force applied to the mass on the gripper is the weight of the hung masses which do not touch the plane. In the sequence of Fig.3.35 low friction is imposed to the Active Surfaces so that the external force on the mass overcomes the friction resistance even when the lower hung mass touches the table (3.35 b)).

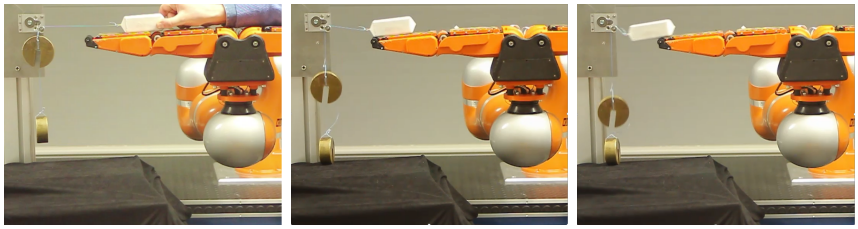

(a) (b) (c)

Figure 3.35: Low friction level: the mass on the finger moves even when the lower load touches the table. The tangential force applied by the only upper load is larger than the imposed friction between the object and the belt. The maximum emulated friction is smaller than the weight of the upper mass.

In the next sequence (Fig.3.36), medium friction is set. With this setting, the weight of the two masses is larger than the friction force as in the previous experiment and the white mass and the belt are dragged in a retrograde motion (a). Differently, in this case, when the lower mass reaches the ground, the only weight of the upper mass is not any more large enough to overcome the emulated friction and the mass stops (c).

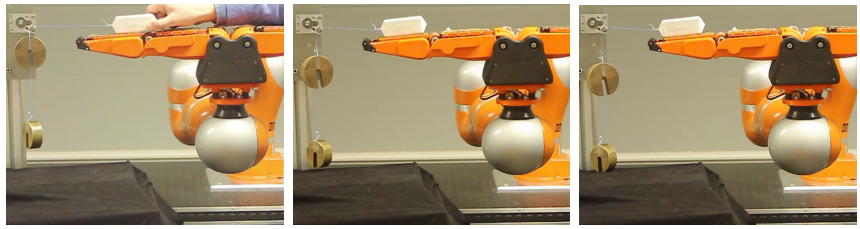

(a) (b) (c)

Figure 3.36: Medium friction level. After the lower mass reaches the table, the tangential force applied only by the upper mass is not sufficient to move the white mass. The maximum emulated friction is larger than the weight of the upper mass and smaller than the sum of the weights of the hung masses.

Lastly, the emulated friction is high and the weight of the two masses is not large enough to drag the mass on the finger. The emulated high friction prevents any movement, hence the white mass is still and the two masses stay hung.

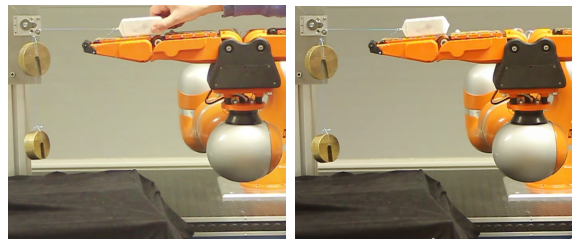

(a) (b)

Figure 3.37: High friction level. The maximum emulated friction is larger than the sum of the weights of the hung masses and the system does not move.

As said in Sec. 3.4.2 the emulated kinetic friction coefficient depends on the normal load on the belts, since their retrograde motion is due to tangential forces whose maximum value is given by the normal load times the real static friction coefficient between the material of the grasped

object and the high friction gum covering the belts. To evaluate the upper and lower bound of the fictitious friction coefficient relative to a mass of 1.09 kg, the tilted plane experiment, with the mass on a finger of the gripper, was led, mounting the Velvet Fingers on the KUKA LWR IV's wrist. Such mass applies on the belt a typical normal load that might rise during grasping of a general object with the Velvet Fingers. The initial position of the finger of the gripper is horizontal with the mass lying on it. As Fig.3.38(a) and 3.38(b) show, when low friction is set, the mass starts moving after a rotation of19° around the axis of the wrist, while, with high friction, the rotation angle reaches 42°. In this experiment the emulated friction coefficient ranges from 0.34 to 0.91 and in general the lower bound decreases at the increasing of the mass while the upper bound remains substantially unchanged.

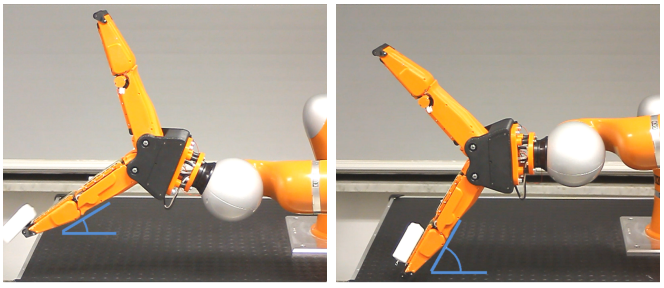

(a) (b)

Figure 3.38: Demonstration of different friction levels implemented on the Velvet Fingers. When a lower level of friction is set (a) the mass slides away after a rotation of a small angle. The highest friction prevents the mass from sliding until a much higher angle is reached (b).

In reference to the tilted plane experiment, Fig.3.39 shows the maximum and minimum emulated friction coefficient as function of the mass lying on the Active Surface. Furthermore the graph highlights the empirical value of 0.407 kg, which is the smallest mass on the belt able to

drive the conveyor belt system in a retrograde motion through a tangential force. Indeed, with a smaller mass, the sliding of the object on the belt occurs instead of the integral motion of the mass and the belt, since the actual static friction coefficient between the object and the material of the belt is overcome.

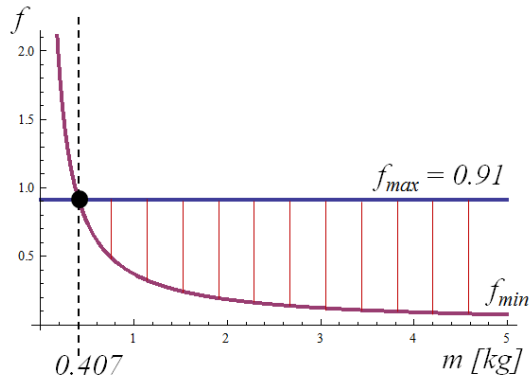

Figure 3.39: Upper and lower bound of the emulated friction coefficient as function of the mass in the tilted plane experiment. The range of the emulated friction coefficient $f_{max} - f_{min}$ increases at the increase of the mass.

Grasping a cylinder can be a challenging task when it is not possible to contact the object under its diameter. To do it, it is necessary that the contact forces exerted by the gripper have a vertical component large enough to balance the weight of the object, otherwise the piece tends to fall down. To avoid the last situation we can squeeze the cylinder and at the same time impose high friction on the Active Surfaces (see Fig. 3.40).

Another example where application of high friction is demanded is when an external torque, normal to the plane of the gripper, is applied to the grasped object. Under this condition it is necessary to compensate this torque to maintain the object unmovable. See Fig. 3.41 where a task of bottle opening is presented as an example.

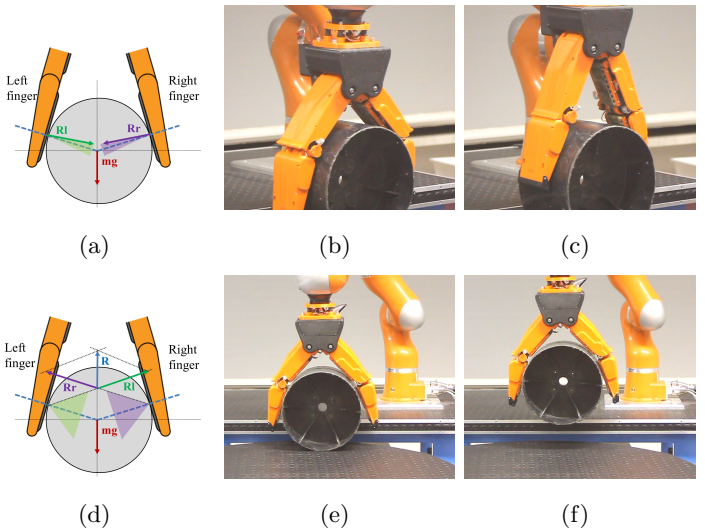

Figure 3.40: Grasping a cylinder with low and high friction. The upper three frames shows the unsuccessful attempt to grasp a big cylinder above its diameter due to the low friction. On the other hand, in the three lower frames, high friction is set on the Active Surfaces. The wide friction cones (d) allow to balance the weight of the cylinder and then to lift it (f).

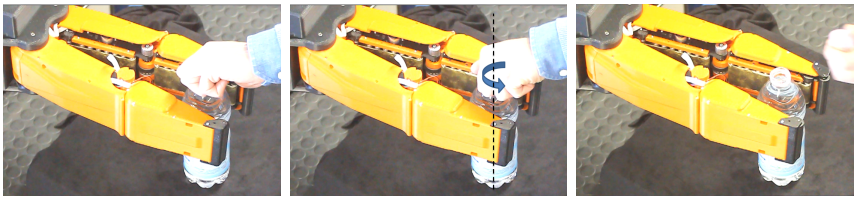

Figure 3.41: High friction can be used to balance the torque applied to screw-open the cap of a grasped bottle.

The aim of the following experimental tests is to point out the performance of a gripper able to switch from "sticky fingers" to "slippery

fingers". Next experiment shows the skill of the Velvet Fingers to grasp a cube by its edges. With one sticky finger (red) and one slippery finger (green) the cube can rotate and get a bigger contact area (blue) with the second finger as illustrated in the top sequence of Fig. 3.42. Doing this, it is not necessary to precisely plan the pose of the Velvet Fingers to perform a stable grasp, instead, it can be achieved using Active Surfaces to drive the object to change its orientation with a passive in-hand manipulation. Two sticky fingers (bottom sequence) ensure a stable tip grasp even if the cube is in a strongly asymmetric pose with respect to the bisector of the fingers.

3.5 Discussion

In this chapter we discussed the theoretical concept, design, implementation and test of a novel gripper which was employed on the wrist of the Parcel Robot within the RobLog project. The experiments on the Velvet Fingers highlighted some qualities as well as some drawbacks. The qualities, which can represent starting points or simply some clues for developing new gripping devices, can be summarized in the following few points:

1. Good adaptability to simple primitive shapes of the objects, obtained through the employment of two RR manipulators as fingers.

2. Ease of control. The number of actuators is reduced to the minimum. In particular the coupling of the first joints, allows to command the closure of the gripper with one motor leaving the capability to embrace the objects to the intrinsic adaptability of the under-actuated structure of the fingers.

3. In-hand manipulation capability. The use of conveyor belts as grip-

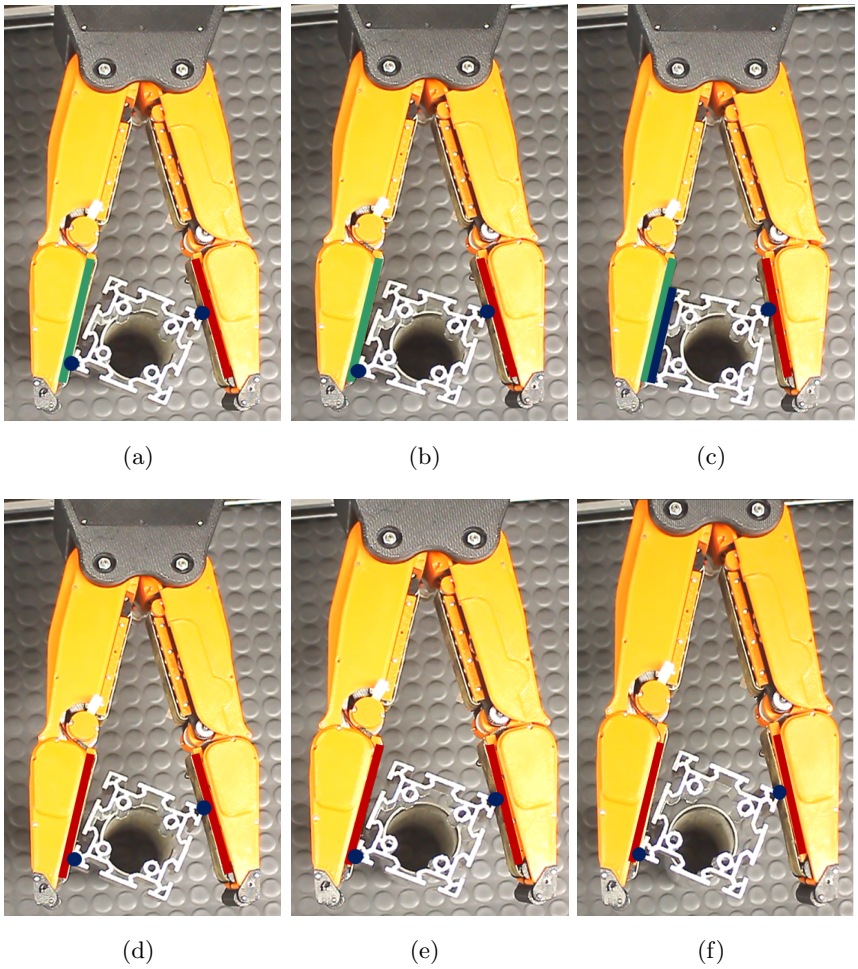

(a) (b) (c)

(d) (e) (f)

Figure 3.42: Different grasp equilibria triggered by different levels of friction. The two sequences, on the two rows, show the evolution of two grasps starting from same initial conditions but yielding different final configurations thanks to different levels of controlled friction. While on the top sequence a low friction level let the grasped object slide in a different configuration, on the bottom high friction ensures stability for the initial grasping configuration.

per/object interface, which are sliding surfaces with no end-strokes, allows to move the contact point resulting also in big and continuous displacements of the object.

4. Variable friction control. The system is able to control and tune the slippage of the objects along the belt direction. The effect of this type of belt control can be considered as a sort of variable and tunable friction perceived by the grasped objects. This skill allows to passively change the arrangement of an object between the fingers or to increase the slippage avoidance.

   The experiments performed with the Velvet Fingers were been also very helpful to identify the main drawbacks, which can be seen as improvement motivations.

The main drawbacks of the Velvet Fingers can be briefly gathered in the following bullet-points:

1. Complex assembling and intervention for regulations and component replacements. This issue was solved in the final version of the Velvet Fingers.

2. No feedback from the grasped object. The sensors used in the Velvet Fingers do not give any information, neither about the local contact force nor the contact point locations. The current sensor employed in the autonomous grasp procedure described in Cap.[ref], gives the overall effort of the motor to squeeze an object

3. As mentioned in Sec.3.4.2 the variable friction control implemented on the Velvet Fingers allows to tune the friction resistance, not the friction coefficient, since the normal force is unknown given that the gripper is not provided of force sensors.

4. The presence of high parasitic internal friction in the conveyor belt system and in the transmission chain between the distal and the proximal belts prevent to emulate low friction resistance.

Chapter 4

Autonomous grasp acquisition with the Velvet Fingers

In the previous chapter a novel under-actuated gripper with active surfaces, named Velvet Fingers, has been introduced. Numerous tests were performed aiming at characterizing the capabilities of the gripper. In some experiments where the pose of the gripper did not change, the palm of the Velvet Fingers was mounted on a fixed support. In other cases, when the execution of the experiment required a change in the relative pose between the target object and the gripper, the Velvet Fingers was attached to a KUKA robot arm. However in the latter case, the hardware behind the gripper merely played the role of holding the gripper with the robot still or manually jogged; in other words no cooperative tasks were performed by the gripper and the robot. In this chapter the gripper is regarded an integrated part in a more complex system in order to investigate the capabilities of the Velvet Fingers as a device for autonomous grasping. To this end, a grasp planning and execution pipeline which take advantages of the under-actuation and the manipulation capability of the

gripper to achieve robust power grasps in cluttered scenes were proposed in [55]. In this chapter, we first describe the optimization-based grasp planner and grasping pipeline proposed in that work. After illustrating the grasp acquisition strategy, we report the results of preliminary tests aimed at evaluating the gripper capabilities in combination with the proposed pipeline. After analyzing the results from this preliminary study, a re-design of the gripper was deemed necessary to facilitate more robust grasp acquisition. In the main contribution of this chapter, we discuss the mechanical re-design of the Velvet Fingers prototype and present an extensive evaluation of the gripper in the context of autonomous grasping in the RobLog project. To this end, the gripper was mounted on the Parcel Robot platform (see Fig.4.1) at the *Bremer Institut für Produktion und Logistik GmbH (BIBA)* in Bremen, Germany and used in a dedicated system for automatically unloading shipment containers filled with randomly packed goods.

Figure 4.1: The Parcel Robot platform equipped with the Velvet Fingers is an autonomous system for unloading shipment containers filled with randomly packed goods.

4.1 Grasp planning for an under-actuated gripper with Active Surfaces

An interesting use of the active surfaces previously touched on in Sec.3.1.2 is the pull-in grasping strategy depicted in Fig.3.11. This strategy relies on the capability of the active surfaces to pull in an object towards the palm. Here the object, after being contacted at the fingertips, is manipulated in a grasp acquisition stage and then firmly grasped in an embracing configuration. The pull-in strategy turns out to be very useful in untidy environments where the scene is populated by many objects in a cluttered disposition. In this context, a nimble fingertip grasp is more likely to be feasible than a robust enveloping grasp, since the first minimizes the bulky presence of the gripper in the scene. The pull-in strategy then aids in obtaining a firm grasp which would not be achievable without the active surfaces. In this section we investigate two issues:

- the effect of the under-actuation in the grasp synthesis, namely the process of determining the gripper's joint configuration and wrist pose with respect to the target object, such that a successful grasp execution is ensured
- the contribution of the active surfaces to the grasp execution process.

Grasp planning and execution in cluttered scenes is subjected to intrinsic difficulties since many pre-planned grasps are not reachable in such environments. The initial fingertip grasp of the pull-in strategy allows to simplify the grasp synthesis, since for planning purposes, the Velvet Fingers can be regarded as a fully actuated structure with extended and rigid fingers, with one DoA which controls the α angle of the first joint (that is the natural configuration of the gripper when no mechanical interaction with the environment occurs). Moreover for our application, we took

into consideration two important observations which further contribute to simplify the planning framework:

1. it has been shown, that most successful grasps usually approach along a surface normal of the object [56, 57].

2. preliminary experiments showed that in many successful grasps the gripper's lateral axis (the x-axis in Fig. 4.2) is normal to one of the principal component directions of the object.

With these assumptions the goal of the grasp planning is to find an appropriate gripper wrist pose $\boldsymbol{P}$ and a proper approaching α angle. Here, we investigate a data-driven approach to grasp synthesis, where a knowledge base is populated offline with target object models which are associated to pre-planned grasps. During execution, the database is used to retrieve grasps and rank them according to the expected quality in the current scene. Our grasp planning methodology is built upon the work by Ciocarlie and Allen [58], who generate pre-grasps in low-dimensional hand joint subspaces by minimizing an energy function based on distance/alignment between pre-defined contact locations on the hand and the target object. In accordance with the first observation, we constrain the approach direction (the y-axis in Fig.4.2) to be along a surface normal $\boldsymbol{n}$ of the object and plan wrist poses $\boldsymbol{P} = \boldsymbol{P}(d, \phi, \psi) \in \mathbb{R}^3$ over the approach distance d and wrist roll and pitch angles ϕ and ψ.

To this end, we minimize the following energy function E: $\mathbb{R}^4 \rightarrow \mathbb{R}$ which was introduced in [58]

$$E(\boldsymbol{P}, \alpha) = \sum_{c=1}^{n_C} \left(1 - \frac{\boldsymbol{n}_c^T \boldsymbol{o}_c}{\|\boldsymbol{o}_c\|_2} + \frac{\|\boldsymbol{o}_c\|_2}{s} \right), \tag{4.1}$$

where n_C indicates the number of preset target contact locations on the phalanges of the gripping device (see Fig. 4.2), $\boldsymbol{n}_c \in \mathbb{R}^3$ denotes the

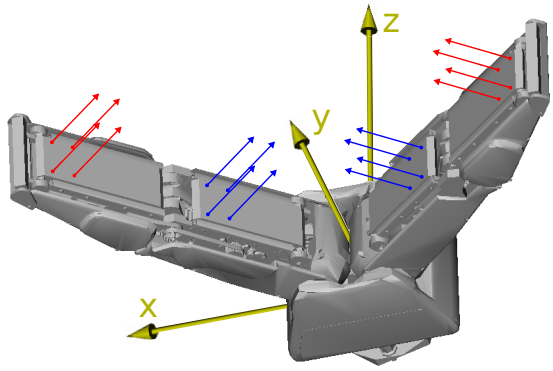

Figure 4.2: Preset contact locations and corresponding surface normals $\hat{\boldsymbol{n}}$ on the Velvet Fingers. For the synthesis of fingertip grasps the set of contacts shown in red were used, while the contacts in blue result in power grasp.

outward-pointing surface unit normal at a preset contact, $\boldsymbol{o}_c \in \mathbb{R}^3$ is the vector from contact c on the hand to the closest point $\boldsymbol{p} \in \mathbb{R}^3$ on the object and s is a scaling parameter (for sake of clarity, the implicit dependence of $\boldsymbol{o}_c$ and $\hat{\boldsymbol{n}}_c$ on $\boldsymbol{P}$ and α was omitted in the notation). The first term in Eq. (4.1) captures the alignments between the object and target contact locations on the hand, the second term indicates the distances of the target contacts to the object. As in [58], the grasp energy in (4.1) is minimized using the simulated annealing algorithm which is able to escape local minima through possible "uphill moves" during optimization via generating random neighbors.

Given a vertex $\boldsymbol{p}$ with associated vertex normal $\boldsymbol{n}$ on the target object's discretized surface, we account for the second observation by providing the solver with appropriate initial conditions. To this end, the gripper is positioned at a fixed offset distance from $\boldsymbol{p}$ along the negative approach direction which coincides with the normal $\boldsymbol{n}$. The initial wrist rotation is determined such that the gripper's lateral axis is normal to the object's principal component direction with the largest eigenvalue which is not parallel to the approach vector. This rotation is then offset by an

initial roll angle ϕ_0. During optimization, box constraints are enforced to ensure that the variables do not diverge too far from the initial condition. The proposed method allows to put bounds on the resulting grasp poses while, opposed to approaches solely relying on heuristic sampling [56, 59], still retains the flexibility to adjust them to the specific object geometry.

An example for the planners output is depicted in Fig.4.3.

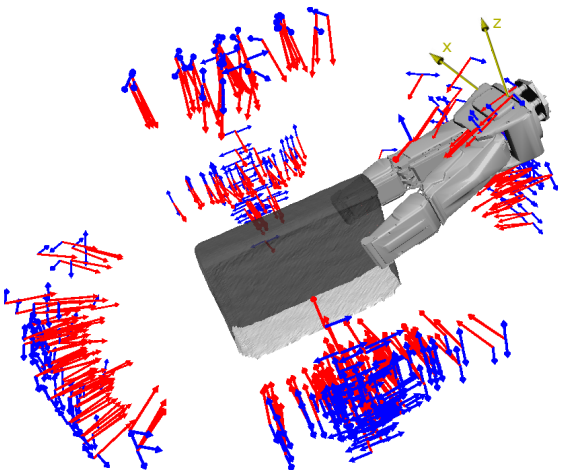

Figure 4.3: A set of fingertip grasps as computed by the planner. Wrist poses are indicated by the approach direction (y-axis) in red and the x-axis in blue. As intended, the resulting wrist orientations are roughly normal to principal component directions of the target object.

4.2 Grasping pipeline

To carry out the experiments in Section 4.4 we employ the grasping pipeline illustrated in Fig. 4.4.

Our approach employs an offline and an online stage. In the offline stage, we acquire 3D models of the target objects, train a perception module and compute grasps. After reading a set of RGB-D images of each

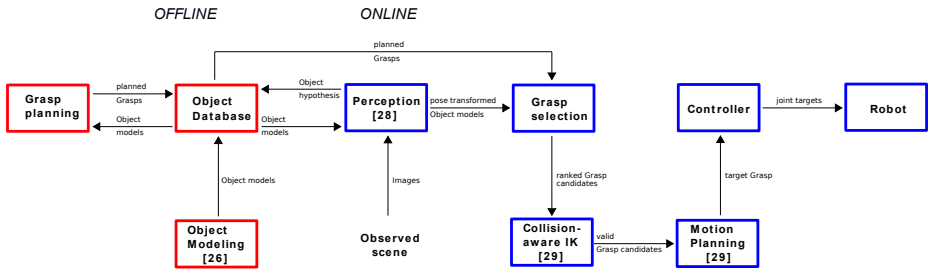

Figure 4.4: The pipeline uses an offline created database storing object models together with grasps provided by the grasp planner. The perception module creates object hypotheses from the observed scene and matches them to the models in the database. Found models are forwarded to the grasp selection module which ranks the associated grasps according to their score in the current scene. Subsequently, inverse kinematics and goal pose collision checks are performed on a chosen grasp before a motion plan is generated which is executed by the controller.

target object placed in a scene with augmented reality markers we reconstruct a discretized representation of the of the object with the TSDF tracker algorithm in [60]. By fusing consecutive views of an object in the TSDF representation we effectively eliminate a big amount of the vision system noise. The reconstructed models are then stored in the database and used by the previously described grasp planner to generate grasps.

The online stage of the proposed pipeline starts with the acquisition of an RGB-D image of the target scene. Following the work in [61], the image is then over-segmented in patches. Local visual features from each patch are then extracted and compared against the feature graphs stored in the database. Once the perception system obtains a list of detected objects, the grasp selection module is used to associate a set of grasps to each of the pose-transformed object candidates.

For evaluation purposes, as described in Section 4.4, this module tests all grasps from the database for feasibility and subsequently executed using a fast RRT planner. An example is shown in Fig. 4.5. Given a high

number of objects and possible grasps, this strategy may not be feasible for online operation. To this end, we employ a grasp ranking procedure and a first-feasible execution strategy. We follow an approach similar to the one outlined by Berenson et. al. [56] and compute, for the given environment, a composite score for each grasp by summing the following two parts:

- grasp energy score
- gripper-relative position score

Here, the grasp energy score is the value of the grasp energy in (4.1) for the current grasp configuration, normalized by the largest energy value over all grasps for an object. The gripper-relative position score captures the similarity of the grasp pose to the current gripper pose and is expressed as one minus the cosine of the angle between the current and target wrist orientation. All grasps are ranked by increasing scores and successively tested for feasibility as described above. Once a valid candidate is found, joint motion trajectories are generated and passed on to the controllers to execute the movement. In all experiments, inverse kinematics, collision checking and motion planning were carried out with the MoveIt! framework [62].

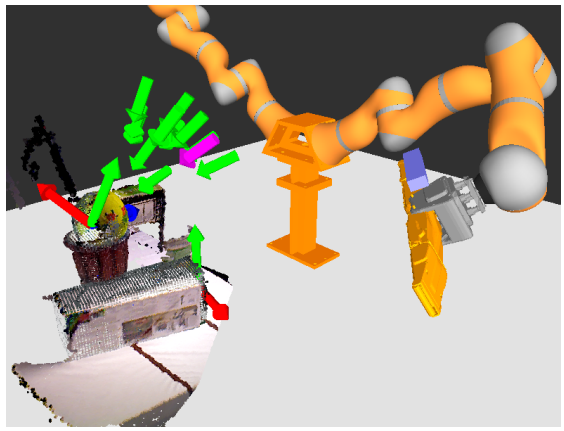

Figure 4.5: Grasp retrieval: Shown is a scene as observed by the robot with two detected objects (ball and box). Also depicted are the feasible grasps $\mathcal{G}^*$ for the ball which are indicated by their approach vectors in green, the purple vector signifies the grasp chosen by the grasp selection module.

4.3 Grasping execution for cluttered scenes

The pull-in routine is triggered after an initial pinch grasp is achieved. Then tangential pushes of the belts drag the object towards the palm. From pure geometrical considerations, as the object moves inwards the opening angle α increases since the fingers, which are still extended, are tangent to the object and constrained to rotate around the first joint. Since in this configuration the fingers are not compliant, we employed a compliant low-level current control of the gripper's actuator of opening and closing whose current absorption, under certain conditions addressed in the following, increases with the increasing of the output. Our grasp execution procedure can be split in three stages (schematically depicted in Fig.4.6) and takes advantages of the pull-in strategy.

First, a relatively low current threshold (LT) is given to the open/close motor controller and the fingers start closing. The V-like closure leads to a pinch grasp and the powering of the motor continues until the cur-

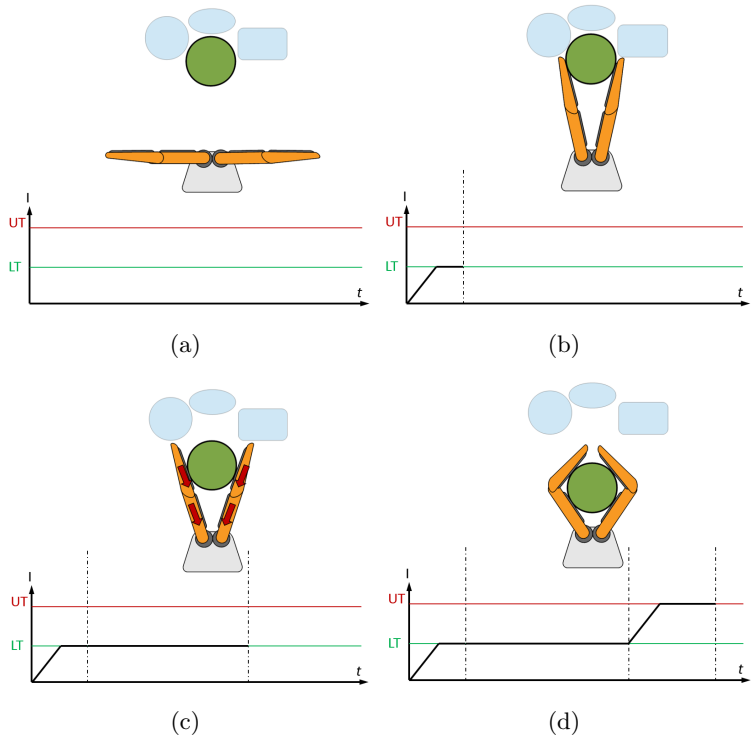

Figure 4.6: In picture a) is shown the gripper fully open ($\alpha = \pi$) at pre-grasping pose. Picture b), c), and d) depict the three stages of the pull-in strategy with an explanatory trade of the current absorption. Picture b) represents the initial pinch grasp after which the belts pull the object towards the palm (Fig.4.6 c)). The pull-in routine results in a final embracing grasp (Fig.4.6 d)).

rent absorption indicates a proper tip grasping force to ensure sufficient friction between the object and the belts (Fig.4.6 b)) for the next step. Then stage two is triggered and the control moves the belts a pre-defined offset towards the palm to pull in the object. The controller strives to maintain the current absorption of the closing motor on LT, by closing or releasing the gripper during in-hand manipulation. In this grasp acquisi-

tion step, the encoders of the belts and the encoders of the joints between the phalanges are monitored (Fig.4.6 c)). When the belts block and the phalanges have wrapped around the object, the final stage starts. Here, a higher current set-point UT is given to the open/close motor controller to ensure a firm grasp (Fig.4.6 d)).

During the grasp acquisition phase the target object has to move from a fingertip contact to a configuration in which the phalanges have wrapped around it. As the object moves towards the palm, this forces the fingers, and consequently the opening joint motor, to be back-driven. If the friction in the transmission chain from the motor to the first joint is low, the object, pulled by the active surfaces can easily drive the system in a retrograde motion by employing tangential forces with the belts. Conversely, high friction in the transmission chain can hinder or even prevent the dragging of the object. This strategy, hence, relies on the monitoring of the current absorption of the opening/closing motor and the ease of the gripping mechanism to be back-driven. In order to perform the autonomous grasp acquisition strategy and evaluate the suggested grasping pipeline, the experiments described in the next section were carried out with a modified version of the Velvet Fingers in which a new closing motor and electronics are employed.

In order to make the pull-in strategy effective, the ratio-motor that closes the fingers must have a small reduction ratio. Yet, reducing the transmission ratio of the gearhead decreases the maximum grasping force. The combination of motor $DCX22L$ with gearhead $GPX22$ 83:1 by *Maxon Motor Company*, is a very good trade off among reduction ratio, grasping force, size, weight and cost. The most important specifications of this ratio-motor are listed in Tab.4.1 and compared with the specifications of the original choice. The new actuator is easily back-drivable with a reduction ratio 3.8 times smaller. Despite the lower gear ratio, the

resulting output force the gripper can output is 67% higher in continuous operation and of 114% in short term condition, while size and weight are comparable. Instead, power consuming and cost are clearly in favor of the original solution.

Table 4.1: Comparative table of the two motors used in the palm

Motor specification	**Symbol**	**RE-MAX22**	**DCX22**
Nominal voltage	V	24 V	24 V
Maximum continuous torque	τ	6.89 mNm	29.2 mNm
Stall torque	τ_m	27.8 mNm	150 mNm
Torque constant	k_τ	25.3 mNm/A	45.2 mNm/A
Motor power	Pot	6 W	19.8 W
Efficiency	η_m	76 %	89.3 %
Reducer specification	**Symbol**	**GP22A**	**GPX22**
Reduction ratio	i_g	316:1	83:1
Number of stages	n_g	4	3
Efficiency	η_r	49%	74%
Ratio-motor		**old solution**	**new solution**
Weight		123g	120g
Size [L x ϕ]		77.65x22mm	80.65x22mm
Force on the tips (continuous operation)		9N	15N
Force on the tips (short term operation)		36.4N	78N

The monitoring of the current absorption is entrusted to a custom electronic board with a PID controller on board and provided of current sensors on the power inputs. Fig.4.7 and Fig.4.8 show the current-based control scheme of the gripper and the electronic board used with the main components indicated.

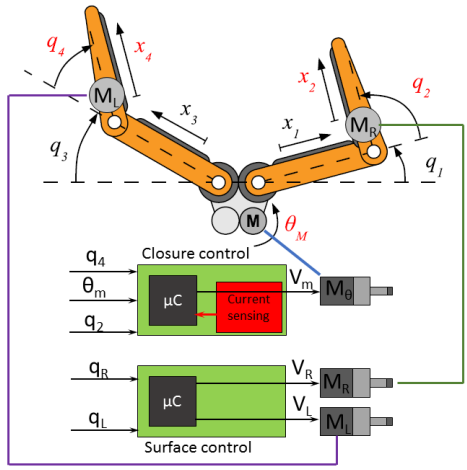

Figure 4.7: Control architecture of the pull-in strategy: one electronic board controls the motor M for the opening and closing, monitors the joints q_2 and q_4 and limits the current absorption. The second boards takes care of the belt motors M_R and M_L.

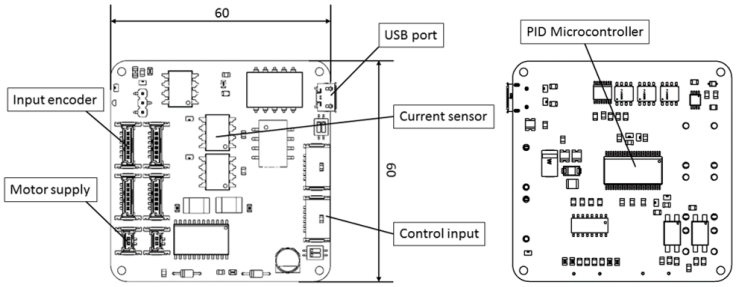

Figure 4.8: Custom electronic board employed for the pull-in strategy: communication protocol RS485 with USB-port for programming. Micro-controller PSoC3 CY8C3246PVIa147 8 bit with FPGA. Possibility to power two DC motors up to 5A and to drive them with PID controller. One current sensing for each driving channel and 4 inputs for magnetic encoders.

4.4 Evaluation and results

In order to evaluate the suggested grasping pipeline, two sets of experimental evaluations were performed. In the first set of experiments we investigate the quality of the proposed grasp planning approach under different environment configurations. We then proceed to analyze the performance of the system in a tabletop grasping scenario including a preliminary performance analysis of the proposed 'pull-in' strategy.

We used a database containing the five target objects shown in Fig. 4.9. For all object recognition and collision detection tasks an ASUS Xtion structured light camera, which is mounted on top of the gripper's palm, is used.

Figure 4.9: The platform utilized in the tests comprises the Velvet Fingers gripper with three actuated DoF and a seven-DoF KUKA lightweight arm. Perception is done with an ASUS Xtion structured light camera mounted on the gripper. Also shown are the five test objects used in the experiments - two different boxes, a beer barrel, a ball and a drum.

To evaluate the planning, we computed three sets of 400 grasps for

each object, containing pinch grasps $\mathcal{G}^P$, enveloping grasps $\mathcal{G}^E$ and an equal mixture of both $\mathcal{G}^M$ respectively. Next, the experimental platform was used to collect two data sets of depth and color images. The first scene data set $\mathcal{S}^I$ contains three observations of each target object in isolation (*i.e.*, only one object in the scene). The second data set $\mathcal{S}^C$ contains observations of scenes with various amount of clutter (*i.e.*, multiple objects in the scene). Here, a total of fifteen different scenes with all five objects, which are incrementally cleared by a human removing one object at a time, were recorded resulting in a total of sixty observed scenes containing at least two objects each. For each observed scene we executed our grasping pipeline using the differently planned grasp sets. In these sets of experiments we evaluate all grasps up to the motion planning module, but do not select or execute a grasp since we aim to evaluate how many of the planned grasps are feasible (*i.e.*, reachable by a collision free path) under different conditions. The predefined parameters for the box constraints, wrist rotation discretization and energy threshold are summarized in Table 4.2.

The outcome of the first experiment is visualized in Fig. 4.10. It is clear that pinch grasps are much more likely to be feasible, even if only a single target object is in the robot's workspace. Many enveloping grasps are rejected because they necessitate large opening angles resulting in bulky gripper silhouettes for which no collision free approach trajectories can be found.

Table 4.3 shows the feasible grasps per object depending on the number of objects in the cluttered scene and the chosen planning flavor (pinch, envelope or mixed grasps). We note that two out of the 15 scenes containing all five objects yielded an exceptionally high number of feasible pinch grasps, which biased the according entry in Table 4.3. This is due to the fact, that the number of feasible grasps found also significantly depends

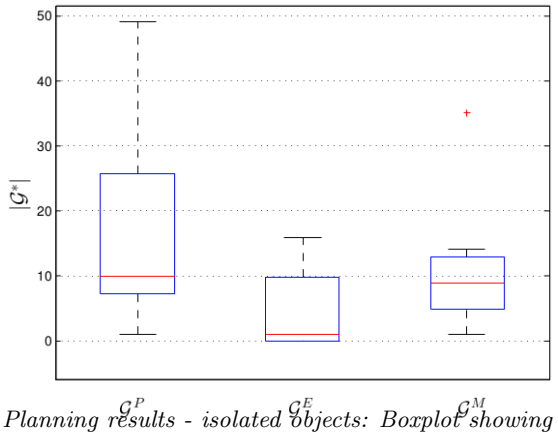

Figure 4.10: Planning results - isolated objects: Boxplot showing the number of feasible grasps $|\mathcal{G}^*|$ per object (out of a total number of 400 pre-planned grasps) as a function of the chosen planning flavor (pinch, envelope or mixed grasps). The grasps were extracted from data set $\mathcal{S}^I$ which contains observations of isolated target objects only.

Table 4.2: Predefined parameters

$\Delta\phi$ [rad]	$\Delta\psi$ [rad]	Δd [m]	n_J	E_{max}
$\pm\ \pi/10$	$\pm\ \pi/10$	$\pm$ 0.4	4	20

on the location of the objects in the robot's workspace which favored pinch grasps in these cases. Nevertheless, it is evident that the difficulty of finding feasible enveloping grasps increases with the amount of clutter, whereas it still possible to obtain pinch grasps with multiple objects in the scene. Also, the set of mixed grasps does not perform significantly better than enveloping grasps. These results provide a strong motivation to exclusively use dexterous initial pinch grasps, coupled with a strategy for subsequent robustness improvement such as using active surfaces to pull the object into a firm enveloping grasp.

Table 4.3: Planning results - cluttered scenes: Mean and 1-STD values of the number of feasible grasps $|\mathcal{G}^*|$ per object depending on the planning flavor (pinch, envelope or mixed) and the number of objects in the scene.

	$\|\mathcal{G}^{*^P}\|$/Obj	$\|\mathcal{G}^{*^E}\|$/Obj	$\|\mathcal{G}^{*^M}\|$/Obj
5 Obj	7.5 ± 12.3	1.3 ± 3.4	3.3 ± 8.0
4 Obj	4.7 ± 6.2	1.4 ± 3.2	2.1 ± 3.5
3 Obj	5.1 ± 8.9	1.5 ± 2.5	2.1 ± 4.2
2 Obj	8.4 ± 9.3	4.0 ± 5.7	4.6 ± 8.0

4.5 Velvet Fingers upgrade

After developing, testing and experimentally verifying skills and performances of the Velvet Fingers in Chap.3.5, in this Chapter we present a strategy that takes advantages of the under-actuation and active surfaces of the gripper to autonomously achieve a firm power grasp even in cluttered environments. In order to make the grasping procedure as reliable as possible, a big amount of optimization of the entire grasping pipeline, tuning of the control parameters of the pull-in sequence (the thresholds of the current, stroke and speed of the active surfaces and many others) and tests with different configurations of the gripper (several types of belts, motors of the conveyor belts, motors for driving the fingers of the gripper, etc.) had to be performed. The first prototype of the Velvet Fingers was not suitable for repeated interventions aimed at testing different solutions, because the assembling and disassembling is complicated and often the replacement of one component entails the disassembling of many parts. Moreover the structure of the Velvet Fingers is in ABS,

hence the risk of damaging parts during disassembling and re-assembling is very considerable. All these considerations make clear the need of an upgrade of the Velvet Fingers towards a version suitable to be integrated on the Parcel Robot platform for the final evaluation and test. The goals of the redesign of the first prototype can be summarized in the following bullet points:

- *Ease of assembling and disassembling enhancement.* This target is directed to a rapid replacement of the hardware components in case of failure or simply to proof different solutions: for instance different drivers or to test the behavior of different types of belts or again to try different tighteners.
- *Complexity reduction.* Another major aim is to decrease the number of components, to reduce the number of potential sources of failure and consequently to increase the constructive simplicity and the reliability of the gripping device. This target also fosters the previous point, increasing the ease of assembling.
- *Optimization of the pull-in strategy.* The actuator for opening and closing must ensure a firm grasp with a low reduction ratio to be easily back-drivable. Since the pull-in strategy relies on the tangential forces exerted on an object in tip grasp, the driver of the active surfaces must ensure a traction force in the belt large enough to drag the target objects inside the fingers of the gripper. To this end we opted for four independent active surfaces. In this fashion the loss of energy for each conveyor belt module reduces, increasing the efficiency of each active surface.
- *Mechanical reliability enhancement.* The majority of the parts of the Velvet Fingers is in ABS, for the ease of fabrication. The downside of the parts in ABS is their lacking mechanical resistance; this

means that they can be easily be damaged by mechanical stress or even during assembling or disassembling. To overcome this issue the most stressed and important part of the new version of the Velvet Fingers are made in a mechanically more resistant material. This objective is also pursued with an accurate design of the components in order to reduce the mechanical stress.

In the following we will provide a summary description of the resulting gripper after the review and the redesign phase. That is because many aspects have been already discussed previously and we wish above all to spotlight the improvements introduced with respect to the first prototype.

The improved version of the Velvet Fingers is depicted in the cut view of Fig.4.18. As clearly visible from the overall view, the conveyor belt system has been completely redesigned, with two independent active surfaces (B1) and (B2) driven by motor cylinders (M2) and (M3) with a ratio-motor embedded to spare space inside the phalanges. Also the arrangements of the mechanical systems, which will be described later, like the conveyor belt, the transmission chain, the tensioning system and others, result, in this version in neat separation and easy accessibility of all mechanical components.

As mentioned before, in order to spare space inside the fingers, the motor of the conveyor belts is embedded in the driver cylinder. Preliminary experiments demonstrated that a traction force in the belt of 10N is large enough to accomplish the tasks. This solution leaves large space inside the fingers to set up others mechanical parts and reduces the total number of components, the cost and the weight of the gripper since the power is directly transmitted from the reducer of the motor to the driver cylinder without any further transmission chain. Fig.4.12 illustrates the mechanical solution adopted in the driver cylinder of the conveyor belts.

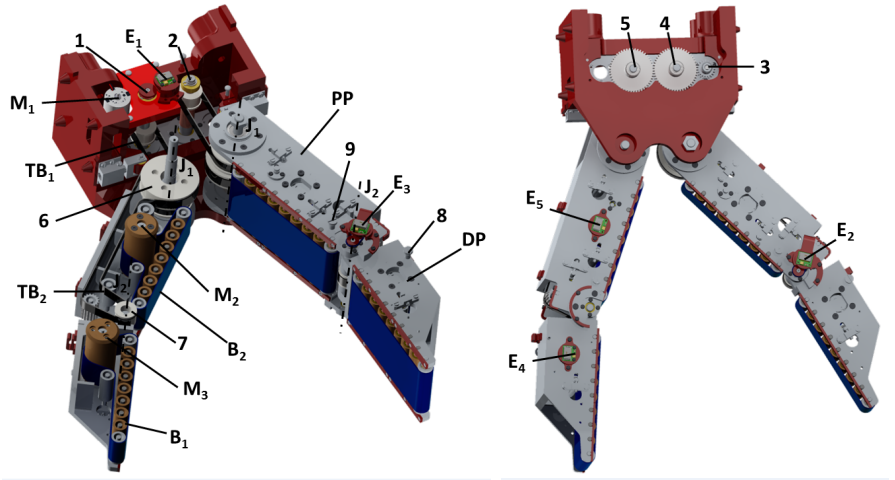

Figure 4.11: CAD design of the final version of the Velvet Fingers.

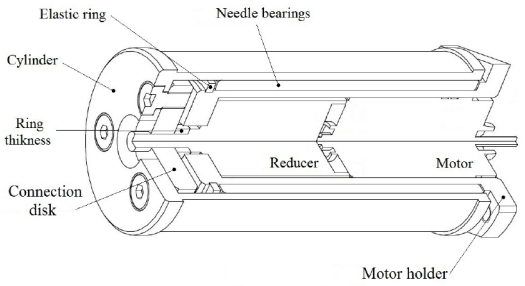

Figure 4.12: The motor is embedded in a housing fixed to the frame of the phalanges. A disk is keyed on the shaft of the reducer and fixed to it with a grub screw. The cylinder is screwed to the disk on the frontal side and is radially supported by needle bearings between the motor holder and the inner hole of the cylinder.

The ratio-motor employed is a DC motor REMAX17 24V 4.5W with a reducer GP16 of reduction ratio 84:1 that is produced by *Maxon Motor Company*. Tab.4.4 lists the main specifications of the actuator.

Table 4.4: Characteristics of the motor REMAX17 *and the gear head* GP16.

Motor specification	**Symbol**	**Value**
Nominal voltage	V	24 V
Maximum continuous torque	τ_m	4.06 mNm
Stall torque	τ_m	16.1 mNm
Torque constant	k_τ	20.9 mNm/A
Motor power	Pot	4.5 W
Maximum speed	n_m	10700 rpm
Efficiency	η_m	75 %
Moment of inertia	J_m	$0.859gcm^2$
Reducer specification	**Symbol**	**Value**
Reduction ratio	i_g	84:1
Number of stages	n_g	3
Efficiency	η_r	73%

The resulting driver cylinder is a very compact solution with an external diameter $D = 27mm$ and a length of $56mm$. The traction force T in the belt exerted by the driver cylinder with the motor in continuous operation is given by:

$$T = \frac{2\tau_m i_g \eta_r}{100D} \tag{4.2}$$

which results in about $18N$ of traction force in the belt. The belts used in this redesigned version are made in polyurethane with a fine textured pattern, $50mm$ wide and thickness of $1mm$. Moreover, in order to increase

the friction coefficient, the belts are coated with a bi-component of liquid polyurethane with high chemical affinity with the base material that results in a final conveyor belt with high friction, a uniform thickness and a well-bonded and resistant coating. The cylinders and rolls with a large winding angle have a slightly convex contour and guide edges which are fundamental to prevent the belts from sliding along the axis and enhance the efficiency of the conveyor belt. Fig.4.13 depicts the driver cylinder (left) and a passive roll (right), with the guide edges clearly visible on the edge of each cylindrical profile.

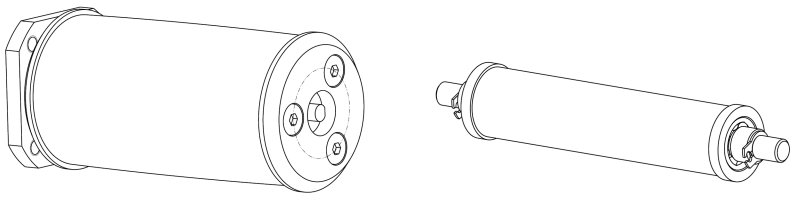

(a) (b)

Figure 4.13: A view of the driver cylinder on the left and a guide roll on the right. The guide edges are visible at the extremities of the cylindrical bodies, while the slightly convex profile is barely perceivable.

Fig.4.14 shows the distal phalanx of the fingers. The frontal part of the phalanx is tapered with a thin tip to approach as much as possible the target object free from collisions with other objects or obstacles. The location of the driver cylinder inside the frame (indicator (Md) in Fig.4.14 b)) of the phalanx has a number of advantages; it is not directly subjected to the grasping forces, therefore the cylinder, stressed only by the torque of the motor and by the preloading in the belt, can be mounted free-standing resulting in an higher ease of assembling and manufacturing and in a more robust structure of the frame.

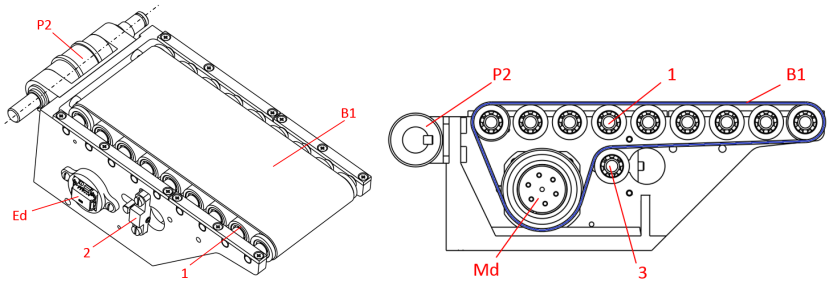

(a) (b)

Figure 4.14: A 3D view of the distal phalanx on the left and a cutaway view on the middle plane of the phalanx on the right. The driver cylinder (Md) of the belt (B1) is mounted free-standing inside the frame. Magnetic encoder (Ed) directly reads the angular displacement of (Md). The belt is properly tensioned by roll (3) whose position can be regulated by stop-dowels (2) and is supported by rolls (1) at the outer surface.

Fig.4.15 depicts a finger of the gripper. The phalanges are maintained aligned by means of two extensional springs whose extremities are anchored to anchor pins (4)(5) on one side of the finger and (9) (10) on the other side (the springs are not represented in the picture). The springs are dimensioned to satisfy three requirements:

- balance the torque around the second joint due to the weight of the distal phalanx, through a proper initial pre-load
- minimize the resistant torque when the proximal phalanx is blocked and the distal phalanx turns around the second joint
- allow a rotation of 90° of the distal phalanx without exceeding their maximum elongation.

From Fig.4.16 it is possible to see the arrangements of the main mechanical parts on the finger in a section on the middle plane. The blue and the black lines are the path of the active surfaces (B1) (B2) and the

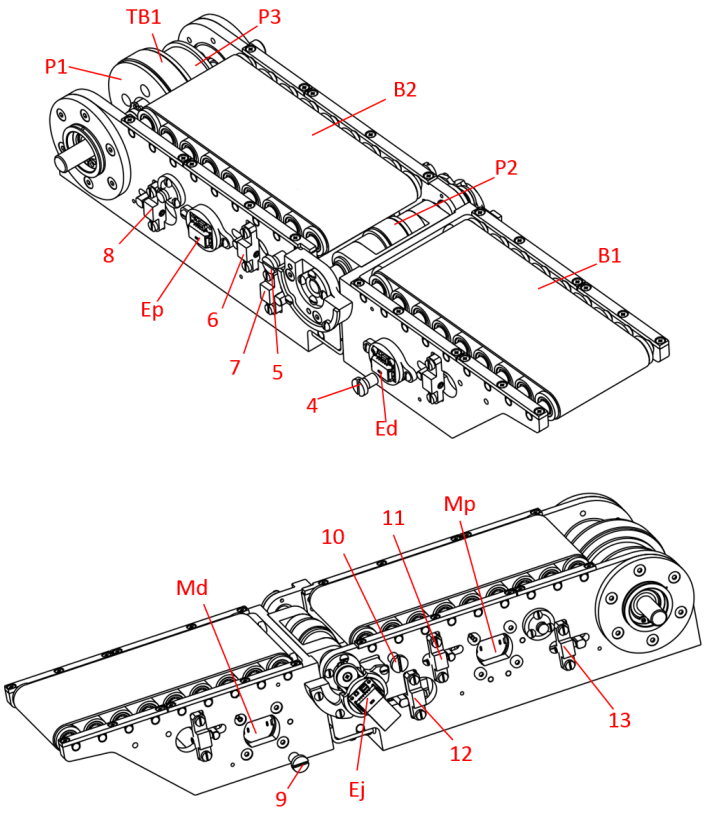

Figure 4.15: Every finger has two independent active surfaces actuated by driver cylinders (Md) and (Mp) on the distal and proximal link respectively. Each finger is equipped with two encoders to drive the motors of the active surfaces, (Ed) and (Ep), and an additional encoder (Ej) on the second joint to discern a tip grasp ($q_2 = 0$) from a power grasp ($q_2 \neq 0$). The belt of the proximal phalanx is preloaded by rolls whose position can be regulated through stop-dowels (6) and (11). Timing belt (TB1) transmits the power from idle pulley (P1) on the first joint to pulley (P2) integral with the distal phalanx and is properly tensioned acting on stop-dowels (7), (8) and (12), (13) which are easily accessible on the sides of the proximal link.

timing belt (TB) respectively. All components, especially the ones more involved in testing, are easily accessible and replaceable.

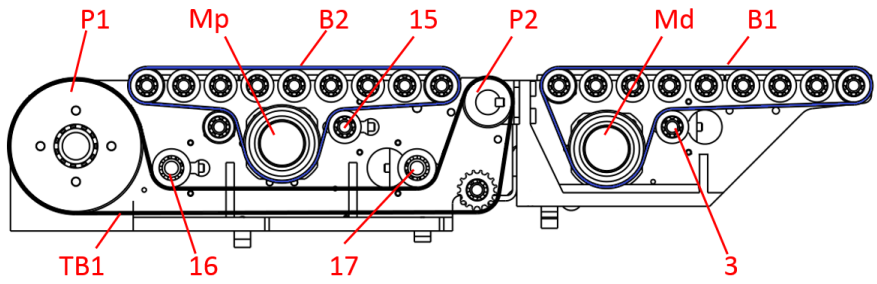

Figure 4.16: Arrangement of the main mechanical components in a cutaway view on the middle plane. The active surfaces (B1) (B2) represented in blue are tensioned by rolls (3) and (15)respectively. Rolls (16) and (17) tension timing belt (TB1).

The structure of the palm in *ABS* (Acrylonitrile Butadiene Styrene) (Fig4.17), has been redesigned and reinforced. Ratio-motor (Mm) in the palm is the same as the one described in Sec.4.3. Three electronic boards (EBl), (EBr) and (EBm), described in Sec.4.3, drive the active surfaces of the fingers and the motor for opening and closing.

Fig.4.18 shows a picture of the final version of the Velvet Fingers

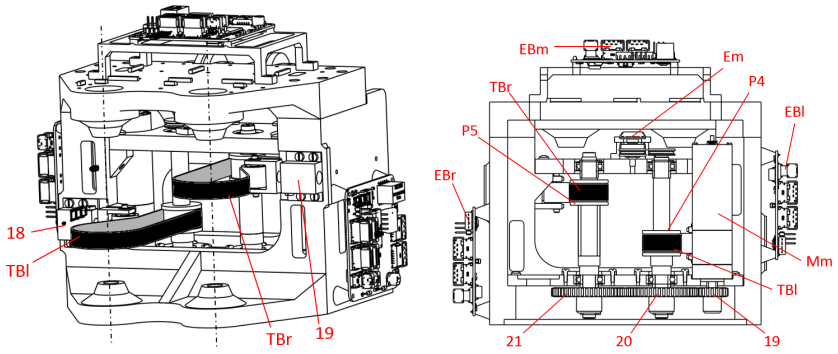

Figure 4.17: A 3D view of the palm on the left and a section with a plane passing for the axes of the motor shafts on the right. The tensioner (18) and (19) are placed on the frontal side of the palm and allow to tighten or loosen timing belts (TBl) and (TBr) simply acting with a screwdriver from the side of the palm without any disassembling intervention. Electronic boards (EBl), (EBr) and (EBm) take care of the active surfaces of the left finger, the right finger and the palm respectively. Ratio-motor (Mm) and electronics are the same described in Sec.4.3.

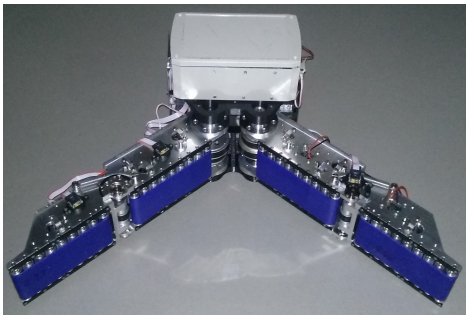

Figure 4.18: A picture of the final version of the Velvet Fingers

4.6 Grasp execution on the Parcel Robot

The RobLog autonomous system was created and evaluated in an incremental fashion, with one external review per year. Here, we report on the

final grasping performance as of the last review of the project. To this end a multitude of different container configurations was set up with the aim at evaluating the robustness of the system to various object stacking arrangements. Test scenes for this scenario contained on average between 20 and 25 objects from 7 to 9 different object classes. Tab.4.5 reports on the ratio of successful grasps over the total number of attempts and the relative percentage of success for the 8 objects modeled in the database (some scenarios included also unknown objects). On average, the system was capable of unloading successfully of 87% the target objects with the percentage of success which ranges from 75% to 97%.

Table 4.5: Results of the grasps for the final review of RobLog

Object	**Success/Total**	**% Successful Grasp**
Aloe-bottle	23/25	92%
DHL-box	97/111	87%
Maisels-barrel	62/78	79%
Pauli-suitcase	45/48	94%
Persil-detergent	20/23	87%
Teddy-bear1	69/71	97%
Teddy-bear2	27/36	75%
Vanish-detergent	36/43	84%

Fig.4.19 shows the initial pinch grasp of a cylindrical and a square section object (the left column) which evolves in a stable power grasps (the right column) after executing the pull-in strategy. The grasping

execution is performed by the final version of the Velvet Fingers mounted on the wrist of the Parcel Robot platform inside the moke-up of a shipping container.

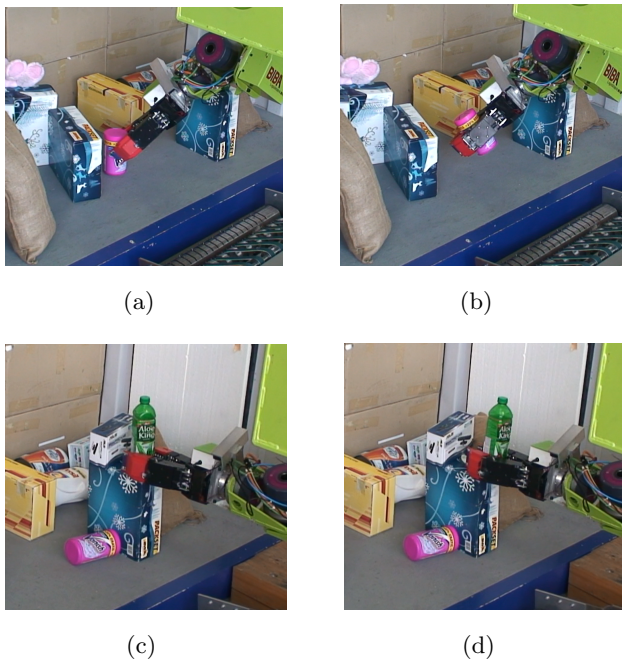

(a) (b)

(c) (d)

Figure 4.19: Two sequences of the pull-in strategy for two primitive shape objects: a cylindrical object (first row) and a square object (second row). In the first frame, the initial fingertip grasp is depicted, which evolves in an embracing grasp after the grasp acquisition depicted in the second frame.

In Fig.4.20 is shown a whole sequence of an autonomous grasp of a big box placed on a second box lying on the floor of the container. In picture a) the Parcel Robot moves the gripper towards the target object until reaching the grasping pose in b). In picture c) the gripper closes its fingers performing an initial pinch grasp. Frame d) shows the achieved power grasp as result of the pull-in procedure. After the power grasp

is achieved the gripper squeezes more energetically the box before the escape phase (picture e)) and the home position return of the platform in f).

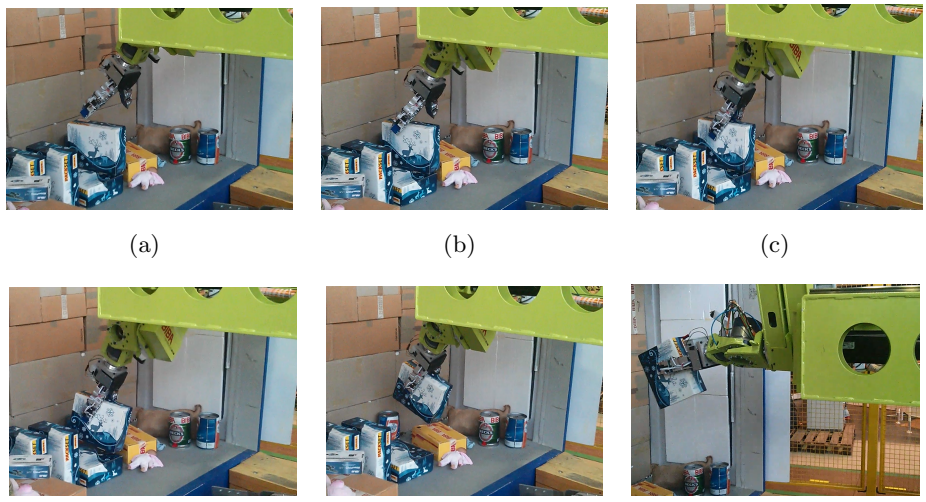

(a) (b) (c)

(d) (e) (f)

Figure 4.20: A sequence of an autonomous grasp of a big box with the final version of the Velvet Fingers mounted on the wrist of the Parcel Robot. The frames depict: a) approach b) grasping point c) pinch grasp d) pull-in e) escape f) home.

4.7 Discussion

In this chapter we contribute a grasp execution routine which takes advantages of the Active Surfaces of the Velvet Fingers to achieve a robust power grasp from an initial nimble fingertip grasp through a grasp acquisition stage in which the object is in-hand manipulated and dragged towards the palm. This strategy turned out to be very useful in cluttered environments since a fingertip grasp is much more likely to be feasible

than a bulky power grasp. Moreover the re-design of the Velvet Fingers, aimed at improving the gripper functionality, at facilitating the integration and test on the robot and at simplifying the calibration of the parameters involved in the pull-in strategy, was crucial for the general improvement of the robotic platform.

Chapter 5

The Velvet II

After analyzing the pro's and con's in the design of the Velvet Fingers, we decided to pursue the development of a new and enhanced gripper prototype. In particular, the new device was designed with the goal to improve the sensing capabilities of the fingers in the process of grasping. This ability is achieved through an advanced concept of active surfaces endowed with the capability to reveal the position of the contact point with the object and the grasping force components. The active surfaces become, hence, Sensitive Active Surfaces hereafter referred to as SASs. Moreover, in order to make the new gripper suitable even for small manipulators with low payload and to further widen the applicative scenario with respect to the one the Velvet Fingers was conceived for, we focused on small household objects which can be found on tables or desks (such as cans, small bottles, spheres like baseball or tennis balls, small boxes etc.) The theoretical concept, design, implementation and test of the new gripper, named Velvet-II, is be discussed over this chapter.

In the last Sec.5.5 the Velvet-II is utilized as gripping device on a research platform for logistic applications developed in collaboration with

AASS Research Center, of the University of Örebro (Sweden) within the the KUKA Innovation Award 2015.

5.1 Concept and specifications

Given the target objects, the gripper must ensure a grasping force, able to hold an object of $2.5kg$ in the worst object/gripper configuration. Moreover, for a quick closing and releasing we demand a time limit of $1s$ for the whole trajectory of the fingers, from completely open to completely closed. Since one of the most interesting features of the previous grippers developed in this thesis, is the adaptability to the shape of the grasped objects, the kinematic of the fingers of the Velvet-II will be inspired by the mechanism adopted in the Velvet Fingers.

In order to elicit information from the object in terms of grasping force and location of the contact point, traditional approaches fall into two camps: tactile sensing and force/torque sensing.

The first category relies on tactile sensors, namely surfaces with arrays of force sensitive elements which are widely employed on the fingertips of many robotic hands. The main transduction methods are resistive, piezoresistive, based on tunnel effect, capacitive, optical, ultrasonic, magnetic and piezoelectric (a brief overview of tactile sensors for robotic applications is available in [63]). Tactile sensors turn out to be useful in manipulation tasks (grasp force control, contact point estimation and grasping stability assessment), in surface exploration and in slippage detection [64]. The main advantages of tactile sensors are that they can be made to cover a large area and that the point of contact is explicitly measured.

The second category relies on intrinsic Force/Torque (F/T) transducers, placed between the contacting surface (for instance the fingertip of a robotic finger) and the frame of the structure, to reveal the contact point location and the force components. The contact sensing problem

with an intrinsic sensor can be formulated as follows: *given an external wrench on the contacting surface and the surface equation, determine the location of the contact point and the force components.* The theoretical aspects of intrinsic contact sensing can be found in [65]. It states that the solution of the contact sensing problem exists and is unique if the following requirements are satisfied:

- a solution exists if the components of the wrench are either unidirectional or limited by the friction cone
- the solution is unique if and only if the surface is convex

Intrinsic sensors using strain gauges are typically more accurate than a tactile sensor but the mass they support (often the whole fingertip), makes them sensitive to the direction of the gravity force and to accelerations. A further downside is then that they can not distinguish between multi-point and single-point contact. Fig.5.1 schematically shows the application of an extrinsic tactile sensor on the fingertip of a robotic finger on the left and of an intrinsic F/T sensor on the right.

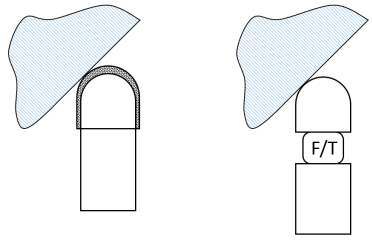

Figure 5.1: On the left a distributed extrinsic tactile sensor covers the fingertip surface of a robotic finger. On the right an intrinsic F/T sensor is placed between the fingertip and the frame of the finger structure.

Since the employment of an extrinsic tactile sensor on sliding surfaces is demanding because of the wiring, we opted for an intrinsic solution with

the sensor located between the frame supporting the conveyor belt and the phalanx. Given the small size of the gripper, a single SAS is simply composed of **i)** a driver cylinder where the torque is applied **ii)** a driven cylinder, **iii)** a belt winding around the cylinders **iv)** a support cylinder that supports the belt in between the driver and the driven cylinder **v)** a frame of the conveyor belt which is fixed on the tool plate of the F/T sensor and **vi)** the F/T transducer that mechanically isolates the conveyor belt from the rest of the finger. Fig.5.2 a) shows a sketch of the SAS with the main components.

Every phalanx of the gripper is therefore endowed with a SAS with the same structure of Fig.5.2 a). From Fig.5.2 b) is also clear that the space between the frame of the phalanges and the frame of the conveyor belts is partially occupied by the sensor and this entails that the train transmission must be located on the sides of the fingers.

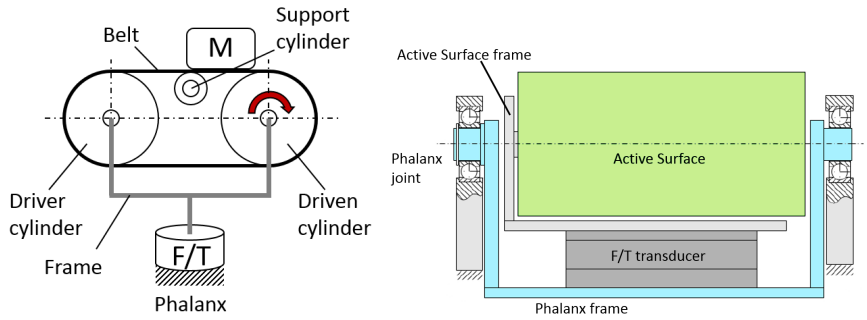

Figure 5.2: On the left is depicted a sketch of a single SAS where the main components are indicated . The picture on the right shows the F/T transducer located between the frame of the conveyor belt and the frame of the phalanx.

The relative position between the joints of the fingers and the cylinders of the SASs is chosen in order to maintain constant the center to

center distance between two consecutive cylinders of the SASs in any configuration of the gripper. That allows to have a constant gap among the SASs of two consecutive phalanges and makes the SASs form a continuous surface in any configuration except the gaps, which can be decided in the design stage. With this end, the joint J_2 and the axis of the second cylinder of the proximal SAS coincide and the same can be said of the first joint J_1 and the first cylinder of the proximal SAS as brought out in Fig.5.3. In this fashion, the gap g_2 is also the distance of the fingers when they are parallel (gripper closed).

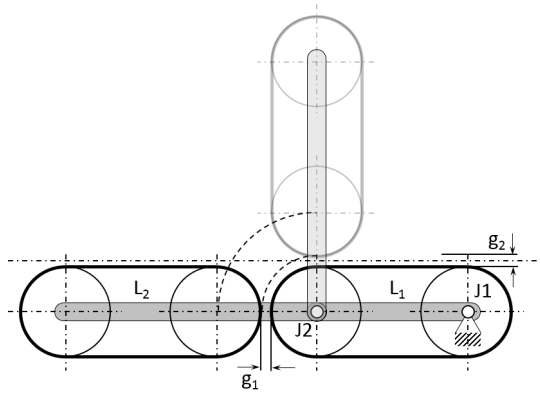

Figure 5.3: Joints and axes of the SAS arrangements to form a continuous sensitive active surface along the entire finger of the gripper and for any configuration of the links, except the gaps g_1 and g_2.

With reference to one finger of Fig.5.4 a), the under-actuation constrain links the joint variables q_1 and q_2 with the generalized displacement of the motor s through the following equation:

$$s = r_1 q_1 + r_2 q_2 \,. \tag{5.1}$$

The ratio r_1/r_2 as stated in Sec.3.1.3, determines the evolution of the gripper configuration after the fingertips touch together (which might

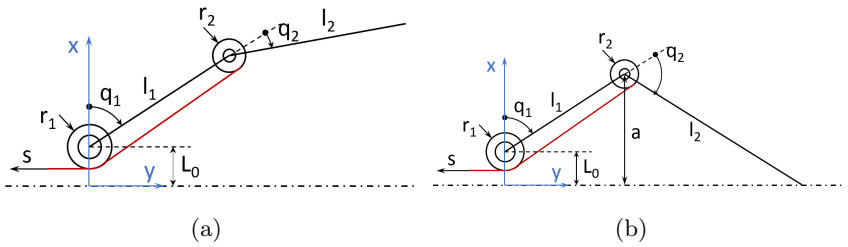

Figure 5.4: Reference frame, kinematic parameters and notation for the kinematic design on the left. On the right, a configuration of the links with the tip on the symmetry plane which represents a grasp with touching fingertips.

occur when a small object blocks the proximal links and the distal ones come into contact). To promote the straightening of the fingers, inequality 3.6 (reported below) must be satisfied (see Fig.5.4 b)):

$$\frac{r_1}{r_2} > \frac{l_1 \sin(q_1)}{l_2 \sin(q_1 + q_2)} + 1\,. \tag{5.2}$$

Given the particular configuration, with the fingertip on the axis of symmetry of the gripper, the previous inequality can be rewritten as function of the high a of the second joint over the axis.

$$\frac{r_1}{r_2} > \sqrt{\frac{l_1^2 - (a - L_0)^2}{l_2^2 - a^2}} + 1 = c(a) + 1\,. \tag{5.3}$$

Given the length of the links and the distance L_0 between the first joint and the axis of symmetry, Eq.5.3 provides the minimum ratio r_1/r_2 which guarantees the desired behavior for any configuration of the gripper.

Moreover, given that the target objects are rather small, we decided to locate the transmission chain on one side of the Velvet-II (as depicted in Fig.5.5) to permit the gripper to approach as much as possible to the surface on which the objects lie. Then, to further reduce the width of the

fingers the transmission between the first and the second joint is carried out by tendons, while the transmission between the motor and the first joint is due to a timing belt.

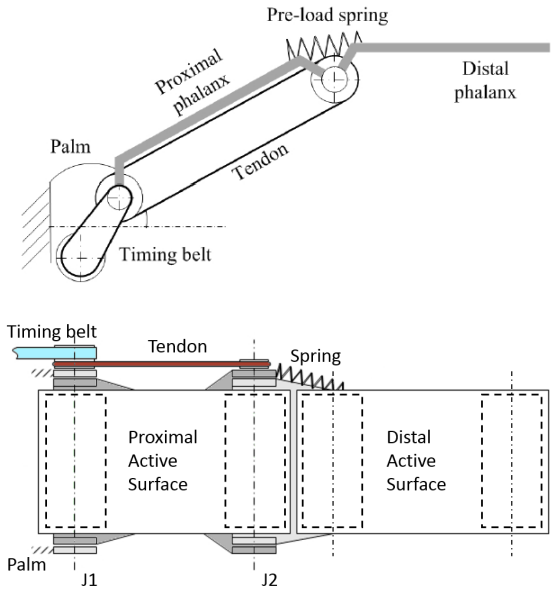

Figure 5.5: Kinematic scheme of a finger of the Velvet-II. The transmission is on one side of the gripper to approach as much as possible to the surface on which the objects lie. The transmission between J_1 and J_2 is due to tendons to reduce the width of the finger, while the transmission between the motor and J_1 is carried out by means of a timing belt.

5.2 Sensitive Active Surfaces

The conveyor belt depicted in Fig5.6 of the Velvet II comprises a driver cylinder, a driven cylinder and a support roll. Since the performances of the conveyor belts of the final version of the Velvet Fingers are satisfactory also for the Velvet-II, the driver cylinder is the same as the one employed in the former gripper. The driven cylinders permits to properly preload the belt thanks to slots on the frame. The belt wraps around the driver and the driven cylinders and is supported in between the cylinders by a small idle roll. The frame supporting the conveyor belt components is screwed to the tool-plate of the F/T transducer.

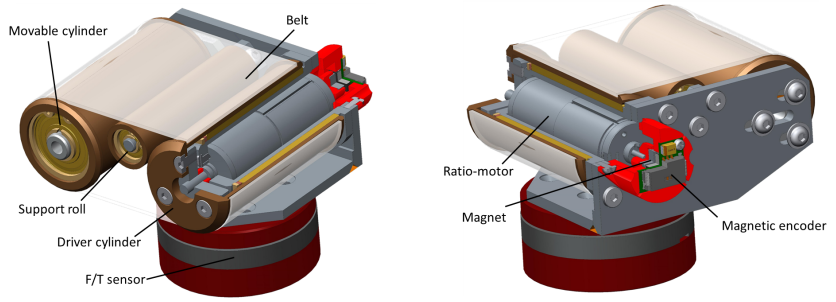

(a) (b)

Figure 5.6: SAS physical implementation. The picture refers to the SAS of the distal phalanx of the Velvet II. The belt winds around a driver cylinder and a driven cylinder. A central idle roll supports the belt on the upper side. An AS5045 Austriamicrosystem magnetic encoder reads the angular position of the motor shaft. The ratio-motor, embedded in the driver roll, is a 4.5W Maxon RE-MAX brushed DC motor with a 84:1 gear-head.

The sensor is a custom 6 axes transducer using a CAN bus line to transmit data in digital form. The frequency of data acquisition is 1kHz and it allows a fine and rapid control of the grasping forces. Forces and

torques that occur in this application fall into the measure range of the transducer with a large margin of safety. The mechanical solution of the sensor is quite compact despite containing all the signal conditioning electronics and the micro-controller for communication and it fits with the size of the phalanges. Tab.5.1 reports the main specifications of the transducer.

Finally, a magnetic encoder monitors the angular displacement θ_m of the rear shaft of the motor, which is related to the displacement of the belt x through the following equation:

$$\Delta x = R_c n_m \theta_m \tag{5.4}$$

where R_c is the radius of the cylinders, n_m is the reduction ratio of the motor.

Table 5.1: Main specifications of the custom F/T transducer

Specification	**Value**
Measure range	$2000N$ (Fx, Fy, Fz) $40Nm$ (Tx, Ty) $30Nm$ (Tz)
Resolution	$0.25N$ (Fx, Fy, Fz) $0.049Nm$ (Tx, Ty) $0.037Nm$ (Tz)
Output data	16 bit, 6 channels, up to 1kmessages/sec
A/D converter	16 bit, $250ksps$
Dimensions [ϕ, H]	45x18mm
Weight	$122g$

Since the custom F/T sensors were not available at the time of the assembling the gripper, preliminary tests with a module of SAS were carried out with the experimental set up represented in Fig.5.7 which makes use of a commercial F/T sensor (ATI-Gamma). The sensor, which communi-

cates with the PC over an RS-232 serial port. A custom electronic board with an embedded PSOC3 micro-controller, controls the actuator and communicates with the higher level control (a PC with Matlab/Simulink) through an USB interface.

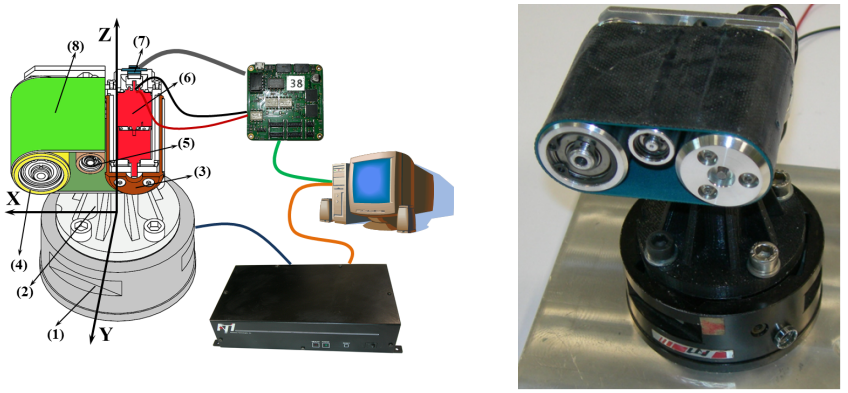

(a) (b)

Figure 5.7: The experimental set up formed by a small conveyor belt mounted on an ATI-Gamma F/T transducer (1), by means of the interface (2). The F/T sensor communicates with the PC over an RS-232 serial port. A PSOC3 micro-controller embedded in a custom electronic board, controls the actuator in a control loop closed on the angular displacement of the motor.

5.2.1 Contact point location

In this section several preliminary contact point experiments are described aimed to validate the contact point algorithm explained in detail in Appendix A. Since the following experiments are performed with an edged tool to have a limited contact area approximable to a point, they were conducting assuming negligible the torque exerted by the tool perpendicular to the surface. The geometrical portion of the belt involved in a possible contact with a grasped object is formed by a plane corresponding

to the outer conveyor belt surface and two cylindrical surfaces associated with the belt rollers (see indicators (3), (4) and (8) in Fig.5.7). Since the sensing surface is convex, the contact point location and the corresponding applied wrench can always be computed from the F/T sensor readings ([65]).

In the first experiment we tested the capability of the SAS to track the trajectory of the contact point which moves on the belt. For this purpose, the greeting "HI" was previously written on the upper plane of the belt with the aid of a ruler as visible in Fig.5.8 a), then the text was followed manually with a sharp tool. The estimated trajectory by the contact point algorythm is shown in Fig.5.8 b) where the units are expressed in mm.

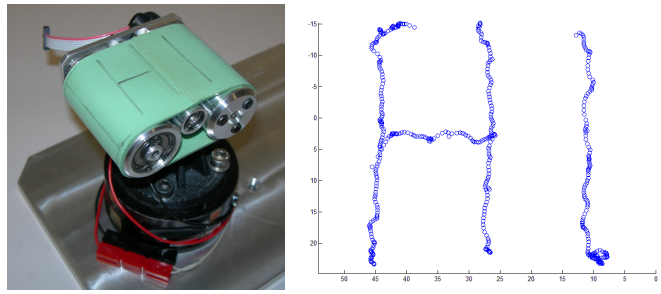

(a) (b)

Figure 5.8: On the left, the conveyor belt with the greeting "HI" drawn on it. On the right the reconstructed trajectory obtained by manually tracking the text with a tipped object.

In the next experiment a straight line was traced on the upper plane with a guide located over the belt. The purpose of this experiment is to compare the trajectory estimation when the motor is off and when the belt is actuated. The pictures in Fig.5.9 show the straight lines estimated with the motor on and off; on the left, the motor was off and the belt still,

conversely, on the right, the line was traced as the belt moves. Comparing the two pictures, there are not any substantial influence of the motor actuation on the trajectory estimation with the contact point algorithm.

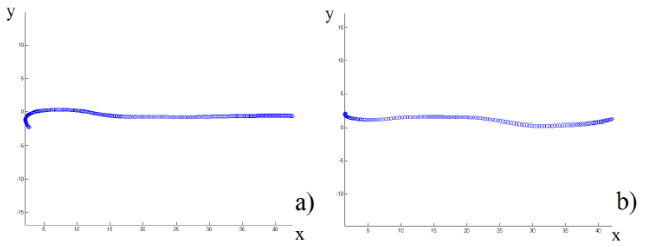

Figure 5.9: Trajectories traced with the contact point algorithm when the belt was still, on the left and when the belts was actuated, on the right (units in mm). The movement of the belt under the tool and the vibrations induced by the motor do not affect much the trajectory estimation.

The purpose of the next experiment is to validate the algorithm over the three geometrical portions forming the SAS: the plane and the two cylindrical surfaces. To this end, a random and continuous trajectory was traced with a tipped object over the three parts of the belt, from the left cylinder to the right cylinder through the upper plane. The trajectory does not have evident discontinuity signs, even on the transition zones between two adjacent portions (see Fig.5.10). Similarly, in Fig.5.11, the perimeter of the active area of the SAS where contacts occur, was followed and then tracked by the algorithm.

In general, the accuracy of the contact point estimation depends on the precision and resolution of the F/T sensor utilized. In our applicative case, the surface on which an external wrench can be applied is a deformable mechanical component: a belt of polyurethane. Therefore the exact geometry of the surface depends on the external forces and this fact constitutes a source of error. However, the magnitude of the error due to the compliance of the belt can be contained by tightening it.

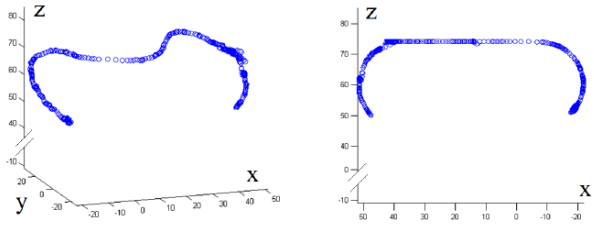

Figure 5.10: Estimation of a random and continuous trajectory all over the external surface. The traced trajectory does not have evident signs of discontinuity between the cylinder and the upper plane.

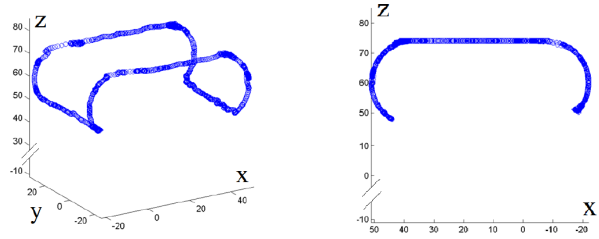

Figure 5.11: Perimeter of the active area of the SAS traced by the algorithm.

In order to estimate the accuracy of the contact point algorithm, an external wrench was applied to a known point on the surface with the edge of a tool and the response of the algorithm compared with the actual contact point location. The next two pictures show the trade of the estimated coordinates of a given contact point in time on the plane and on the driven cylinder. The actual values of the coordinates are indicated by a green line and the red lines define the upper and lower displacement of the output (in blue) respect to the real value.

Several tests performed on different points all over the SAS indicated a magnitude of the error contained in $\pm 2mm$ for the linear dimensions and $\pm 3°$ for the angular dimensions.

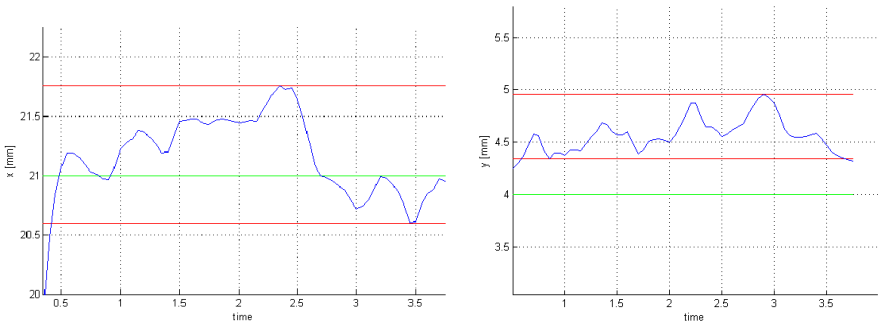

Figure 5.12: Estimated coordinates of a given contact point on the plane. The green line represents the real coordinates in the local reference frame of the plane: $x = 21mm, y = 4mm$. The red lines define the range in which the output (in blue) is contained. (See Appendix A for the local reference frame definition).

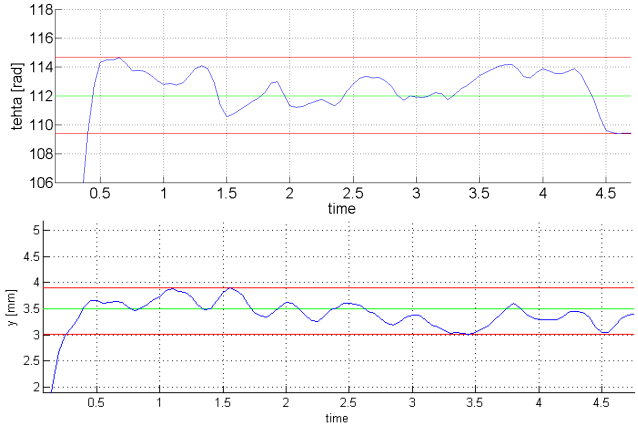

Figure 5.13: Estimated coordinates of a given contact point on the driven cylinder. The green line represents the real coordinates in the local reference frame of the driven cylinder: $\theta = 112°, y = 4mm$ (See Appendix A for the local reference frame definition).

5.2.2 Variable friction coefficient control of the SAS

In this section we first present the variable friction coefficient control implemented on the SAS of the Velvet-II and afterward we discuss several experiments aimed at validating the control algorithm. The variable friction coefficient control is built upon the same simplifying assumptions adopted in the Active Surfaces of the Velvet Fingers (Sec.3.4.2). It is a reformulation of the computational model of friction presented in Sec.3.4.2 aimed at improving the performances of the Active Surfaces and at emulating the friction coefficient rather than the friction force as in the Velvet Fingers. Two important modification are introduced into the system 3.15:

1. the saturation of the tension $V(i)$ at the motor is expressed in terms of the desired friction coefficient μ^* and the normal force component F_N on the external active area of the SAS, which is computable given the response of the F/T sensor and the geometry of the surface where the point of contact occurs (see Appendix A for for the calculation of Fn)

2. the internal parasitic friction is compensated by supplying a proper additional amount of tension at the motor.

The voltage supplied to the motor is comprised of two terms:

$$V(i) = V^*(sgn(Ft)) - V_H(f^*, Fn, \theta_m(i))). \tag{5.5}$$

The first addend V^*, which was empirically established, is the tension necessary to compensate the internal friction of the conveyor belt system due to the friction inside the ratio-motor, on the rotating components, friction from the sliding of the belt on the guide edges of the cylinders and other minor losses of energy. Given an external tangential force Ft acting on the belt, whose direction can be determined as described in Appendix

A from the output of the F/T sensor, a tension V^* (with the proper sign according with the direction of the tangential force) can be supplied to the motor to drive it in incipient motion. In this fashion, theoretically, any $Ft > 0$ is able to drive the device in retrograde motion. The term V^* constitutes an improvement with respect to the control implemented in the Velvet Fingers since it allows to achieve very low fictitious coefficient of friction. This improvement is here feasible since the direction where to compensate the internal friction is now available from the output of the F/T sensor.

The second addend V_H is simply a re-formulation of the last equation of system 3.15. It can be made explicit with respect to the desired coefficient of friction f^* and to the outputs of the F/T sensor and the encoder at the rear shaft of the motor as explained in the following. Given the stiffness K_s, the maximum elongation of the virtual spring z_{max} can be now expressed as $z_{max} = f^* Fn/K_s$; it is now function of the coefficient of friction f^* and and the normal force components Fn which in general is variable in time.

Expressing the displacement of the belt x and the reference position w as function of the angular position θ_m of the rear shaft of the motor as:

$$\begin{aligned} x &= R_c n_m \theta_m \\ w &= R_c n_m \theta_{ref} \end{aligned} \tag{5.6}$$

where R_c is the radius of the cylinders of the SAS, the system 3.15 can be reformulated as follows:

$$\begin{cases} \theta_{ref}(i+1) = \begin{cases} \theta_m(i) - \frac{f^*Fn}{k_s n_m R_c} & \text{if} \quad n_m R_c(\theta_m(i) - \theta_{ref}(i)) > z_{max} = \frac{f^*Fn}{k_s} \\ \theta_{ref}(i) & \text{if} \quad |n_m R_c(\theta_m(i) - \theta_{ref}(i))| < z_{max} = \frac{f^*Fn}{k_s} \\ \theta_m(i) + \frac{f^*Fn}{k_s n_m R_c} & \text{if} \quad n_m R_c(\theta_m(i) - \theta_{ref}(i)) < -z_{max} = -\frac{f^*Fn}{k_s} \end{cases} , \\ \\ V_H(i) = \frac{k_\tau n_m}{R_c R} K_s SAT_{-\frac{f^*Fn}{K_s}}^{\frac{f^*Fn}{K_s}} \left(R_c n_m \left(\theta_m(i) - \theta_{ref}(i)\right)\right) \end{cases} \tag{5.7}$$

In the system the first block is the updating of the virtual reference θ_{ref} and the last equation constitutes the second contribution of Eq:5.5 at the sampling time i. Here, the variables Fn and $\theta(i)$ come from the F/T sensor and the encoder respectively and the desired coefficient of friction f^* is set by the user.

The variable friction experiments are performed in two different conditions: applying a constant tangential force to an object lying on the surface and applying a variable force in time. The first experiment is directed to assess the accuracy of the emulated friction coefficient with respect to the one actually obtained. To carry out this assessment we utilized the experimental set up shown in Fig.5.14.

The experiment is performed placing an object of mass M_1 on the belt and applying to it a constant tangential force along the direction of the Dof of the SAS. To exert a constant tangential force, a wire is horizontally linked to M_1, wraps a round a pulley and at the vertical segment of the wire a second object of mass M_2 is hung as visible in Fig.5.14. The weight of the latter object is equal to the applied constant tangential force. With this set-up, after providing the motor of the tension V^* and setting a desired coefficient of friction f^*, if M_2 is large enough to bring M_1 in the process of moving, the ratio between the tangential force and

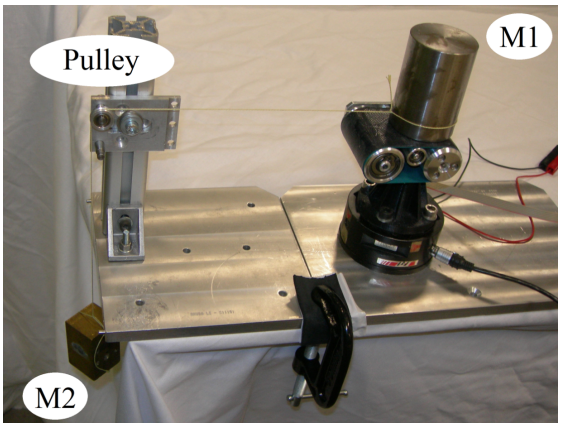

Figure 5.14: Experimental set up for the accuracy assessment of the emulated friction coefficient

the normal force on the SAS is equal to the coulombic friction coefficient $f = M_2/M_1$ "perceived" by the object on the belt. The correspondence between the ratio of the masses f and the desired friction coefficient f^* was estimated following the procedure described here. A set of masses M_2 were selected. For each mass M_2, the value of f^* was decreased in the algorithm from a high value (large enough to prevent any movement of the mass on the belt) until achieving a continuous movement of M_1. Then the corresponding values f and f^* were reported in a diagram $f - f^*$. The result of the experiment is reported in Fig.5.15. The green line, which bisects the first quadrant of the graph, is the ideal line representing the ideal match between the emulated friction and the ratio of the masses. The red line is the regression line which interpolates the results of the experiment (the blue dots) whose equation is $f^* = 1.024f - 0.037$. The red line is almost parallel to the green one and it is vertically shifted of 0.037 towards the negative values with respect to the latter. Given a ratio of the masses, for instance $f = 0.3$ indicated by the vertical blue line, the

mass M_1 moves imposing a lower value of the emulated friction (about $f = 0.26$). The shifting of the regression line with respect to the green line is the result of the necessity to reserve a little margin from a complete friction compensation to avoid undesirable movements of the belt.

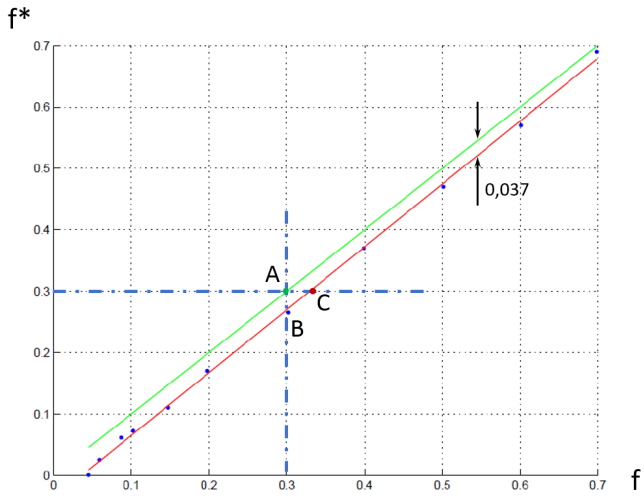

Figure 5.15: Graph of the evaluation of the error in the friction coefficient emulation. The green line is the bisector of the first quadrant and represent the ideal match between the actual and the emulated friction. The red line is the linear interpolation of the results of the experiment.

Another implication of the shifting of the regression line is that there is a lower limit (around 0.05) of the friction coefficient which can be emulated. However, the lower bound of the emulated friction is considerably low and does not depend on the mass of the object lying on the belt as in the Velvet Fingers. The sequence in Fig.5.16 shows a big cylinder in steel on the SAS dragged by a mass twenty times smaller ($\mu = 0.05$).

The following experiment is aimed at validating the emulation of an imposed coefficient of friction f^* in presence of a variable wrench applied to the SAS. In this situation, the movement of the belt is triggered any-

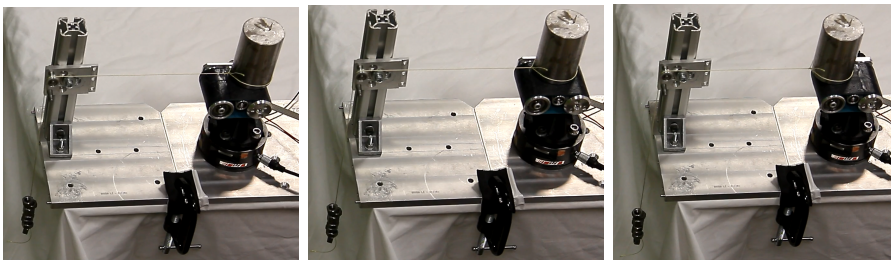

(a) (b) (c)

Figure 5.16: The sequence shows a big cylinder in steel on the SAS dragged from position a) to position b) by 7 small nuts. The total mass of the nuts is twenty times smaller than the mass of the cylinder ($f = 0.05$)

time the ratio between the tangential component Ft (along the direction of the DoF of the belt) and the normal component Fn of the external wrench overcomes f^*. The experiment was performed setting off-line a desired friction coefficient f^* (in the case reported on here $f^* = 0.2$) and afterwards a randomly variable external wrench was applied manually with a tipped tool on the SAS. Fig.5.17 shows the trend of the point of contact location x and the ratio Ft/Fn in time (the contact point location and the components of the wrench are calculated with the contact point algorithm). In Fig.5.17 the shaded rectangles indicate the time intervals in which Ft/Fn is smaller than the emulated friction coefficient. In these intervals the friction force prevents the displacement of the contact point and x maintains constant. On the contrary, out of the shaded rectangles Ft/Fn is larger than the emulated friction coefficient and the contact point moves. However when x changes, the exerted tangential force on the SAS can be larger than the emulated friction force, as can be seen in the graph. This is possible because of the inertia of the conveyor belt which have to be driven in a retrograde motion by the tangential component of the external wrench and the virtual damping effect due to

the uncompensated counter electro-motive force.

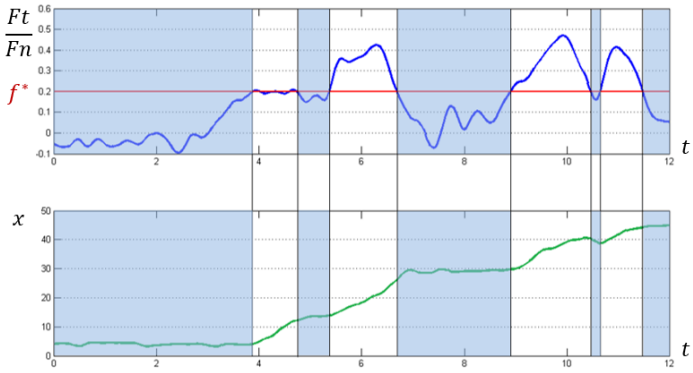

Figure 5.17: Trend of the contact point location under a randomly variable external wrench. In the shaded rectangles the ratio Ft/Fn is smaller than f^* and x does not change. Out of the rectangle Ft/Fn is larger than f^* and the belt moves.

Variable friction control can be utilized to let the object passively reach a pose were the stability is locally maximal. Indeed, sometimes after the pull-in strategy, a cylindrical object (for example) is not well centered because of the resistance offered by the belts and contact can occur on two points only as depicted (exaggerated) in Fig.3.9 a). An active compliant control does not solve the problem because a robust grasp with four contact points depends on the diameter of the object (for cylindrical parts) and therefore the necessary displacement of the belt is unknown. A more traditional way to improve the robustness of the grasp might be to squeeze the object more in order to overcome resistance of the belts. However, this might be risky for the integrity of the object. On the contrary, variable friction control (imposing low friction) might allow for a more robust grasp without increasing the grasping forces by letting the object passively find the most robust configuration inside the gripper.

5.3 The Velvet II: physical implementation

In this section an overall description of the mechanical implementation of the Velvet-II, the electronics and sensors on board is provided. The Velvet-II has many common traits with the Velvet Fingers in terms of its kinematic structure. As in the Velvet Fingers, three main parts can be discerned in an overall view like the one depicted in Fig.5.18. A palm, that is the fixed part of the gripper and can be attached at the wrist of a manipulator through a proper interface, and two facing fingers forming a rotary-rotary planar manipulator each, which constitute the jaws of the gripper. Each finger comprises a distal and a proximal phalanx on which the SASs are mounted. Given the specifications and for the sake of dimension we decided to utilize one small motor for each finger rather than one bigger motor and a transmission chain to simultaneously drive the fingers. The gripper has three electronic boards on board, the same described in Sec.4.3. The SASs of each finger have a dedicated electronic board while the board on the top of the palm drives the motors of opening/closing.

The indicated dimensions in Fig.5.19 reveal the small size of the device. The active surfaces of each finger cover a total area of 50 mm wide and 150 mm long with a gap between two consecutive SASs $g_1 = g_2 = 3mm$ (see Fig.5.3 for the meaning of the notation). When fully open the gripper is 303mm wide, 133mm high and 135.5mm long with a mass of about 3kg. The high thickness of the phalanges is due mainly to the dimensions of the 6-axis sensor and to reduce it, sensors of smaller size should be utilized, which however restricts considerably the applicable loads and increases the overall cost.

Fig.5.20 shows a CAD model of the gripper in a tip grasp of a pencil and an enveloping grasp of a can.

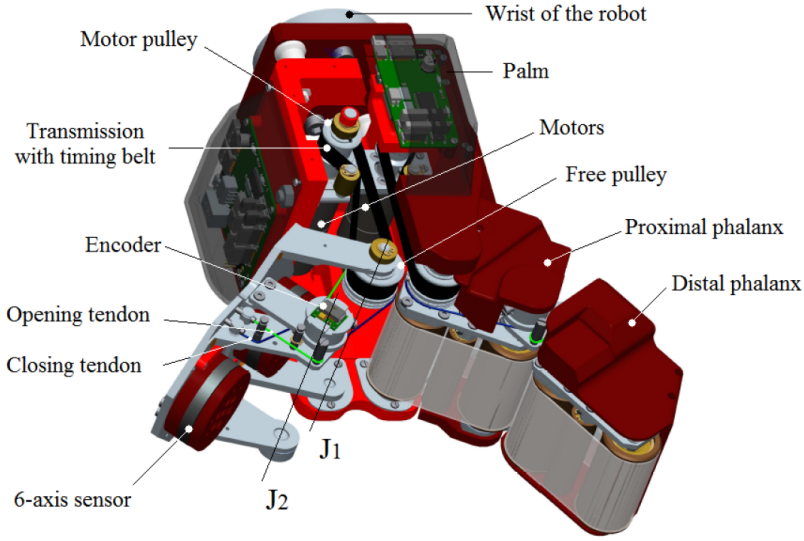

Figure 5.18: Overall view of the Velvet-II. Three main parts can be discerned: a palm, that is the fixed part of the gripper and two fingers with independent SASs on the distal and the proximal phalanges. Each finger is independently driven by a ratio-motor housed in the palm. The transmission chain is formed of a toothed belt from the motor shaft and the idle pulley on the first joint and of tendons between the joints of the finger.

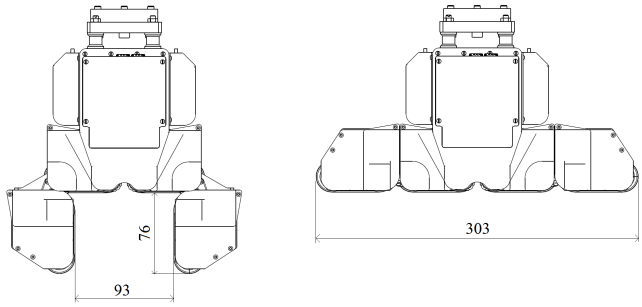

Figure 5.19: Two different postures of the gripper, with some significant dimensions.

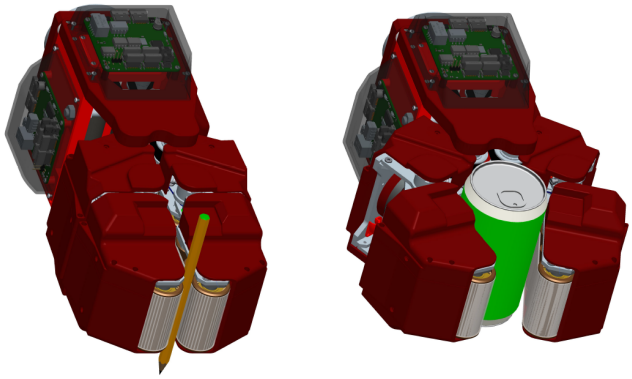

Figure 5.20: Cad design of two grasps: a tip grasp of a pencil on the left and a power grasp of a can on the right.

5.3.1 The fingers

Fig.5.21 shows an assembled finger without the active surfaces and the covers, where all the main components are visible except the spring at the second joint for the sake of clarity. F/T transducers (1) and (2) are screwed at the frame of the distal and the proximal phalanx. The finger is driven by a timing belt (not visible in this picture) that engages idle pulley (7), on first joint J_1. Integral with (7) is pulley (6) for tendons (3) and (4) which are tensioned in closing and opening respectively. They are anchored at pulley (6), wrap around second joint J_2 and are fixed to anchor pins (p1) and (p2), that provide the proper pre-load to the tendons compensating errors in their length. Pins (p3) and (p5) guide the tendons around J_2 and direct them to anchor pins (p1) and (p2). An extension return spring around the second joint is fixed, at one end, to pin (p6) integral with the proximal phalanx and, at the other end, to pin (p4) integral with the distal phalanx and maintain the links aligned in free opening and closing. When the proximal phalanx is blocked by an object keeping on powering the motor, idle roll continues to rotate,

turning the distal phalanx around J_2 as the spring elongates. The angular displacement of the distal link around J_2 is monitored by magnetic encoder (5).

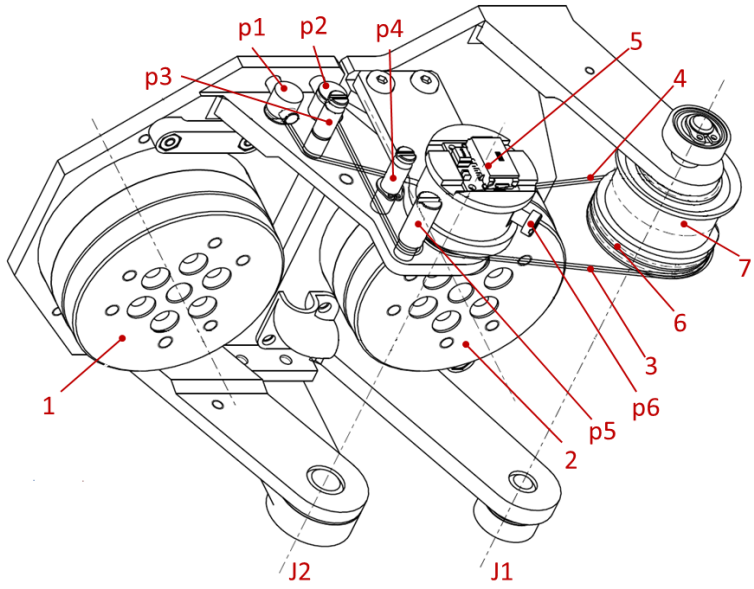

Figure 5.21: A drawing of a finger of the Velvet-II without the conveyor belts and the covers with indicated the main components. For the sake of clarity the spring at the second joint is omitted.

The transmission with tendons has the advantage to occupy a little space but, unlike the timing belts, they need anchors and their stroke is limited. The tendons are made in polyester with a flexible abrasion resistant cover easy to splice, a diameter of $1mm$ and a high breaking strength of $195kg$. Fig.5.22 shows the paths of the tendons which ensure them to be in contact with the guides of the joints in any configuration of the finger and the maximum angle of winding θ_1 and θ_2 which occur when the finger is completely extended and the links are aligned. Since

$q_2 \in [0, 2\pi]$, the maximum angle of winding around the second joint of the red wire θ_2 must be larger than $\pi/2$ ($\theta_2 > \pi/2$) to guarantee the contact with the pulley over the entire stroke of the link around J_2. When $q_2 = \pi/2$ the maximum angle of winding around the first joint of the blue wire reduces of r_2/r_1 times $\pi/2$ hence θ_1 must be larger than $\frac{\pi r_2}{2r_1}$ ($\theta_1 > \frac{\pi r_2}{2r_1}$). Referring to Fig.5.22, the red tendon is tensioned in closing and grasping, conversely the blue wire is charged in opening and releasing.

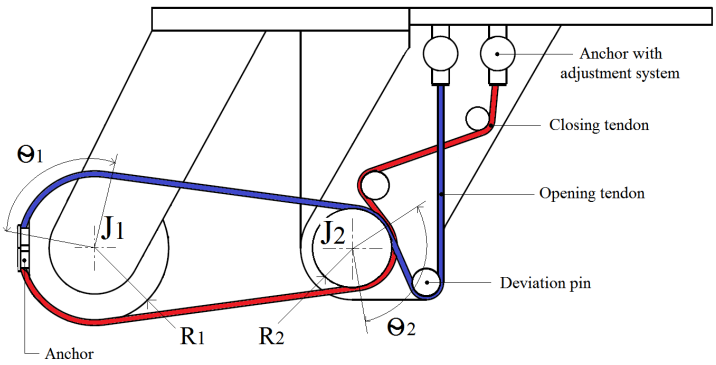

Figure 5.22: The paths and the winding angles of the tendons which transmit the torque from the idle pulley on the first joint to the distal phalanx. The red tendon is tensioned in closing and grasping and the blue tendon in opening and releasing.

The transmission ratio between the first and the second joint $r_1/r_2 \approx 1.86$ satisfies the constrain 5.4 and ensures the straightening of the fingers when the fingertips meet. Indeed, given the length $L_0 = 16mm$, $l_1 = 45mm$ and $l_2 = 75mm$ of Fig.5.4, the function $c(a)$ has a maximum in a range of a compatible with the dimension of the gripper which corresponds to a ratio around 1.62. Fig.5.23 shows the trend of the function $c(a)$.

Fig.5.24 shows the mechanical details of the first and the second joints. Fig.5.24 a) shows the coupling of the toothed pulley for the timing belt

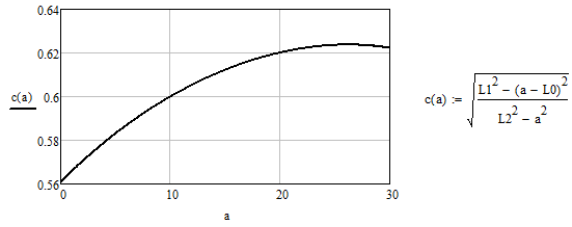

Figure 5.23: Trade of the function c(a) for the Velvet-II.

and the pulley for the tendons with the anchor pins. The coupled pulleys are mounted free to turn on the pin of the joint. In Fig.5.24 b) is depicted the pin of the second joint forced in the frame of the distal phalanx and the encoder fixed on the arm of the proximal phalanx.

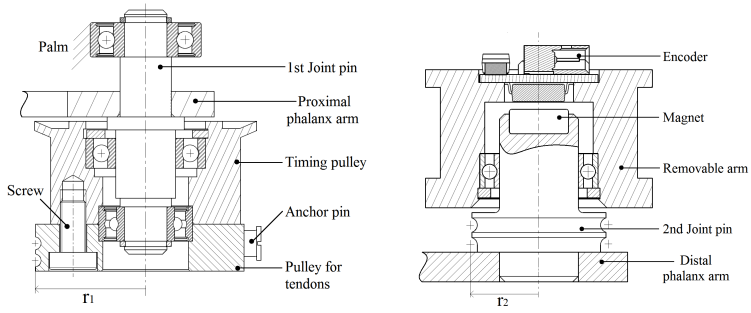

(a) (b)

Figure 5.24: On the left a drawing of the idle pulley mounted on the pin of the first joint. The toothed pulley of the timing belt and the pulley for the tendons are made integral by screws. On the right depicted is the pin of the second joint with the slots for the tendons and the magnet for the encoder on the top.

To anchor the extremities of the tendons at the pins, they must be prepared utilizing the splicing, that allows to carry out eyelets at the ends of the wire with a rather precise center-to-center distance, as shown in Fig.5.25.

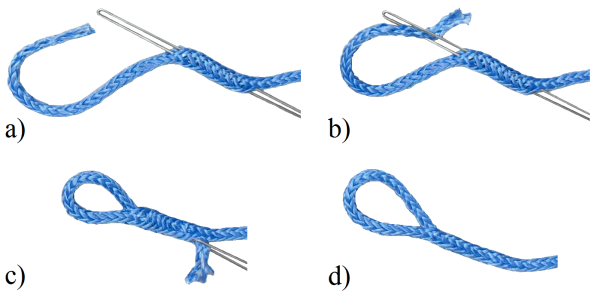

Figure 5.25: A sequence of the splicing procedure to prepare the eyelets at the extremities of the tendons with the aid of a thin steel wire bended on oneself.

The parts of the fingers which are welded, that are the frames of the phalanges, are made in Aluminum AlSi1MgMn (EN AW 6082) (trade name: Anticorodal6082-UNI9006/4) for the suitability of the material to be welded. The other parts are made in AlZn5,5MgCu (EN AW 7075) (trade name: Ergal55-UNI9007/2) that is mechanically more resistant. Moreover the parts which further demand high mechanical resistance like the pins and the anchor pins of the springs are made in stainless steel AISI-316 UNI EN 10028-7.

5.3.2 Palm

Fig.5.26 shows the palm of the Velvet-II. In this picture the upper plates are cut to show the components inside the palm. Moreover the covers, the electronic boards and the timing belts are omitted for the sake of clarity. Motor (1) and (2) are ratio-motors $DCX22S$ with a supply voltage of $24V$, power $14W$ and with a planetary gear-head $GPX22C$ of transmission ratio $231:1$ (by *Maxon Motor Company*) which drive one finger each. Tab.5.2 reports the specification of the employed ratio-motors. The timing belt, properly tensioned by tighteners (3), transmits power from motor pulley (4), directly keyed on the axis of the ratio-motor, to the

pulley at the first joint with a transmission ratio $\tau \approx 1.5$. Angular displacements of the motor shaft are monitored by magnet (5) and magnetic encoder (6).

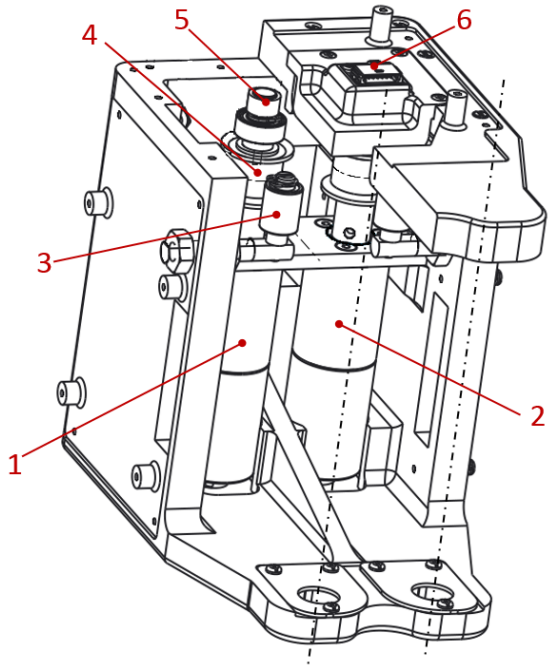

Figure 5.26: An inside view of the palm of the Velvet-II. The carter and the upper plates are made in ABS (Acrylonitrile Butadiene Styrene).

Table 5.2: Characteristics of the motor DCX22 *and the gear head* GPX22C.

Motor specification	**Symbol**	**Value**
Maximum continuous torque	τ_m	0.0154 Nm
Maximum power	Pot	14 W
Maximum speed	n_m	12400 rpm
Efficiency	η_m	86 %
Moment of inertia	J_m	$5.2 \cdot 10^{-7} kgm^2$
Gear-head specification	**Symbol**	**Value**
Reduction ratio	i_g	231:1
Number of stages	n_g	3
Efficiency	η_r	74%

5.4 Grasping experiments

As previously said the gripper is built with the frame of the fingers in Aluminum while the palm and some non-structural parts on the fingers are in *ABS* (Acrylonitrile Butadiene Styrene) printed by a rapid prototyping machine using the *FDM* technique (Fused Deposition Modeling). Fig.5.27 is a picture of the Velvet-II without the covers. Since at the time of assembling the F/T sensors were not yet available, they were replaced with four spacer in *ABS* (the red cylinders between the conveyor belts and the frame of the phalanges in the picture).

Some preliminary experiments on grasping, performed with a simplified control (with a PID embedded in the electronics, without resorting to any kind of impedance control), show the adaptation capability of the gripper to small objects which can be associated to primitive shapes like

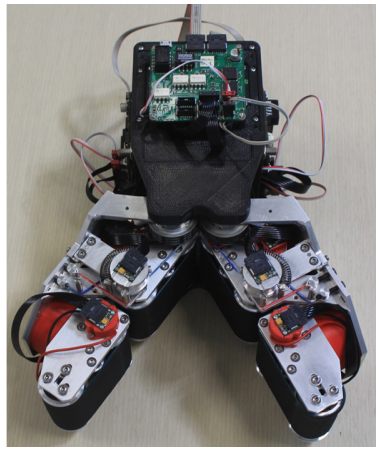

Figure 5.27: A picture of the Velvet-II.

cylinders parallelepipeds, cubes and spheres as can be seen in Fig.5.28.

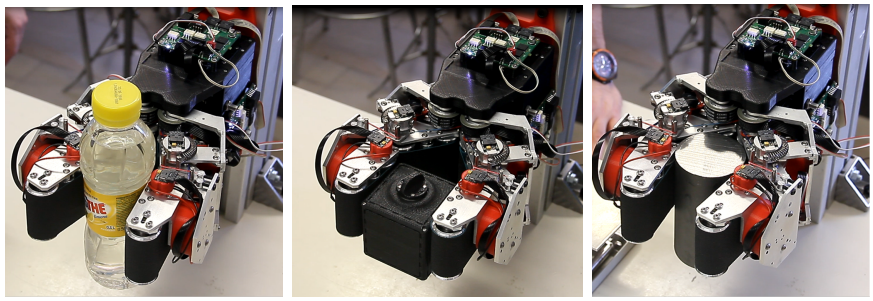

(a) (b) (c)

Figure 5.28: The object grasped are: a bottle of 0.5 liter, a cube and a cylinder made of steell with a weight of about $2.5kg$

In a final set of experiments, we used the SAS in a preliminary investigation of the contact forces occurring in incipient slippage conditions. Gunji et al. [64] observed a significant decrease of the grasping force (detected by a tactile sensor) immediately before the slip displacement of a

pinch grasped object. Our experiments have been conducted in power grasp configurations by slowly decreasing the internal grasp force until the grasped object slipped. As shown in Fig. 5.29 and Fig. 5.30, which refer to the grasping of a battery and an hammer, dropping the object is predated by a rapid redistribution of the components of the total grasping forces on each phalanx of the gripper, highlighted in the graphs with shaded areas.

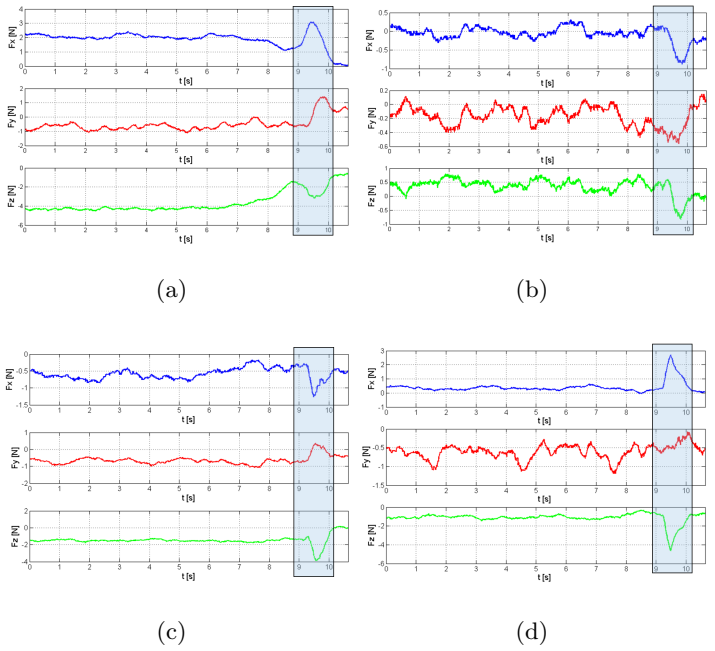

Figure 5.29: Sliding experiments of a grasped battery. Every graph is relative to a phalanx of the gripper and in every graph the Fx, Fy, Fz components are shown. In the pale blue rectangles the redistribution of the forces is clearly evident.

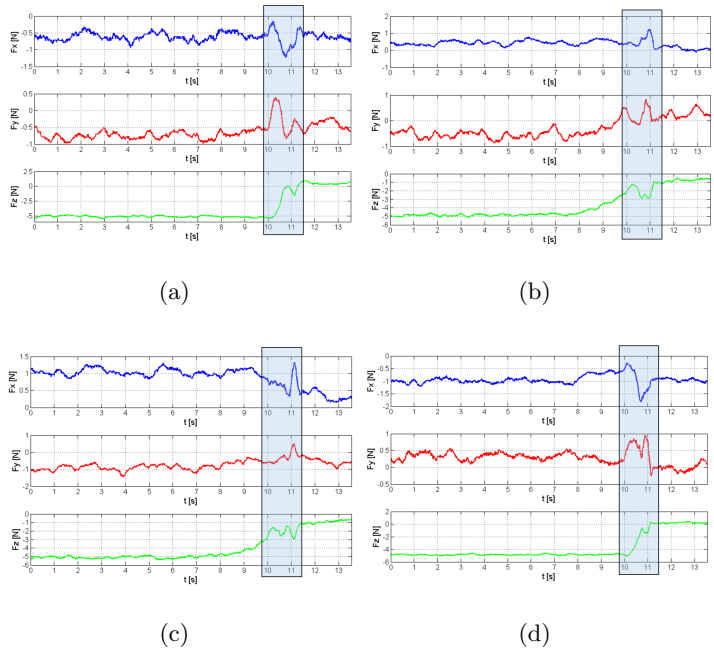

Figure 5.30: Sliding experiments of a grasped hammer. Every graph is relative to a phalanx of the gripper and in every graph the Fx, Fy, Fz components are shown. The pale blue rectangles highlight the force redistribution in the pre-sliding phase.

5.5 The Velvet-II on an autonomous picking and palletizing platform

In this Section the Velvet-II is utilized as gripping device on a research platform for fully autonomous commissioning tasks from storage compartments in warehouses, developed in collaboration with AASS Research Center, of the University of Örebro (Sweden) within the the KUKA Innovation Award 2015. My contribution in this project was mainly the setup of the hardware devices, the tuning of the grasping control parameters and the performing of the test runs. The need for automating this typol-

ogy of task, lies in the general trend of humanizing workstations, relieving operators to the dull and strenuous nature of commissioning which might cause mental and physical illness in human workers [66].

There exist partial solutions for the automated commissioning problem in controlled environments. The system described in [67] coordinates a fleet of Autonomous Ground Vehicles (AGVs) which transport shelves filled with goods to a human worker who picks the corresponding objects to complete the order. The key obstacles for a fully automatized solution applicable in general warehouse settings can be summarized in the following two bullet points:

- the safe cooperation with humans in industrial environments
- the autonomous grasping/manipulation of unstructured goods at satisfactory cycle times

During the course of this project we tried to address these problems, providing a preliminary solution of a safe and autonomous pick and palletizing platform.

The Autonomous Picking & Palletizing (APPLE) research platform (see Fig. 5.31) which we developed to accomplish the following sub-task chain which occurs during commissioning in prototypical warehouses: **i)** autonomous picking of goods from a storage location, **ii)** subsequent placement on a standard EUR pallet and **iii)** transport of the filled pallet to a target location. Furthermore, this process has to be carried out in a manner which is safe for humans operating in the same environment. The platform's mobile base consists of a retrofitted nonholonomic Linde CitiTruck forklift AGV [69] which is able to detect and pick up pallets in designated loading zones. A KUKA LBR iiwa [70] lightweight arm which is fitted with the Velvet-II is used for robust grasping and object manipulation. The next Section describes the autonomous forklift.

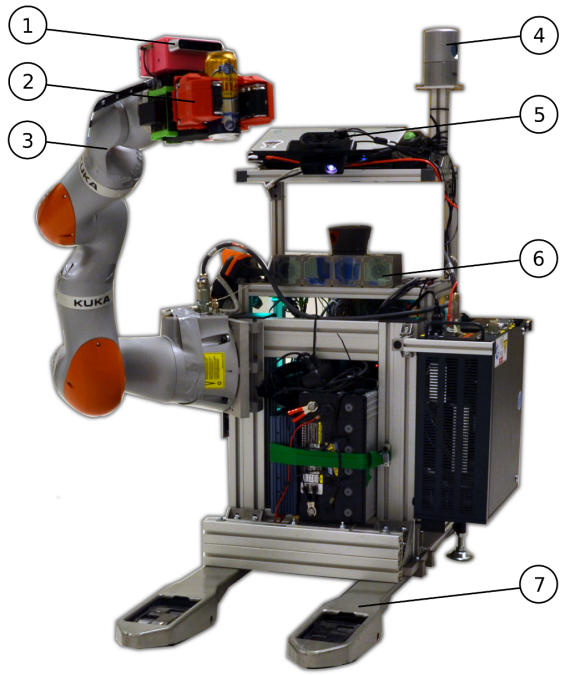

Figure 5.31: The APPLE platform. A KUKA LBR iiwa arm (3) with the Velvet-II (2) on its wrist is mounted on a retrofitted Linde CitiTruck AGV (7). For localization, a Velodyne HDL-32 Lidar (4) is used, human co-workers are detected with our RefleX camera system (6) presented in [68]. In order to detect pallets, we employ an Asus Xtion Pro Live structured light camera (5). Object detection is done with a Structure IO device (1) which is mounted on the gripper's palm.

5.5.1 Autonomus forklift

The mobile base is built upon a manual forklift which originally was equipped with motorized forks and a drive wheel only. The forklift has been retrofitted with a steering mechanism and a commercial AGV control system which is used to interface the original drive mechanism as well as the steering servo. To assure safe operation, the vehicle is equipped with a SICK S300 safety laser scanner [71] and an industrial prototype system

for detecting human workforce using reflective safety vests as described in the following.

Challenges in Autonomous Navigation

The industry standard for autonomous navigation of forklifts is to use pre-defined trajectories which are either manually defined or learned through teaching-by-demonstration from a human operator [72, 73]. Although conceptually simple, pre-defining trajectories limits pallet handling to occur only at pre-defined poses. In addition, only overly simple strategies for handling unforeseen obstacles can be applied. The fundamental difficulties of motion planning for a forklift lie in the nonholonomic constraints and the large sweep area it needs to occupy while operating in a limited work space.

In order to obtain reliable localization in large dynamic warehouses with high accuracy, it is common to mount reflectors in the environment and to use a dedicated sensing device [74]. This approach provides reliable navigation in smaller facilities where walls are commonly observed. However, without additional infrastructure, navigation in large and dynamic environments remains a challenge.

Navigation

The navigation module ensures that the forklift is capable of moving safely and autonomously through the work space environment to arbitrary load/unload poses with high accuracy. According to the AGV system provider Kollmorgen [75], the required end pose accuracy for picking up pallets is ± 0.03 m in position and ± 1 degree in orientation. The navigation module comprises trajectory generation, tracking control and a localization system.

The online trajectory generation is done in two steps. First, a kinematically feasible path with discretized start and goal poses is generated using a lattice planner [76]. Second, this path is post-processed using a path smoother [77] which assures a smooth, collision-free and continuous trajectory, which allows to drive the vehicle with high accuracy. Subsequently, the obtained trajectory is driven using a model predictive tracking controller. For localization, a Velodyne HDL-32 3D laser scanner [78] is utilized to construct a 3D map (using the 3D-NDT-OM map representation) of the static parts of the environment [55]. The map and odometry information is then used to localize the vehicle in the presence of dynamic entities using a dual timescale approach [79]. The complete navigation system has been implemented, extensively tested and successfully integrated on the APPLE demonstrator. A detailed description can be found in [77].

The current system for pallet detection and pickup requires a rough estimate of the location of the pallet (*i. e.*, a pre-defined pickup zone). In order to compute the final pose based on sensory data from an Asus Xtion Pro Live [80] mounted on the AGV, a Signed Distance Function (SDF) tracker [60] is used with a given SDF model of the pallet. The tracking is done while driving towards the pickup zone and the trajectory is recomputed on the fly which, depending on the pose offset, may include a reverse driving operation.

Human Detection

As the envisioned mobile manipulation system will operate in environments shared with human workforce, robust human detection is crucial to ensure a safe work environment. We address this problem by using the recently developed RefleX workforce protection system [68]. RefleX is a camera-based safety system designed for industrial vehicles and machin-

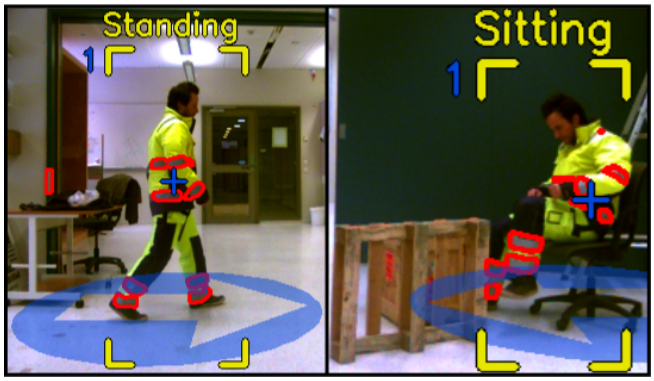

Figure 5.32: For safe navigation, the robot detects and tracks humans in the close neighborhood, estimates their position, and infers body pose information. Active infrared vision in combination with reflective safety clothing ensures robust performance independent of the illumination conditions.

ery, that detects and tracks human workers wearing off-the-shelf high-visibility clothing (Fig. 5.32). Using active near-infrared stereo vision, RefleX detects and locates the reflective markers on the safety garments in order to estimate position and relative velocity of the observed person, and to infer further body pose information. The underlying sensing principle thereby ensures that the detection performance is nearly independent of external illumination conditions. A classification of the observed reflective patterns further allows the APPLE system to discriminate between a worker's safety garments and other reflective navigation markers placed in the environment.

5.5.2 Grasping & Manipulation System

In this section we present our approach for grasp representation/planning and manipulator motion generation. The main idea is to provide a functional representation of grasps as intervals in task space, which allows redundancy in the gripper pose prior to executing the grasp. Subsequently,

we leverage the obtained redundancy to generate reactive motions by formulating a representation of the corresponding tasks as a hierarchical Stack of Tasks (SoT) which is executed by the prioritized motion control framework proposed by Kanoun et al. [81].

Object Detection

A typical commissioning scenario in a warehouse environment generally involves as a first step the identification and localization of an object targeted for picking. In this work, we assume a simple scenario where objects of the same type are stored on a single pallet. As shown in Fig. 5.31, the Velvet-II is equipped with a Structure IO structured light depth sensor [82]. We use the 3D point clouds generated by this sensor as an input for a simple object detection module which identifies clusters of points matching our expected object models using the Point Cloud Library (PCL) [83]. Identified target clusters are then passed on to the grasp planning module described below.

Grasp Representation and Planning

Traditional data-driven grasp synthesis [84] relies on precise knowledge of the target object geometry and frictional properties. Since this information is often not available in practice, grasps planned in simulation might fail. Here, we represent grasps as pre-defined pose intervals associated with primitive object geometries as exemplary shown in Fig. 5.33 for side grasps on cylindrical objects. These intervals bound the grasping device's position and orientation, but do not fully constrain its pose. In this work, for simplicity, we limit ourselves to the illustrated grasp interval defined for cylindrical shapes. In a concept originating from observations of human grasping behavior, it has been shown that the grasping device should be roughly aligned with the target object's principal components

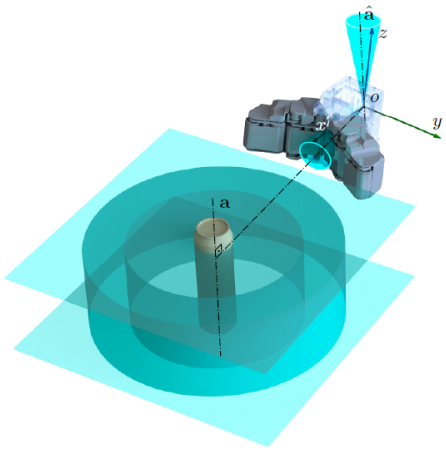

Figure 5.33: The shaded cyan regions illustrate the side grasp interval constraints for a cylindrical object. For a successful grasp, the palm frame origin $\boldsymbol{o}$ *needs to lie inside the depicted cylindrical shell which is aligned with object axis* $\boldsymbol{a}$*. The cylinders height is limited by two planes which are normal to* $\boldsymbol{a}$*. Additionally, the gripper's vertical axis (z) is constrained to lie in a cone whose axis* $\hat{\boldsymbol{a}}$ *is parallel to the object axis* $\boldsymbol{a}$*. Furthermore, the gripper's approach axis (x) has to lie inside a cone centered on the normal which connects axis* $\boldsymbol{a}$ *and point* $\boldsymbol{o}$*.*

to achieve robust grasps [85]. This property is achieved by the cone constraints depicted in Fig. 5.33. Currently, the parameters of the grasp intervals such as the distance range between gripper and object have to be evaluated experimentally for each primitive shape category. During operation, after the target object pose is detected, the grasp interval needs to be adapted to the specific scene and target object dimensions as illustrated in Fig. 5.34. Our strategy is to pre-compute a gripper collision map and use it for determining the valid grasping configurations around the target object. Once invalid grasping configurations have been pruned by using the scene model, the remaining configurations can be

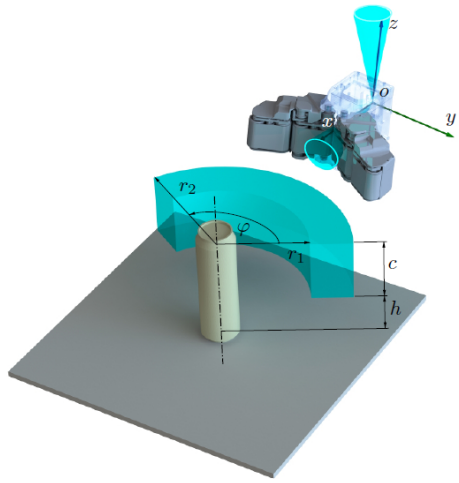

Figure 5.34: During the online stage, the corresponding grasp interval shown in Fig. 5.33 needs to be truncated (i. e., parameters for r_1, r_2, c, h and φ need to be determined) to accommodate the specific target object dimensions and to account for the fact that some regions of the grasp interval might not be feasible due to obstruction by the environment.

clustered into continuous regions and used to determine the constraints in an automatic manner.

Manipulator Motion Generation

To leverage the freedom in pre-grasp position and orientation gained from the previously described grasp representation, we use a control-based approach for reactive, on-the-fly motion generation. More specific, the method of choice is the one developed by Kanoun et al. [81] which allows to formulate the grasp interval, as well as additional desiderata such as joint limit avoidance, in form of task functions which subsequently are utilized to form a hierarchical SoT. In this paradigm, the SoT is then

used to compute prioritized controls during movement execution.

5.5.3 Robust Grasp Execution

Since the F/T sensors were not available at the time of the APPLE Project, we implemented the pull-in strategy, relying on the current absorption of the gripper's actuators as described in Sec.4.3. In order to enhance the effectiveness of the grasp acquisition strategy, the original actuators of the Velvet-II were replaced with two less reduced motors, the same type utilized in the final version of the Velvet Fingers (see Sec.4.3 for more details about the need of low reduced actuators).

The main parameters to the pull-in routine (the current thresholds for contact and final enveloping grasp), which depend on the target object properties (friction coefficient and mass) were experimentally tuned and good values were found for a set of household objects. Fig.5.35 shows four sequences of intermediate grasp states. From the left to the right depicted are the following stages: tip grasp, pull-in, embracing grasp and lift of the object.

5.5.4 Evaluation

For an early evaluation of the APPLE platform, we set up a simplified commissioning scenario as illustrated in Fig. 5.36. To this end, the previously described software components were implemented in the Robot Operating System (ROS) [86] framework. The trials were successfully carried out at a run-time of approximately four minutes for the whole procedure, of which two minutes were spent on object detection and grasping.

5.5.5 Discussion

In this Chapter a new gripper has been introduced from the basic idea to its employment in an applicative case. The gripper is designed for relatively small objects such as cans or small bottles. It is endowed with Sensitive Active Surfaces on the inner side of its fingers, implemented by conveyor belts with intrinsic F/T sensors, which allow for in-hand manipulation, contact point detection, friction coefficient emulation and slippage detection. Since the sensors were available only in the very last period of this work, we implemented on the gripper only the in-hand manipulation control and we tested the SASs as slippage detectors. Contact point algorithm and friction emulation were previously implemented and tested on a SAS module, separately from the gripper, making use of an available commercial F/T sensor. The full integration of the features of the SAS on the already existing control architecture of the gripper, constitutes the next future work in order to investigate their actual benefits on a gripping device. The contact point detection might be used to identify objects from a database which were previously in-hand rotated and their contact point trajectories recorded. Indeed, different objects can carry out different contact point trajectories when in-hand rotated. Moreover, low friction on the phalanges of the gripper, enabled at the end of the grasp acquisition stage, might foster the link wrapping around the goods allowing them to passively arranged between the links in the most stable position among the phalanges, by minimizing the resistance on the object at moving.

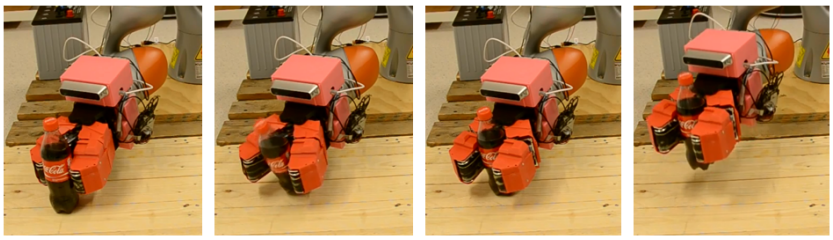

(a)

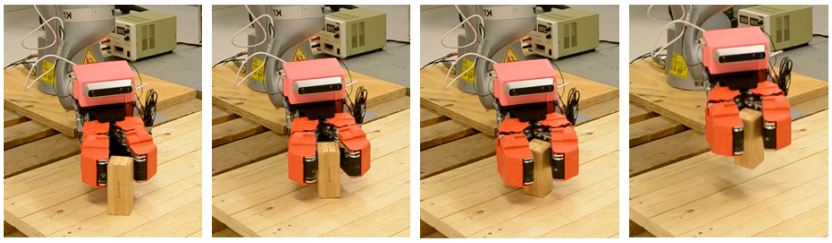

(b)

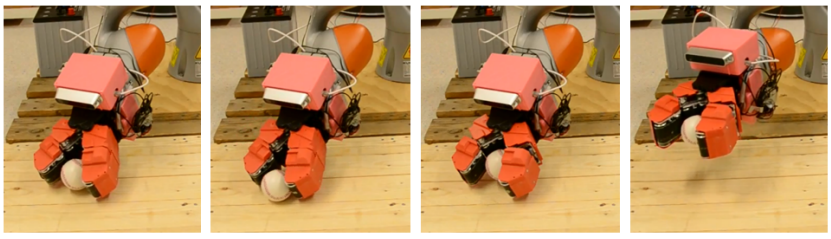

(c)

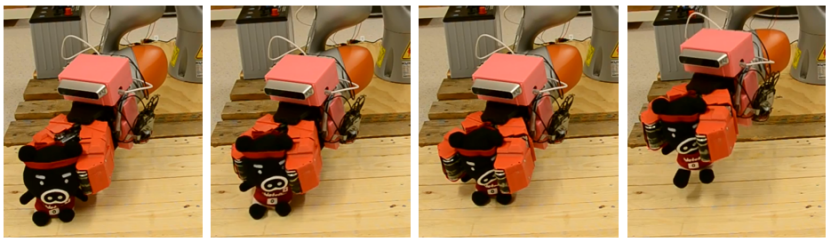

(d)

Figure 5.35: Sequences of autonomous grasping of four objects: a cylindrical object a), a sphere (baseball) b), a cube c) and a deformable object d)

Figure 5.36: On the left, the robot picks up an empty pallet in a designated zone; in the middle, the robot navigates to a loading zone where a can is detected and picked up; finally, on the right, the loaded pallet is transported to a drop-off location.

Chapter 6

Conclusion and future works

This thesis was carried out within the FP7 IP European Project RobLog with the aim of developing an end effector to be mounted on the wrist of a robotic platform for unloading of goods from a container. The scene in which the gripping device operates is filled with loose heterogeneous objects, hence the gripper works in unstructured environments with cluttered arrangements of objects. Moreover the goods differ in shape, dimension, weight and solidity (rigid or deformable). The characteristics of the environment and the objects indicate some desirable features the gripper should have. The basic idea was to take a simple mechanical planar gripper with one degree of actuation and to endow it with some further features.

The adaptation capability to the shape of objects is achieved with a rotary-rotary kinematic structure of the fingers and an under-actuated structure to drive all the links with only one actuator which results in simplicity of control. Every phalanx of the fingers is endowed with an Active Surface, implemented by a smart conveyor belt, which allows to in-hand manipulate the grasped object. Since the container configurations

contain a lot of clutter, the Active Surfaces are utilized to achieve robust grasps starting from initial fingertip grasps which, in untidy environment, are most likely to be feasible.

After preliminary tests, the first gripper prototype (the Velvet Fingers) has been then redesigned and improved to facilitate the grasp acquisition phase and the integration with the unloading platform. Numerous experiments highlighted the most beneficial gripper features to autonomously grasp objects in cluttered environment, which are summarized below.

Adaptability: the RR kinematic structure of the fingers of the gripper allows to embrace the object resulting in reliable grasps.

Under-actuation: it pursues the hardware and control complexity reduction since it does not involve an active coordination of all joints

Active Surfaces: they allow to achieve robust grasps by in-hand manipulating objects which, otherwise, would not be reachable for a power grasp in cluttered arrangements of the goods.

Compliance: Mechanical compliance and augmented compliance through current control are keys of success for autonomous grasp acquisition

Keeping into account this consideration, a novel gripper (the Velvt-II) for relatively small objects was presented. The gripper is endowed with Sensitive Active Surfaces, an advanced concept of Active Surfaces implemented by a conveyor belt with an intrinsic force/torque sensor. The gripper has adaptation capability to the shape of the goods, in-hand manipulation capability, allows to emulate different friction coefficients between the fingers and the goods, to know the grasping forces, to locate the point of contact and to detect incipient slippage of the grasped objects. Then the Velvet-II formed the end effector of the APPLE platform for

autonomous picking and palletizing within the KUKA Innovation Award 2015.

Since the force/torque sensors were available in the very last period of this thesis the contact point algorithm and friction emulation were not implemented on the gripper. This certainly constitutes a future work to carefully investigate, in order to evaluate the actual benefits of the F/T sensor employment.

Contact point location on the SASs of the gripper might be used to identify objects from a database which were previously in-hand rotated and their contact point trajectories recorded. Indeed, characteristics like shape, dimensions or peculiar geometrical features of an object might result in well recognizable profile of the contact point trajectory during in hand rotation. This might be useful in case of failure of the vision system because of a not suitable lighting, or obstructed view or even when a perception system is not available.

Low friction on the phalanges of the gripper, enabled at the end of the grasp acquisition phase, might foster the link wrapping around the goods allowing them to passively slide towards the most stable position among the phalanges, by minimizing the resistance on the object while moving.

Although Active Surfaces have been implemented by simple conveyor belts, this entails an increase of the complexity of the device, with a consequent increase of the number of components, the size and the weight of the end effector. Recent advances in micro-technology which culminated in engineered surfaces already implemented on robotic devices such as the gecko skin of the Sticky-Bot ([46], [47]), suggest that micro-structured surfaces might be the future active surfaces implementation. In this fashion micro scale adhesion control could make the surfaces of the grippers charged with the task of moving the contact point with the object, main-

taining low the general complexity of the end effector.

Appendix A

Contact Point Algorithm

In this appendix the contact point algorithm is described. It is used in Sec.5.2 to locate the contact point on the SAS given the response of the F/T sensor. The procedure is different depending on the portion of the SAS where the contact occurs: the left cylindrical surface of the driven cylinder, the right cylindrical surface of the driver cylinder and the upper plane. The extension in space of every portion is given since the geometry of the SAS module is known. The contact point algorithm routine is described below. Given that the spatial boundaries of the three portions are known, the algorithm starts assuming that the contact point occurs on the upper plane. If the solution does not belong to the range of the extension of the upper plane, the algorithm enable the calculation assuming a contact on the left cylinder. If even in this case the obtained solution is not compatible with the spatial location of the left cylinder it entails that the contact occurs on the right cylinder and the relative calculation is triggered. In the following we describe the contact point calculation of the three portions.

The left cylinder

The employed 6-axis F/T sensors are placed between each conveyor belt module and the frame of the fingers, in order to estimate the contact point of the grasped object. From this point of view all modules are exactly equal to the others. For the sake of simplicity, we refer to the module of the distal phalanx of the left finger of the Velvet II. Fig.A.1 depicts the reference frame of the sensor $\{Ss\} = \{Os : Xs, Ys, Zs\}$ in blue, the local reference system of the left cylinder $\{Slc\} = \{Olc : Xlc, Ylc, Zlc\}$ in red and the components of the position vector between the origins of the two reference systems along the axes of the sensor $\Delta xl = 37mm$, $\Delta yl = 3.5mm$ $\Delta zl = 19mm$.

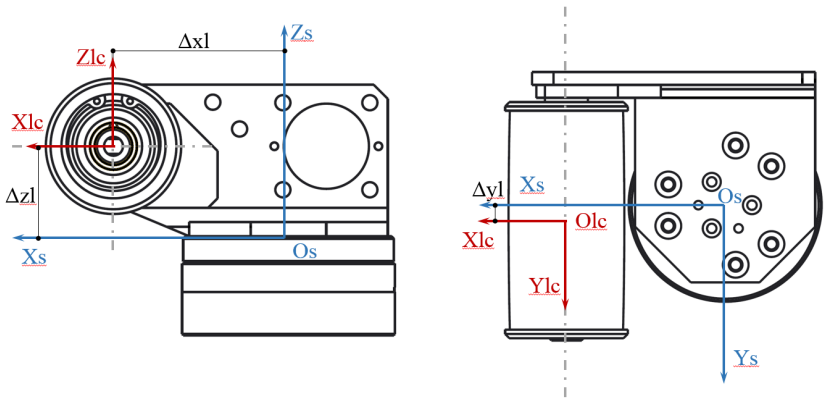

Figure A.1: Reference frames of the 6-axis F/T sensor (in blue) and the left cylinder (in red) and their offsets

The belt implementing the Active Surface wraps around the driver and the driven cylinder. Referring to the left (driven) cylinder, the contact point occurs on the left cylinder of radius $R = 14mm$ (radius of the cylinder + half of the thickness of the belt). The wrench applied on the left cylinder follows the following constrains:

- The normal component of the force (Fn) is directed inwards the surface. Fn is always positive.

- The tangential components of the force (Ft and Fa) are limited by the friction coefficient between the belt and the contacted object by the gripper:
  $\sqrt{Ft^2 + Fa^2} < \mu Fn$. Ft and Fa are positive if concordant with the axes of the cylinder.

- The torque Tn is perpendicular to the surface. It is positive when counterclockwise with respect to the going out normal $n - n$.

Fig.A.2 shows the external wrench in green on the left cylinder with all the components positive (the belt is not visible for the sake of clarity). In the same figures $\{Slc\} = \{Olc : Xlc, Ylc, Zlc\}$ is depicted as well.

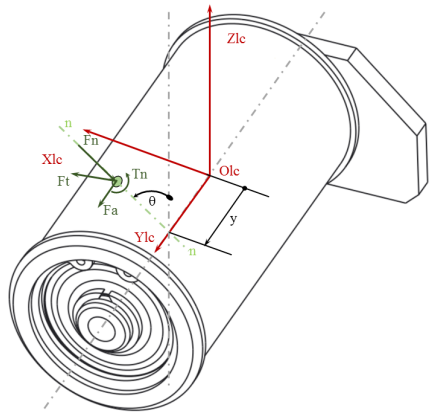

Figure A.2: Reference system on the left cylinder and external wrench applied on it

The unknowns of the problem are the components of the external wrench Fn, Ft, Fa, Tn and the position of the contact point on the left cylinder θ, y while the signal coming from the sensor is the problem data.

Here θ is the angle between the z-axes and the normal $n-n$ to the surface in the contact point and y is the distance between the origin of $\{Slc\}$ and the intersection between $n-n$ and the axis of the cylinder. Given an external wrench on the left cylinder applied to a general θ and y, the corresponding wrench at the reference system $\{Slc\}$ is given by:

$$\begin{cases} Fxlc = & -Fn \cdot Sin\theta + Ft \cdot Cos\theta & (I) \\ Fylc = & Fa & (II) \\ Fzlc = & -Ft \cdot Sin\theta - Fn \cdot Cos\theta & (III) \\ Txlc = & -Fn \cdot y \cdot Cos\theta - Ft \cdot y \cdot Sin\theta - Fa \cdot R \cdot Cos\theta + Tn \cdot Sin\theta & (IV) \\ Tylc = & Ft \cdot R & (V) \\ Tzlc = & Fn \cdot y \cdot Sin\theta - Ft \cdot y \cdot Cos\theta + Fa \cdot R \cdot Sin\theta + Tn \cdot Cos\theta & (VI) \end{cases} \tag{A.1}$$

The local force components at the contact point are easily carried out given the wrench components at $\{Slc\}$. Indeed Fa and Ft come directly from (II) and (V).

$$\begin{aligned} Fa &= Fylc \\ Ft &= \frac{Tylc}{R} \end{aligned} \tag{A.2}$$

Then $(I)^2 + (III)^2 = Fxlc^2 + Fzlc^2$, hence is:

$$Fn = \sqrt{Fxlc^2 + Fzlc^2 - \frac{Tylc^2}{R^2}} \tag{A.3}$$

Once Fn and Ft are known, (I) can be solved in θ with substitution method, being a non-homogeneous trigonometric linear equation:

$$\theta = 2ArcTan[\frac{-\sqrt{Fxlc^2 + Fzlc^2 - \frac{Tylc^2}{R^2}} \pm Fzlc}{Fxlc + \frac{Tylc}{R}}] \tag{A.4}$$

Given Fn and Ft two solutions are possible as depicted in Fig.A.3

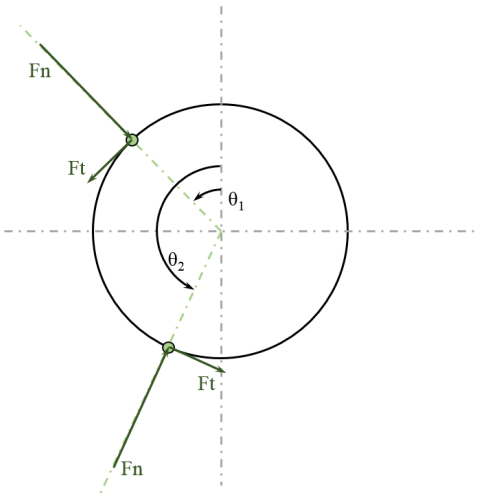

Figure A.3: Two possible solutions θ_1 and θ_2 given Fn and Ft

To disambiguate the solutions coming from Eq.A.4 we use equation (III).

Given Fn, Ft, Fa and θ, equations (IV) and (VI) form a linear system with solutions Tn and y:

$$\begin{cases} Tn = & \frac{FzlcTzlc+FaRFxlcCos\theta+FxlcTxlc-FaRFzlcSin\theta}{FxlcSin\theta+FzlcCos\theta} \\ y = & \frac{Sin\theta(-FzlcTzlc-FaRFxlcCos\theta-FxlcTxlc+FaRFzlcSin\theta)}{Fzlc(FxlcSin\theta+FzlcCos\theta)} + \frac{FaRCos\theta+Txlc}{Fzlc} \end{cases} \tag{A.5}$$

Finally, said:

$$\omega_s = \begin{bmatrix} F_{sx} \\ F_{sy} \\ F_{sz} \\ T_{sx} \\ T_{sy} \\ T_{sz} \end{bmatrix} \tag{A.6}$$

the wrench applied at the sensor and:

$$\omega_{lc} = \begin{bmatrix} Fxlc \\ Fylc \\ Fzlc \\ Txlc \\ Tylc \\ Tzlc \end{bmatrix} \tag{A.7}$$

the wrench with pole O_{lc}, the relation between the two wrenches is:

$$\omega_{lc} = W_{(lc \leftarrow s)} \omega_s \tag{A.8}$$

where

$$W_{lc} = \begin{bmatrix} I_3 & O_3 \\ \widehat{O_{lc} - O_s} & I_3 \end{bmatrix} \tag{A.9}$$

and

$$\widehat{O_{lc} - O_s} = \begin{bmatrix} 0 & \Delta z & -\Delta y \\ -\Delta z & 0 & \Delta x \\ \Delta y & -\Delta x & 0 \end{bmatrix} \tag{A.10}$$

In Eq.A.9 $I_3 \in \mathbb{R}^{3x3}$ is the identity matrix and $O_3 \in \mathbb{R}^{3x3}$ is the null matrix. Summing everything up, when a wrench is applied to the left cylinder the generalized force ω_s is available. Eq.A.8 allows to know the wrench at the local frame of the left cylinder ω_{lc}. Then Eq.A.2 and Eq.A.3 give the main components of the contact force. Finally Eq.A.4 and Eq.A.5 give the contact torque and the position of the contact point on the left cylinder.

The right cylinder

Fig.A.4 depicts the local reference system of the left cylinder $\{Src\} = \{Orc : Xrc, Yrc, Zrc\}$ in red and the components of the position vector between the origins of the two reference systems along the axes of the sensor $\Delta xr = -8mm$, $\Delta yr = 3.5mm$ $\Delta zr = 19mm$.

Briefly, in the local reference frame:

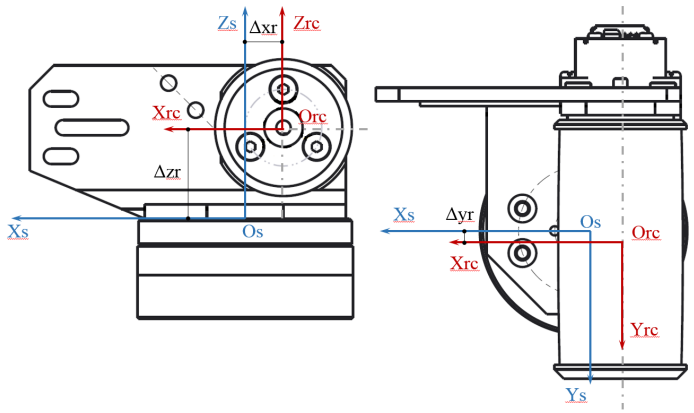

Figure A.4: Reference system of the 6-axis F/T sensor (in blue) and the right cylinder (in red) and their offsets

$$\begin{cases} Fxrc = & Fn \cdot Sin\theta + Ft \cdot Cos\theta & (I) \\ Fyrc = & Fa & (II) \\ Fzrc = & Ft \cdot Sin\theta - Fn \cdot Cos\theta & (III) \\ Txrc = & -Fn \cdot y \cdot Cos\theta + Ft \cdot y \cdot Sin\theta - Fa \cdot R \cdot Cos\theta - Tn \cdot Sin\theta & (IV) \\ Tyrc = & Ft \cdot R & (V) \\ Tzrc = & -Fn \cdot y \cdot Sin\theta - Ft \cdot y \cdot Cos\theta - Fa \cdot R \cdot Sin\theta + Tn \cdot Cos\theta & (VI) \end{cases} \tag{A.11}$$

Indeed Fa and Ft come directly from (II) and (V).

$$\begin{aligned} Fa &= Fyrc \\ Ft &= \frac{Tyrc}{R} \end{aligned} \tag{A.12}$$

Then $(I)^2 + (III)^2 = Fxrc^2 + Fzrc^2$, hence is:

$$Fn = \sqrt{Fxrc^2 + Fzrc^2 - \frac{Tyrc^2}{R^2}} \tag{A.13}$$

Once Fn and Ft are known, (I) can be solved in θ with substitution method, being a non-homogeneous trigonometric linear equation:

$$\theta = 2ArcTan[\frac{\sqrt{Fxrc^2 + Fzrc^2 - \frac{Tyrc^2}{R^2}} \pm Fzrc}{Fxrc + \frac{Tyrc}{R}}] \tag{A.14}$$

To disambiguate the solutions coming from Eq.A.14 we use equation (III). Given Fn, Ft, Fa and θ, equations (IV) and (VI) form a linear system with solutions Tn and y.

$$\begin{cases} Tn = & \frac{FzrcTzrc - FaFzrcRSin\theta - FaRFxrc - FxrcTxrc}{FzrcCos\theta - FxrcSin\theta} \\ y = & \frac{Sin\theta(FzrcTzrc - FaFzrcRSin\theta - FaRFxrc - FxrcTxrc)}{Fzrc(FzrcCos\theta - FxrcSin\theta)} + \frac{FaRCos + Txrc\theta}{Fzrc} \end{cases} \tag{A.15}$$

Finally, said:

$$\omega_s = \begin{bmatrix} F_{sx} \\ F_{sy} \\ F_{sz} \\ T_{sx} \\ T_{sy} \\ T_{sz} \end{bmatrix} \tag{A.16}$$

the wrench applied at the sensor and:

$$\omega_{rc} = \begin{bmatrix} Fxrc \\ Fyrc \\ Fzrc \\ Txrc \\ Tyrc \\ Tzrc \end{bmatrix} \tag{A.17}$$

the wrench with pole O_{rc}, the relation between the two wrenches is:

$$\omega_{rc} = W_{(rc \leftarrow s)} \omega_s \tag{A.18}$$

where

$$W_{(rc \leftarrow s)} = \begin{bmatrix} I_3 & O_3 \\ \widehat{O_{rc} - O_s} & I_3 \end{bmatrix} \tag{A.19}$$

and

$$\widehat{O_{rc} - O_s} = \begin{bmatrix} 0 & \Delta z & -\Delta y \\ -\Delta z & 0 & \Delta x \\ \Delta y & -\Delta x & 0 \end{bmatrix} \tag{A.20}$$

The plane

In Fig.A.5 the reference frames of the sensor $\{Ss\} = \{Os : Xs, Ys, Zs\}$ and the plane $\{Sp\} = \{Op : Xp, Yp, Zp\}$ are shown. The components of

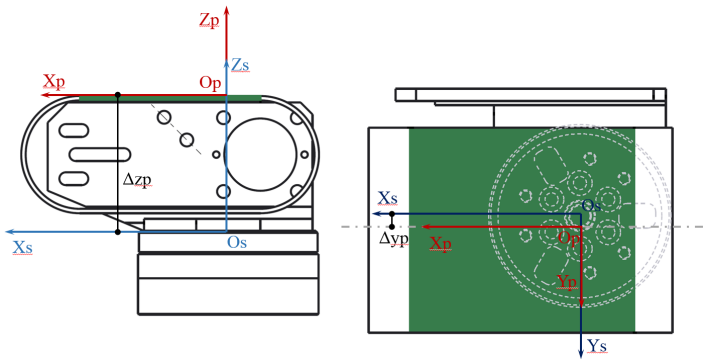

Figure A.5: Reference frame of the 6-axis F/T sensor in blue and the local reference frame of the plane in red.

the position vector between the origins of the two reference systems along the axes of the sensor are $\Delta xp = 0$, $\Delta yp = 3.5mm$ $\Delta zp = 33mm$. Fig.A.6 shows the external wrench in green on the plane with all the components positive. In the same figures $\{Sp\} = \{Op : Xp, Yp, Zp\}$ is depicted as well. In the local reference frame:

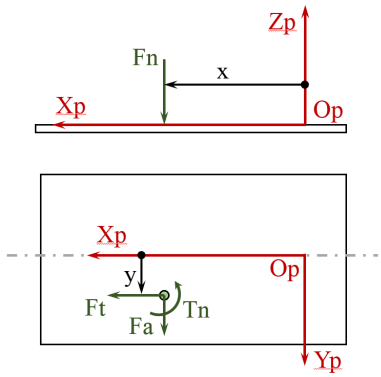

Figure A.6: Reference system of the 6-axis F/T sensor

$$\begin{cases} Fxp = & Ft & (I) \\ Fyp = & Fa & (II) \\ Fzp = & -Fn & (III) \\ Txp = & -Fn \cdot y & (IV) \\ Typ = & Fn \cdot x & (V) \\ Tzp = & Tn + Fa \cdot x - Ft \cdot y & (VI) \end{cases} \tag{A.21}$$

Eq.A.21 can be directly solved to get Ft, Fa, Fn, y, x, Tn:

$$\begin{cases} Ft = & Fxp & (I) \\ Fa = & Fyp & (II) \\ Fn = & Fzp & (III) \\ y = & -\frac{Txp}{Fzp} & (IV) \\ x = & \frac{Typ}{Fzp} & (V) \\ Tn = & Tn + Fxp \cdot y - Fyp \cdot x & (VI) \end{cases} \tag{A.22}$$

Finally, said:

$$\omega_s = \begin{bmatrix} F_{sx} \\ F_{sy} \\ F_{sz} \\ T_{sx} \\ T_{sy} \\ T_{sz} \end{bmatrix} \tag{A.23}$$

the wrench applied at the sensor and:

$$\omega_p = \begin{bmatrix} Fxp \\ Fyp \\ Fzp \\ Txp \\ Typ \\ Tzp \end{bmatrix} \tag{A.24}$$

the wrench with pole O_p, the relation between the two wrenches is:

$$\omega_p = W_{(p \leftarrow s)} \omega_s \tag{A.25}$$

where

$$W_{(p \leftarrow s)} = \begin{bmatrix} I_3 & O_3 \\ \widehat{O_p - O_s} & I_3 \end{bmatrix} \tag{A.26}$$

and

$$\widehat{O_p - O_s} = \begin{bmatrix} 0 & \Delta z & -\Delta y \\ -\Delta z & 0 & \Delta x \\ \Delta y & -\Delta x & 0 \end{bmatrix} \tag{A.27}$$

Bibliography

[1] R. M. Murray, Z. Li, S. S. Sastry, and S. S. Sastry, *A mathematical introduction to robotic manipulation*. CRC press, 1994.

[2] A. Henderson and C. Pehoski, *Hand function in the child: Foundations for remediation*. Elsevier Health Sciences, 2006.

[3] M. Grebenstein, A. Albu-Schaffer, T. Bahls, M. Chalon, O. Eiberger, W. Friedl, R. Gruber, S. Haddadin, U. Hagn, R. Haslinger, *et al.*, "The dlr hand arm system," in *Robotics and Automation (ICRA), 2011 IEEE International Conference on*, pp. 3175–3182, IEEE, 2011.

[4] A. Bicchi, "Hands for dexterous manipulation and robust grasping: A difficult road toward simplicity," *Robotics and Automation, IEEE Transactions on*, vol. 16, no. 6, pp. 652–662, 2000.

[5] A. Namiki, Y. Imai, M. Ishikawa, and M. Kaneko, "Development of a high-speed multifingered hand system and its application to catching," in *Intelligent Robots and Systems, 2003.(IROS 2003). Proceedings. 2003 IEEE/RSJ International Conference on*, vol. 3, pp. 2666–2671, IEEE, 2003.

[6] "Barrett technology inc.." http://www.barrett.com/products-hand.htm.

[7] G. Monkman, S. Hesse, and R. Steinmann, *Robot grippers*. Vch Verlagsgesellschaft Mbh, 2007.

[8] M. Tichem, D. Lang, and B. Karpuschewski, "A classification scheme for quantitative analysis of micro-grip principles," *Assembly automation*, vol. 24, no. 1, pp. 88–93, 2004.

[9] G. Fantoni, M. Santochi, G. Dini, K. Trachtb, B. Scholz-Reiter, J. Fleischer, T. K. T. Lien, G. Seliger, G. Reinhart, J. Franke, H. N. Hans Hansen, and A. Verl, "Grasping devices and methods in automated production processes," *Annals of the CIRP*, vol. 12, 2014.

[10] K. Yatsuzuka, F. Hatakeyama, K. Asano, and S. Aonuma, "Fundamental characteristics of electrostatic wafer chuck with insulating sealant," *Industry Applications, IEEE Transactions on*, vol. 36, no. 2, pp. 510–516, 2000.

[11] J. Stephan and G. Seliger, "Handling with ice-the cryo-gripper, a new approach," *Assembly Automation*, vol. 19, no. 4, pp. 332–337, 1999.

[12] S. Davis, J. Gray, and D. G. Caldwell, "An end effector based on the bernoulli principle for handling sliced fruit and vegetables," *Robotics and Computer-Integrated Manufacturing*, vol. 24, no. 2, pp. 249–257, 2008.

[13] G. Reinhart and J. Hoeppner, "Non-contact handling using high-intensity ultrasonics," *CIRP Annals-Manufacturing Technology*, vol. 49, no. 1, pp. 5–8, 2000.

[14] H. Van Brussel, J. Peirs, D. Reynaerts, A. Delchambre, G. Reinhart, N. Roth, M. Weck, and E. Zussman, "Assembly of microsystems," *CIRP Annals-Manufacturing Technology*, vol. 49, no. 2, pp. 451–472, 2000.

[15] "Da vinci robot." http://www.davincisurgery.com/.

[16] "Eod robots." https://icortechnology.com.

[17] "Uhd-iii." http://www.fmctechnologies.com/en/SchillingRobotics.aspx.

[18] L. B. Bridgwater, C. Ihrke, M. A. Diftler, M. E. Abdallah, N. A. Radford, J. Rogers, S. Yayathi, R. S. Askew, and D. M. Linn, "The robonaut 2 hand-designed to do work with tools," in *Robotics and Automation (ICRA), 2012 IEEE International Conference on*, pp. 3425–3430, IEEE, 2012.

[19] R. O. Ambrose, H. Aldridge, R. S. Askew, R. R. Burridge, W. Bluethmann, M. Diftler, C. Lovchik, D. Magruder, and F. Rehnmark, "Robonaut: Nasa's space humanoid," *IEEE Intelligent Systems*, vol. 15, no. 4, pp. 57–63, 2000.

[20] M. R. Cutkosky, "On grasp choice, grasp models, and the design of hands for manufacturing tasks," *Robotics and Automation, IEEE Transactions on*, vol. 5, no. 3, pp. 269–279, 1989.

[21] "The shadow dexterous hand." http://www.shadow.org.uk.

[22] N. Ulrich, R. Paul, and R. Bajcsy, "A medium-complexity compliant end effector," in *Robotics and Automation, 1988. Proceedings., 1988 IEEE International Conference on*, pp. 434–436, IEEE, 1988.

[23] M. T. Mason, S. S. Srinivasa, and A. S. Vazquez, "Generality and simple hands," in *Robotics Research*, pp. 345–361, Springer, 2011.

[24] L. Birglen, C. Gosselin, and T. Laliberte, *Underactuated robotic hands*. Springer Verlag, 2008.

[25] M. G. Catalano, G. Grioli, E. Farnioli, A. Serio, C. Piazza, and A. Bicchi, "Adaptive synergies for the design and control of the pisa/iit softhand," *The International Journal of Robotics Research*, vol. 33, no. 5, pp. 768–782, 2014.

[26] S. Hirose and Y. Umetani, "The development of soft gripper for the versatile robot hand," *Mechanism and machine theory*, vol. 13, no. 3, pp. 351–359, 1978.

[27] S. Hirose, "Connected differential mechanism and its applications," *Proc. 2nd ICAR*, pp. 319–326, 1985.

[28] M. Ciocarlie, F. M. Hicks, and S. Stanford, "Kinetic and dimensional optimization for a tendon-driven gripper," in *Robotics and Automation (ICRA), 2013 IEEE International Conference on*, pp. 2751–2758, IEEE, 2013.

[29] "2g velo gripper." http://www.willowgarage.com/velo2g.

[30] "Robotiq two-fingers." http://www.robotiq.com.

[31] A. M. Dollar and R. D. Howe, "Designing robust robotic graspers for unstructured environments," in *Workshop on Manipulation for Human Environments*, 2006.

[32] A. M. Dollar and R. D. Howe, "The highly adaptive sdm hand: Design and performance evaluation," *The international journal of robotics research*, vol. 29, no. 5, pp. 585–597, 2010.

[33] R. R. Ma, L. U. Odhner, and A. M. Dollar, "A modular, open-source 3d printed underactuated hand," in *Robotics and Automation (ICRA), 2013 IEEE International Conference on*, pp. 2737–2743, IEEE, 2013.

[34] J. R. Amend, E. M. Brown, N. Rodenberg, H. M. Jaeger, and H. Lipson, "A positive pressure universal gripper based on the jamming of granular material," *Robotics, IEEE Transactions on*, vol. 28, no. 2, pp. 341–350, 2012.

[35] E. Brown, N. Rodenberg, J. Amend, A. Mozeika, E. Steltz, M. R. Zakin, H. Lipson, and H. M. Jaeger, "Universal robotic gripper based on the jamming of granular material," *Proceedings of the National Academy of Sciences*, vol. 107, no. 44, pp. 18809–18814, 2010.

[36] M. T. Mason, "Manipulator grasping and pushing operations," 1982.

[37] K. Y. Goldberg, "Orienting polygonal parts without sensors," *Algorithmica*, vol. 10, no. 2-4, pp. 201–225, 1993.

[38] A. Ambler, H. G. Barrow, C. M. Brown, R. M. Burstall, and R. J. Popplestone, *A versatile computer-controlled assembly system.* School of Artificial Intelligence, University of Edinburgh, 1973.

[39] K. Tadakuma, R. Tadakuma, K. Ioka, T. Kudo, M. Takagi, Y. Tsumaki, M. Higashimori, and M. Kaneko, "Additional manipulating function for limited narrow space with omnidirectional driving gear," in *Intelligent Robots and Systems (IROS), 2012 IEEE/RSJ International Conference on*, pp. 5438–5439, IEEE, 2012.

[40] P. Datseris and W. Palm, "Principles on the development of mechanical hands which can manipulate objects by means of active control," *Journal of Mechanical Design*, vol. 107, no. 2, pp. 148–156, 1985.

[41] P. S. Datseris, A. C. Sayder, and W. J. Palm, "Apparatus for manipulating a workpiece or the like," Aug. 21 1984. US Patent 4,466,768.

[42] "Roll on gripper." `http://www.iml.fraunhofer.de/en.html`.

[43] G. Read, R., "Robotic hand effector," 2009.

[44] A. Bicchi and A. Marigo, "Dexterous grippers: Putting nonholonomy to work for fine manipulation," *Int. Jour. of Robotics Research*, pp. 427–442, 2002.

[45] J. Dejeu, M. Bechelany, P. Rougeot, L. Philippe, and M. Gauthier, "Adhesion control for micro-and nano-manipulation," *ACS nano*, 2011.

[46] K. Autumn, A. Dittmore, D. Santos, M. Spenko, and M. Cutkosky, "Frictional adhesion: a new angle on gecko attachment," *Journal of Experimental Biology*, vol. 209, no. 18, pp. 3569–3579, 2006.

[47] S. Kim, M. Spenko, S. Trujillo, B. Heyneman, D. Santos, and M. Cutkosky, "Smooth vertical surface climbing with directional adhesion," *Robotics, IEEE Transactions on*, vol. 24, no. 1, pp. 65–74, 2008.

[48] J. Lindsay, F. Chen, L. Yu, and N. Efremova, "Nanofabricated gecko-like fasteners with adhesive hairs for disposable absorbent articles," Oct. 12 2010. US Patent 7,811,272.

[49] A. Bicchi and R. Sorrentino, "Dexterous manipulation through rolling," in *Int. Conf. on Robotics and Automation*, pp. 452–457, IEEE, 1995.

[50] M. Gabiccini, E. Farnioli, and A. Bicchi, "Grasp analysis tools for synergistic underactuated robotic hands," *The International Journal of Robotics Research*, vol. 32, no. 13, pp. 1553–1576, 2013.

[51] A. Bicchi and D. Prattichizzo, "Manipulability of cooperating robots with unactuated joints and closed-chain mechanisms," 2000.

[52] D. Prattichizzo, M. Malvezzi, M. Gabiccini, and A. Bicchi, "On the manipulability ellipsoids of under-actuated robotic hands with compliance," *Robotics and Autonomous Systems, Elsevier*, vol. 60, no. 3, pp. 337–346, 2012.

[53] D. Pratichizzo, M. Malvezzi, and A. Bicchi, "On motion and force controllability of grasping hands with postural synergies," in *Robotics: Science and Systems*, IEEE, 2010.

[54] V. Hayward and B. Armstrong, "A new computational model of friction applied to haptic rendering," *Experimental Robotics VI*, pp. 403–412, 2000.

[55] R. Krug, T. Stoyanov, M. Bonilla, V. Tincani, N. Vaskevicius, G. Fantoni, A. Birk, A. Lilienthal, and A. Bicchi, "Velvet fingers: Grasp planning and execution for an underactuated gripper with active surfaces," in *Robotics and Automation (ICRA), 2014 IEEE International Conference on*, pp. 3669–3675, IEEE, 2014.

[56] D. Berenson, R. Diankov, K. Nishiwaki, S. Kagami, and J. Kuffner, "Grasp planning in complex scenes," in *Proc. of the IEEE/RAS Int. Conf. on Humanoid Robots*, pp. 42–48, 2007.

[57] E. Rombokas, P. Brook, J. Smith, and Y. Matsuoka, "Biologically inspired grasp planning using only orthogonal approach angles," in *Proc. of the IEEE/RAS-EMBS Int. Conf. on Biomedical Robotics and Biomechatronics*, pp. 1656–1661, 2012.

[58] M. T. Ciocarlie and P. K. Allen, "Hand posture subspaces for dexterous robotic grasping," *IJRR*, vol. 28, no. 7, pp. 851–867, 2009.

[59] R. Diankov, *Automated Construction of Robotic Manipulation Programs*. PhD thesis, Carnegie Mellon University, Robotics Institute, 2010.

[60] D. R. Canelhas, T. Stoyanov, and A. J. Lilienthal, "Sdf tracker: A parallel algorithm for on-line pose estimation and scene reconstruction from depth images," in *Intelligent Robots and Systems (IROS), 2013 IEEE/RSJ International Conference on*, pp. 3671–3676, IEEE, 2013.

[61] N. Vaskevicius, K. Pathak, A. Ichim, and A. Birk, "The jacobs robotics approach to object recognition and localization in the context of the icra'11 solutions in perception challenge," in *Proc. of the IEEE Int. Conf. on Robotics and Automation*, pp. 3475–3481, 2012.

[62] I. A. Sucan and S. Chitta, ""Moveit!"," 2013.

[63] R. S. Dahiya and M. Valle, "Tactile sensing for robotic applications," *Sensors, Focus on Tactile, Force and Stress Sensors*, pp. 298–304, 2008.

[64] D. Gunji, Y. Mizoguchi, S. Teshigawara, A. Ming, A. Namiki, M. Ishikawaand, and M. Shimojo, "Grasping force control of multi-fingered robot hand based on slip detection using tactile sensor," in *Robotics and Automation, 2008. ICRA 2008. IEEE International Conference on*, pp. 2605–2610, IEEE, 2008.

[65] A. Bicchi, J. K. Salisbury, and D. L. Brock, "Contact sensing from force measurements," *The International Journal of Robotics Research*, vol. 12, no. 3, pp. 249–262, 1993.

[66] W. Echelmeyer, A. Kirchheim, and E. Wellbrock, "Robotics-logistics: Challenges for automation of logistic processes," in *Proc. of the IEEE International Conference on Automation and Logistics*, pp. 2099–2103, 2008.

[67] P. R. Wurman, R. D'Andrea, and M. Mountz, "Coordinating hundreds of cooperative, autonomous vehicles in warehouses," *AI magazine*, vol. 29, no. 1, pp. 9–20, 2008.

[68] R. Mosberger, H. Andreasson, and A. J. Lilienthal, "A customized vision system for tracking humans wearing reflective safety clothing from industrial vehicles and machinery," *Sensors*, vol. 14, no. 10, pp. 17952–17980, 2014.

[69] "Linde material handling." http://www.citi-truck.com.

[70] "Kuka lightweight robotics." http://www.kuka-labs.com/en/service_robotics/lightweight_robotics/.

[71] "Sick s300 laser scanner." http://www.sick.com/.

[72] T. Hellstrom and O. Ringdahl, "Follow the past: a path-tracking algorithm for autonomous vehicles," *Int. Journal of Vehicle Autonomous Systems*, vol. 4, no. 2, pp. 216–224, 2006.

[73] J. Marshall, T. Barfoot, and J. Larsson, "Autonomous underground tramming for center-articulated vehicles," *Journal of Field Robotics*, vol. 25, no. 6-7, pp. 400–421, 2008.

[74] K. Hyyppa, "Method of navigating an automated guided vehicle," 1989. US Patent 4,811,228.

[75] "Automated guided vehicle (agv) controls." http://www.kollmorgen.com/.

[76] M. Cirillo, T. Uras, S. Koenig, H. Andreasson, and F. Pecora, "Integrated motion planning and coordination for industrial vehicles," in *Proc. of the International Conference on Automated Planning and Scheduling*, 2014.

[77] H. Andreasson, J. Saarinen, M. Cirillo, T. Stoyanov, and A. J. Lilienthal, "Fast, continuous state path smoothing to improve navigation accuracy," 2015, to appear.

[78] "Velodyne hdl-32e." http://www.velodynelidar.com/.

[79] R. Valencia, J. Saarinen, H. Andreasson, J. Vallve, J. Andrade-Cetto, and A. Lilienthal, "Localization in highly dynamic environments using dual-timescale ndt-mcl," pp. 3956–3962, May 2014.

[80] "Xtion pro live." http://www.asus.com/Multimedia/Xtion_PRO_LIVE/.

[81] O. Kanoun, F. Lamiraux, and P.-B. Wieber, "Kinematic control of redundant manipulators: Generalizing the task-priority framework to inequality task," vol. 27, no. 4, pp. 785–792, 2011.

[82] "Structured light depth sensor." http://structure.io/.

[83] R. B. Rusu and S. Cousins, "3D is here: Point Cloud Library (PCL)," pp. 1–4, 2011.

[84] J. Bohg, A. Morales, T. Asfour, and D. Kragic, "Data-driven grasp synthesis — a survey," vol. 30, no. 2, pp. 289–309, 2014.

[85] R. Balasubramanian, L. Xu, P. Brook, J. Smith, and Y. Matsuoka, "Physical human interactive guidance: Identifying grasping principles from human-planned grasps," vol. 28, no. 4, pp. 899–910, 2012.

[86] M. Quigley, K. Conley, B. Gerkey, J. Faust, T. Foote, J. Leibs, R. Wheeler, and A. Y. Ng, "ROS: an open-source robot operating system," in *IEEE International Conference on Robotics and Automation - Workshop on open source software*, vol. 3, p. 5, 2009.